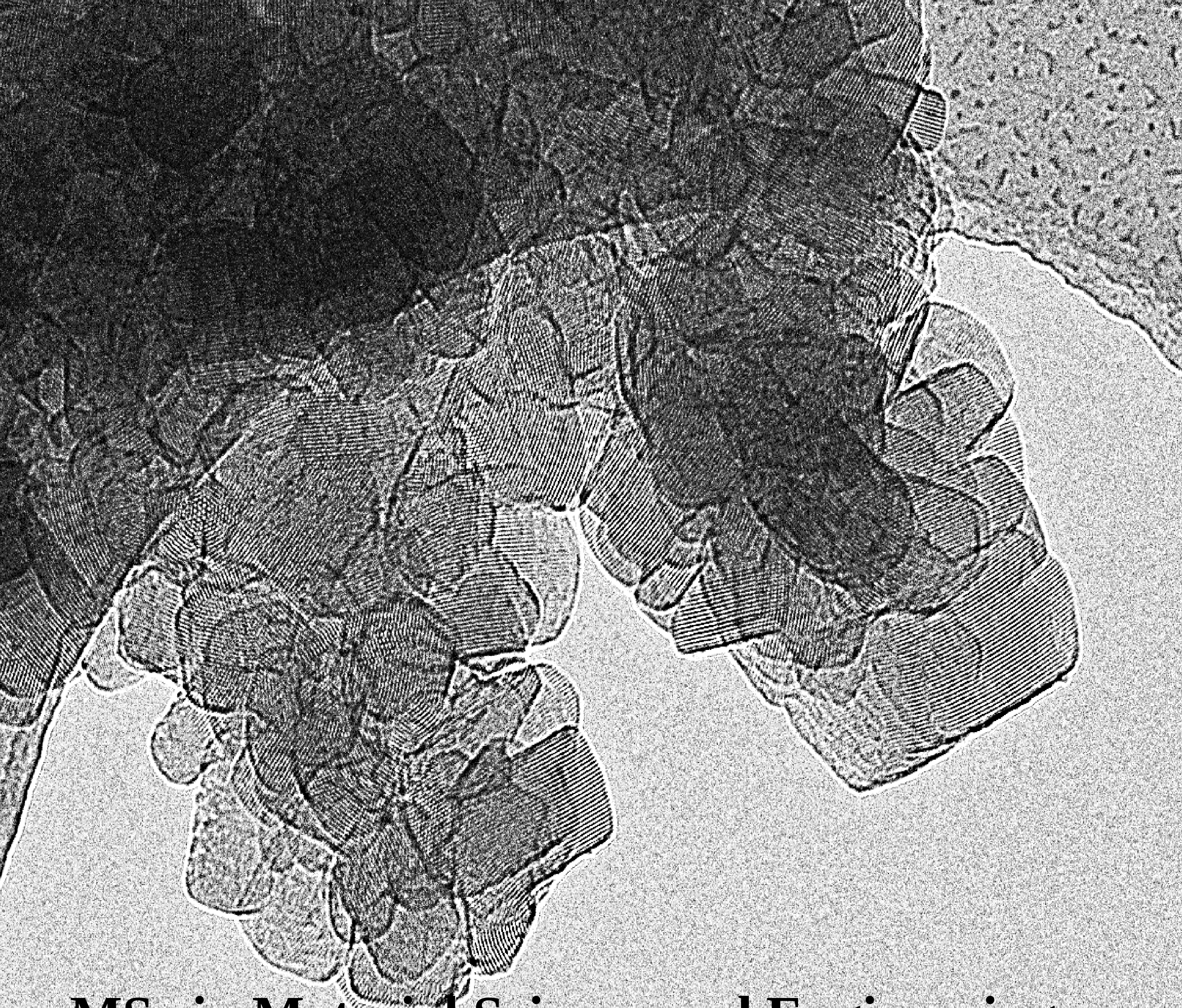

MSc in Material Science and Engineering

Insight on polysulfides harness: COFs for Li-S batteries

Martina Laura Cotti
2018

Insight on polysulfides harness: COFs for lithium-sulphur batteries

A thesis submitted to the Delft University of Technology in fulfillment of the requirements for the degree of

Master of Science
in Materials Science and Engineering

at the Delft University of Technology,
to be defended publicly on Monday December 10, 2018 at 10:00 AM.

By

Martina Laura Cotti

Supervisor: Dr. E.Kelder

Thesis committee: Dr. Erik Kelder
Dr. Amarante Bottger
Dr. Pablo Serra Costa

Abstract

Nine COF designs have been selected for their porosity, surface area and pore surface chemistry, synthesized or reproduced via a solvothermal method with different degrees of success in terms of crystallinity and porosity. Through various spectroscopy techniques (IR, Raman, XPS), together with imaging tools (SEM, TEM) and system specific analysis (XRD, N2 adsorption) it was possible to characterize the samples in all their aspects and reveal the hidden mechanisms of their nucleation. Three COFs (TAPB-DMTP 100, TAPB-DMTP 50 and DhaTab 100) had high degree of crystallinity and reasonable BET surface areas (1906, 1952, 437 m^2 g^{-1}respectively). IISERP-CON1 was quite amorphous and adsorbed the equivalent of 125 m^2 g^{-1}. Nonetheless, as well as TAPB-DMTPs, it became for the first time cathode in sulphur and Li_2S batteries. Once the battery fabrication reached its optimum, the maximum reached capacities have been 470 mAh g^{-1} (B3) and 991 mAh g^{-1} (B6) and 532 mAh g^{-1} (B4) in the first half cycle at 0.01C. When run at 0.1C, B3 could deliver 360 mAh g^{-1} after the first discharge. The fact that IISERP-CON1 delivered the highest capacity must be attributed to the high density of adsorption sites and the strong link in between COF and Li_2S that was observed with XPS. In order to reach longer cycling times, it is important that both an ordered porous structure and a rational trapping sites arrangement are achieved in the same COF.

Preface

Piove su le tue ciglia nere
sì che par tu pianga
ma di piacere; non bianca
ma quasi fatta virente,
par da scorza tu esca.
E tutta la vita è in noi fresca
aulente,
il cuor nel petto è come pèsca
intatta,
tra le pàlpebre gli occhi
son come polle tra l'erbe,
i denti negli alvèoli
son come mandorle acerbe.
E andiam di fratta in fratta,
or congiunti or disciolti
chi sa dove, chi sa dove!

Alcyone,
Gabriele d'Annunzio

This thesis collects roughly 7 months of work on the application of Covalent Organic Frameworks (COFs) in lithium sulfur batteries. Since no one in the SEE group had previous experience with these porous crystalline materials, this research provides knowledge and observations from multiple disciplines, (Organic chemistry, Material Science and Physics) and unfolds from the synthesis of COFs to their characterization and from the assembling of batteries to their understanding through electrochemical tests. Together with the fact that I had no daily supervisor, it can really be said that it was a "one man thesis".

A part from the practicalities, the challenge of dealing with a brand new material, with all its aspects, except for the industrial development, was challenging, inspiring and exciting. At the same time, having to face the difficulties of a chemical synthesis, without being prepared for it or expecting it, was unsettling and often frustrating. This thesis made me understand many things, among which that an engineer cannot be a Chemist and a Material scientist at the same time, despite I thought it was possible, and that understanding complicated concepts and being able to use them is one of the most satisfying and empowering human quality.

Only few people know that these two years at TU Delft have been the marriest and the saddest of my life.

Joining the TUDelft dream has been one of my strongest ambitions and being accepted was extremely rewarding. Despite I have filled my days with events, I am sorry I haven't done, seen or thought even more. On the dark side there is that my mother got diagnosed with cancer in the same period that I was accepted. Having a loved one close to death forces you to face a lot of responsabilities and fears. I honestly don't know how I got up and went to class some mornings, or how I could even learn or talk to people.

The Italian poem at the beginning of this paragraph talks about rebirth. Ermione, the lover of the poet, springs out of the bark of a tree and lets the rain fall on her face, before running blissfully towards the unknown.

Martina L.Cotti
Delft, Nov 2018

Acknowledgments

Intellectual and/or practical contribution to this work was without a doubt provided by Ing. Duco Bosma, PhD. Peter-Paul Harks and PhD. Remco Van der Jagt, for they have helped me advancing in the intricate domains of “hard core” chemistry, lithium-sulphur systems, or just supported me and spent some of their time talking about my work, without which I would have been totally lost. I also thank Frans Ooms for the help and smiles he brings in the grey RID laboratories and briefly my "two supervisors”, Wolter Jager and Erik Kelder, for the chats at the very beginning and very end.

Finally, I want to deliver a lovely thought to my Irek, who is the brightest and most speculative mind I have ever met and whose tender support was essential in making me start writing and clarifying my chaotic ideas. At last but not least, an enormous amount of gratitude goes towards my Parents, who can finally stop worrying because they have managed to give their only daughter what they couldn't have, who I love immensely and who I would like to see age happily and freely.

Table of contents

Introduction

A battery in a nut shell

Batteries are fascinating systems. They are probably one of the easiest to explain, after all, Alessandro Volta could prove their working principles already in 1800 [1] and we are still using his voltaic copper-zinc pile as first example in lecture rooms. Nevertheless, their working principles rely on a wide and twisted network of knowledge that roots deeply in chemistry, physics and material science.

Batteries are a crucial tile in the mosaic that portraits a sustainable future for our world. They are already an essential components of all our electronic devices, they will soon dominate the world of electric vehicles, but are also going to play an important role in the management of the energy produced by environmentally friendly source, which is crucial, if we really hope to preserve our planet for the future generations. [2]

But how do batteries work and how have they changed? Not to start from the origin of the World, it can be claimed that there are atoms, which are particles made of a positively charged nuclei and a negatively charged cloud of electrons, and that these react with each other, exchanging electrons, forming bonds to make molecules, according to the laws of chemistry. Whether a molecule, or an atom, prefers to conserve its actual state or react and transform into something else, it depends on its chemical potential (μ). A system is said to be in equilibrium, either absolute or relative, when its chemical potential is the lowest available. A battery is a system of species that stores energy in the form of a potential difference and coverts it into electric power by lowering its chemical potential spontaneously.

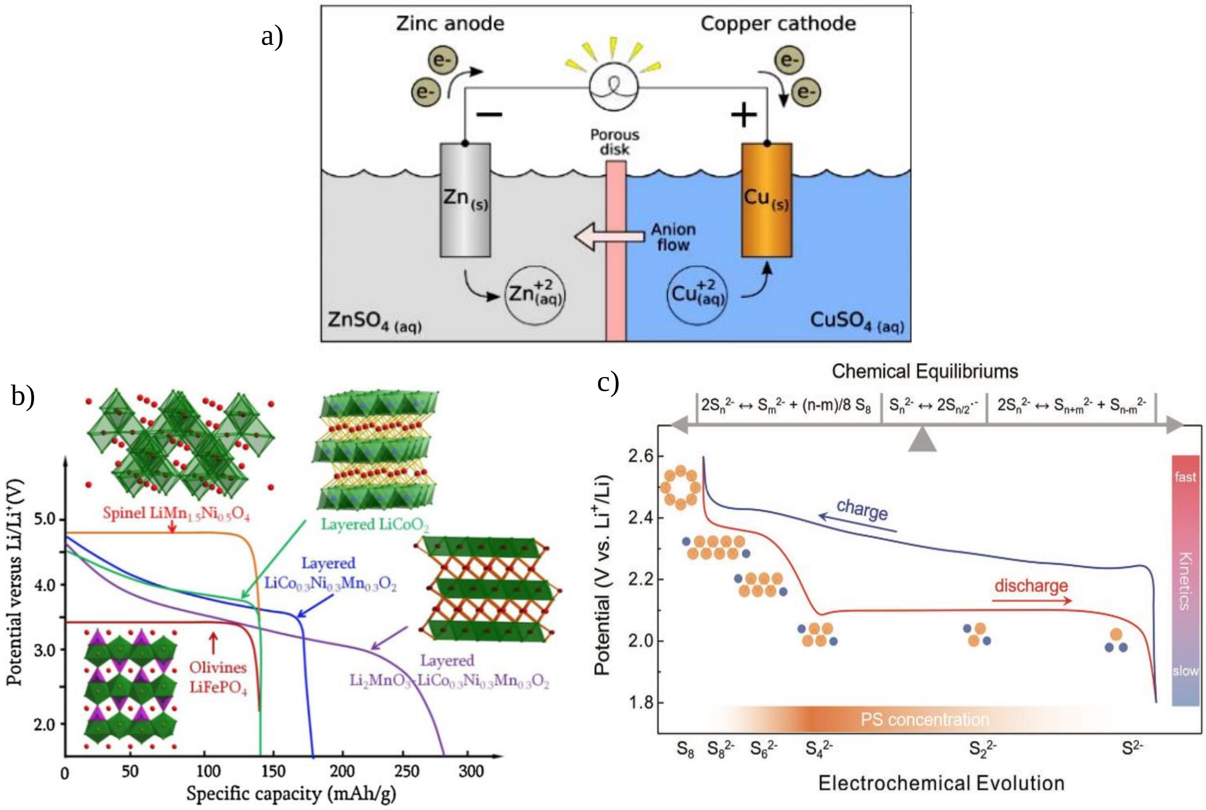

Figure 1:
Concept scheme of the copper-zinc pile in which are shown the movements of the species involved in the redox reaction (a). Voltage profiles for various insertion Li batteries systems (b) [3]. Theoretical voltage profile of a lithium-sulphur battery (c) [4]

The main difference with an ordinary chemical reaction is that electrons and chemical species physically travel along two distinct paths:

1) the specie that releases electrons, in the picture is Zn, will travel from its solid surface into a liquid solution as a cation
2) the specie that accepts electrons, in the picture is Cu, will travel from the liquid solution to its solid surface
3) the electrons lost by Zn will flow along an external circuits

This split is what allows the battery to power whatever load is connected to it.

Zinc wants to move into a liquid, called electrolyte, because there it can bind with $SO4^{2-}$ anions and lower its chemical potential (from μ_{Zn} to $\mu_{Zn}{}^{+}$), for the same reason copper wants to release $SO4^{2-}$ and deposit on the electrode surface (from $\mu_{Cu}{}^{+}$ to μ_{Cu}),. Electrons are "pushed" through a conductive wire by the contribution of both chemical potentials differences, which is called voltage (V), and can produce electricity.

$$V = \frac{\mu_{Cu^+} - \mu_{Cu}}{q} - \frac{\mu_{Zn} - \mu_{Zn^+}}{q} = \varepsilon_{Cu} - \varepsilon_{Zn}$$

To conclude, a battery works because two reactions, that involve ions and electrons, take place at the same time at two physically distinct places connected by a liquid, in which only ions can diffuse, and a conductive wire, in which only electrons can flow. The reaction that provides electrons is called *oxidation*, while the reaction that demands electrons is called *reduction*. The branch of chemistry that deals with reactions that involve charged species is called electrochemistry.

$$(-)\ \text{Oxidation: } Zn(s) \longleftrightarrow Zn^{2+} + 2e^{-} + SO_4^{2-}$$

$$(+)\ \text{Reduction: } Cu^{2+} + SO_4^{2-} + 2e^{-} \longleftrightarrow Cu(s)$$

This process is made reversible by applying a voltage of (almost) equal intensity but opposite sign to the battery. The reactions taking place at this point are not spontaneous.

Lithium batteries [5] are not very different from what depicted above, if not for the facts that there is only one ionic specie contributing to the charge, which is Li^{+}, and that the concentration of ions is constant in the electrolyte but not in the electrodes, therefore the well known Nerst equation fails to describe its voltage curves, Figure 1b. Lithium oxidizes at the anode releasing one electron, it travels through the electrolyte to the cathode, where it meets it again. The cathode material to accomodate lithium is forced to change its structure move towards another minimum energy configuration. The reaction that takes place at the cathode changes its chemical potential and it is observed that the voltage of the battery (at constant current) decreases during *discharge*. The way in which this happens is specific to the Li-cathode system, Figure 1b, and below a certain minimum voltage, called cut-off voltage, the reaction cease to be spontaneous.

In the next paragraph these concepts will be used to describe a very well studied cathode material for lithium batteries: sulphur.

Lithium-Sulphur batteries

Sulphur is one of the most desirable materials that can be chosen as cathode for lithium ion batteries for the amount of Li moles/unit it can store, its low molecular weight and for its ready availability and low cost, being the 17th most available element in the earth crust [6], two positions below carbon, and one of the most produced, 69.000.000 tonnes against 1150.000.000 for iron and 57.000.000 for aluminum (2016) [7]. However, the readers will find out soon that lithium - sulphur batteries are very complex systems, since they require knowledge and control over chemical equilibria and electrochemical reactions, phase transformations, as well as adsorption, desorption and diffusion processes. To add more spice to the mix, they should also learn that sulphur and its intermediates are insulators ($\sigma_S = 5*10^{-16}$ S/m vs. $\sigma_{Cu} = 5.9*10^{7}$ S/m) [8], have different solubilities and different densities (1.96-2.19 g cm^{-3} for S_8 vs 1.63 g cm^{-3} for Li_2S) [9], which means that they expand and contract. But let's go through it step by step [4, 10]

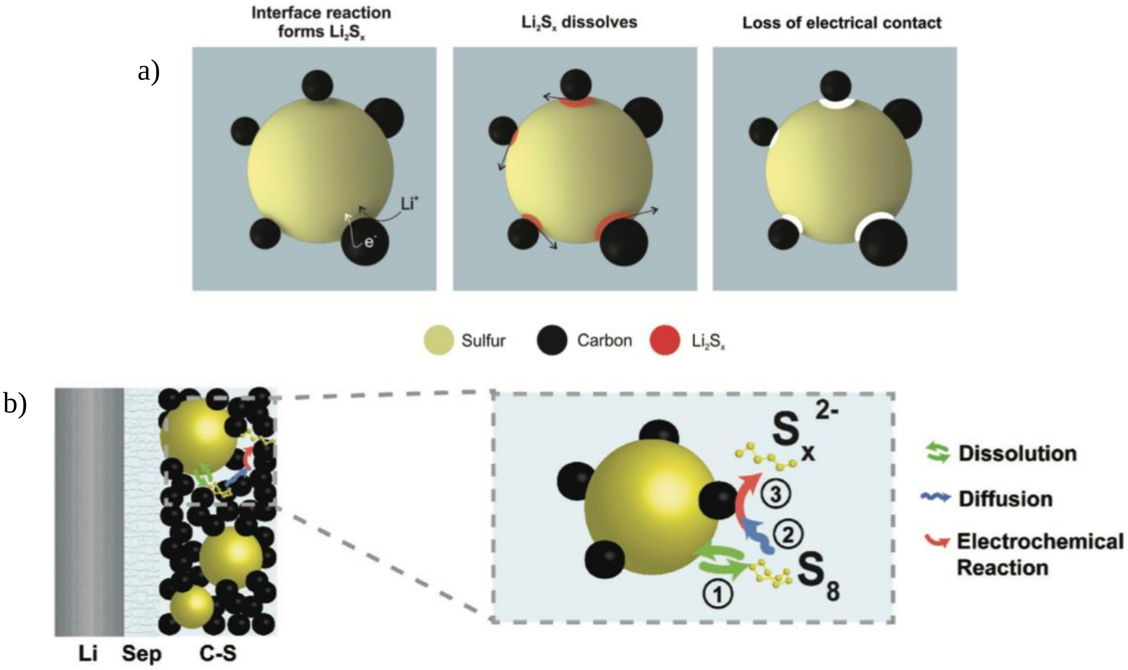

Figure 2:
Abstract representation of a sulphur particle in contact with a carbon particle and reduction taking place at their interaface, followed by loss of electrical contact (top). Schematic of the mechanism of dissolution and diffusion of sulphur (bottom) [11].

In a battery lithium diffuses through the electrolyte and reacts with sulphur according to the following redox reaction:

$$S_8 + 16Li^+ + 16e^- \longleftrightarrow 8Li_2S \text{ [12]}$$

The average voltage at which it takes place is around 2.15 V, which is lower than common intercalation materials (≥ 3 V). However, since each sulphur atom can store up to 2 lithiums, it turns out to have a very high theoretical specific capacity (1675 mAh g^{-1}) and specific energy (2500 W/kg) [12].

The full description of the system can be followed step by step by looking at Figure 1c. In the solid state, sulphur is found in its cyclic form, *cyclooctasulphur* S_8. As electrons income, sulphur undergoes three reduction steps:

1. from S^0 to $S^{0.5-}$ at around 2.3 V vs Li^+/Li
2. from $S^{0.5-}$ to S^{1-} at around 2 V vs Li^+/Li
3. from S^{1-} to S^{2-} below 2 V vs Li^+/Li

During step 1, sulphur rings break and assume a chain like shape known as *polysulfide (PS)*, S_x^{2-}.
It must be realized that this reaction proceeds according to two processes, one faster and dominant, one slower and restricted to the nanoscale [11]. If sulphur could only react through a solid state reaction, being very poorly conductive, Li-S curves would be characterized by large activation energies at the beginning of discharge and quick capacity fading due to contact loss with carbon particles, Figure 2a. Since this does not take place, there must be an alternative path way. It was found

out, for how little, sulphur dissolution is the dominant reaction and that the overall rate is actually dominated by the balance between the dissolution and diffusion of sulphur in the medium and the speed of consumption of sulphur at the current collector surface, Figure 2b. At the end of this particular step sulphur is in the form of S_4^{2-}. These PS chains are willing to accept electrons because in this way the outer electron orbitals of the peripheral sulphur atoms reach the argon configuration. Overall the molecules are negatively charged, which explains how they bind with 2 moles of Li^+ each. Therefore, once sulphur has dissolved, these reactions are kinetically easy to accomplish. During step 2, reaction proceeds until sulphur turns into Li_2S_2, which constitute the first energetic obstacle to overcome. Li_2S chains are insoluble in organic electrolytes and therefore they need energy to nucleate. Finally Li_2S_2 reacts into Li_2S, but often this reaction is impeded by solid state diffusion resistance [12].

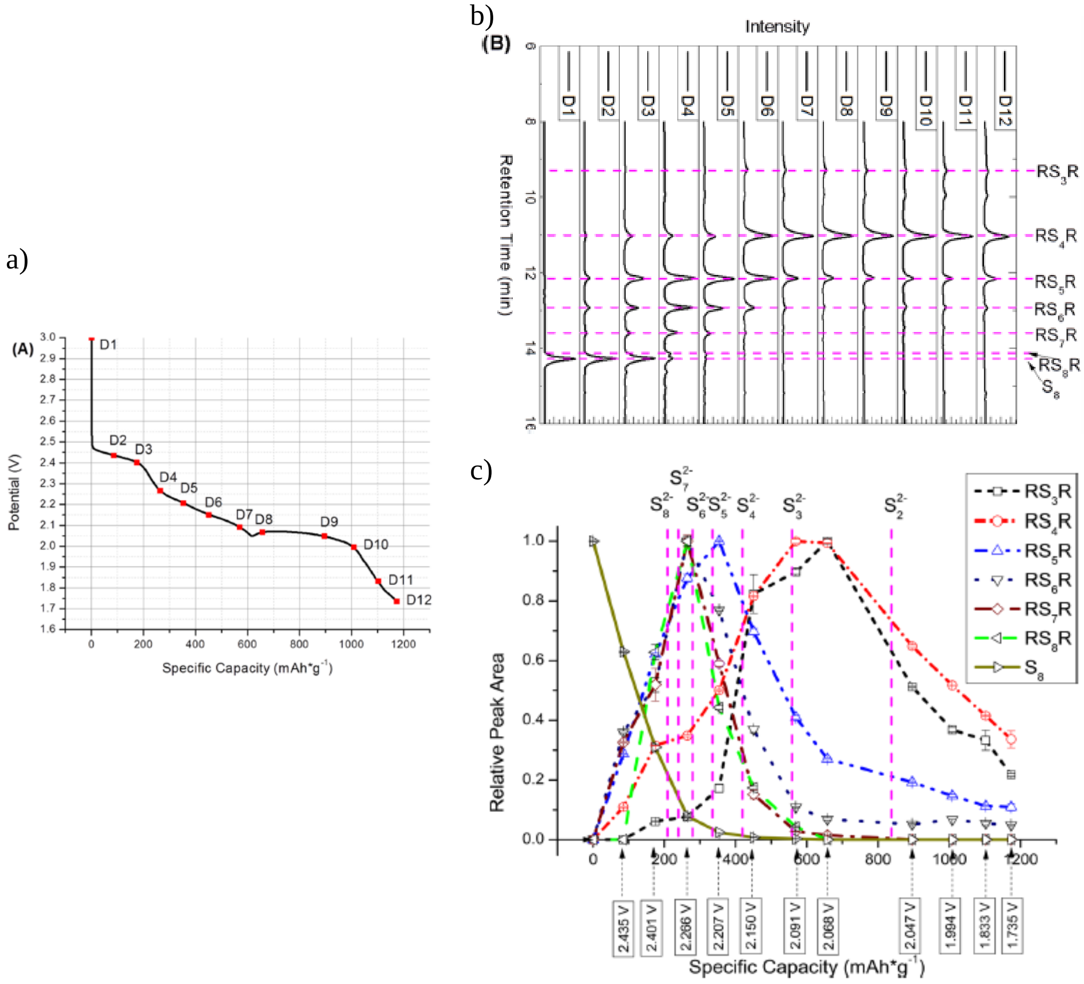

Figure 3:

Discharge curve of the coin cell battery used for the experiment: carbon fibers as cathode, lithium metal anode and reference electrode and sulphur catholyte. Result of the chromatography (HPLC) at the different sampling points revealing the occurence of the different polysulfide species according to the voltage. (a). Plot of the normalized concentrations versus the specific capacity (b). The fact that concentration peaks for S_4^{2-} and S_3^{2}- are moved towards the right is a proof that another species that can-t be detected by HPLC is formed: Li_2S_2 or Li_2S (c). [13]

Polysulfides are not all product of an electrochemical reaction and the voltage shape is better explained taking into account chemical equilibria in between the species. Zhong D. et al. have managed to map the variations in concentration of polysulfides along the voltage curve by analysis of electrolytes samples via HPLC (High Performance Liquid Chromatography). Each plateau stands for a chemical equilibrium between two or more species of polysulfides, see Figure 3a, and falls when one of them is depleted. The reaction overall moves toward short chain polysulfides, as expected. However, by detecting that the experimental concentration of S_4^{2-} and S_3^{2-} peaked at lower voltages than the theoretical one, they could claim that Li_2S_2 and Li_2S do not form at low voltages only, but start to nucleate at 2.1 V, despite the theoretical capacity has not been reached yet. Indeed the reaction is not complete since S_5^{2-},S_4^{2-} and S_3^{2-} are still found at 1.8 V. This is confirmed also by another study [14] that claims that Li_2S needs 100 mV of potential difference to nucleate on carbon. When charging the battery, instead, they could explain the existence of one single plateau by the fact that most polysulfides varied in concentration with the same rate and so remained in equilibrium with each other until oxidation was completed (95% sulphur back at 2.9 V). [13]

As you may have already realized, long chain PS S_n^{x-} with $n \geq 3$ are very different from those short chain PS, $n \leq 2$.

The first ones, to begin with, are slightly more conductive, polar, and they are soluble in many liquid electrolytes. This means that instead of adsorbing on the current collector, they can lose contact with the surface and not react further. This produces decrease in capacity and worsens the rate performance of the battery. In addition, if their concentration in solution are very high, the viscosity of the electrolyte increases and Li diffusion in the electrolyte deteriorates [4]. It is also true, however, that the dissolution of polysulfides encourages the utilization of all the sulfur in the battery: polysulfides can react with sulphur and produce Li_2S_8 and in this way speeding up the kinetics by avoiding the slower dissolution-diffusion step discussed above [11].

Li_2S_2 and Li_2S are instead known as insoluble polysulfides and are insulators. They deposit on the surface of the current collector, creating a highly resistive layer against electron flow. Their behavior determines capacity losses, because there are less and less locations where polysulfides can react, as well as capacity fading with cycling and with high currents, because it is very difficult to make these species react back, since Li_2S has to undergo a solid state reaction [11, 12].

The actual Achilles heel of Li-S batteries, which develops from these combined observations, is that soluble polysulfides can short-circuit the battery by diffusing to the anode side, consuming the electrons that should have powered the external load, then maybe diffuse back. However, if the anode gets widely coated with insoluble Li_2S_2/Li_2S, incoming long-chains will react with them to form other polysulfides, which will diffuse back and be re-oxidized. This is known as “shuttle effect”. The consequence of which are poor mass utilization, lower capacities and low coulombic efficiency [4, 10]

Current research status

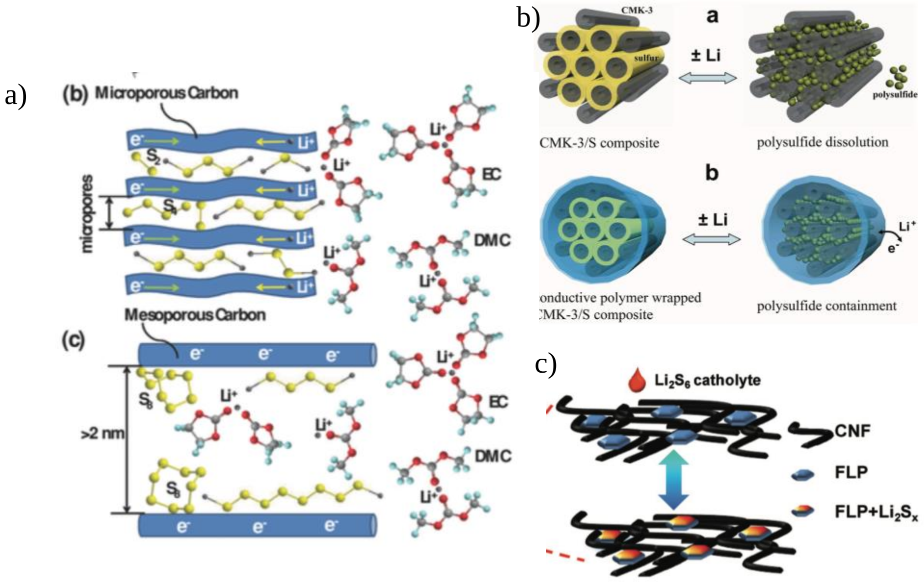

Figure 4:

Example of a microporous system in which PS evolution is skipped by keeping the solvent out of the channels [15] (a). CMK-3 as sulphur cathode wrapped in a polymer band to prevent that PS travel in the solvent [16] (b). A net of carbon fibers mixed together with layers of phosphorene (FLP) as sulphur adsorption sites [17] (c).

The cathode-design strategies developed by the battery community to face the issue of PS shuttling can be organized into two categories [4]: 1) PS formation by-pass [15, 18, 19] and PS confinement [16].

According to the first line of thought, PS formation is inhibited by spatial restriction due to micro pores and/or the loss of contact in between sulfur particles and the electrolyte, whose nature dictates and favors the formation of specific PS [15], Figure 4a. However these configurations often suffer from heavy Li_2S deposition and poor diffusion. One example are “coconut carbon shells (CSC)” in which sulphur was melted [18] that could deliver only 703 mAh g^{-1} at 0.2C after 100 cycles.
The second line of thought agrees to maintain the advantages of PS formation - in particular a liquid solution reaction over solid state reaction - and devotes the design of the cathode structure to the trapping and containment of PS.
Mesoporous carbons have been one of the first materials in which it was tried to achieve PS trapping by use of a porous network, without sacrificing electronic and ionic diffusion. An example is CMK-3 [12, 16], Figure 4b, in which trapping was achieved thanks to the pores and probably some weak Van der Waals interactions, but the shuttle effect couldn’t be completely prevented due to poor adsorption energies [20]. Generally speaking, solutions based on steric hindrance only have a hard time to conciliate the effort to provide enough trapping resistance, with the necessity to have a large specific storage volume where molecular species have also the space to diffuse. It becomes clear that sulphur and polysulfide immobilization has to be supported by other trapping techniques, such as physisorption and chemisorption. They consist on binding molecular species floating into a media to a solid surface by mean of a more or less strong and reversible chemical interaction. In the Li-S system these will be very often in the form of London dispersion forces, since Large molecules like S_8 can be attracted by induced polarization of their electron clouds, while long negatively charged chains like PS are attracted to positively charged groups. During charge instead, electrostatic interaction in between lithium and electron rich atoms can be exploited to achieve an indirect trapping, which is actually more similar to an “hydrogen bond”.

Hippauf F. et al. [21] investigated a series of carbon and carbon N/O-doped matrixes with different pore size distributions and confirmed that an high ratio of ultramicropores ($\leq$ 0.7 nm) is what endows carbon materials with the ability to retain more Li_2S_6 from solution, thanks to the overlap of the adsorption potentials from opposite pore walls. However, the best carbon matrix, CMI2, retained only 0.54 mmol g^{-1} of Li_2S_6. The highest adsorption was obtained when carbon was doped with N and O (30% of total atomic weight), in CMOI2 (1.22 mmol g-1), even if most of the capacity was again due to ultramicropores. For the doped samples the adsorption capacity was also increasing with the concentration of Li_2S_6 in solution, proving that heteroatoms sites have a role into the rearrangement and packing of Li_2S. Carbon matrices probably induce co-adsorption of molecules, hence pores get plugged faster, which is the reason why the adsorbed amount didn’t change with concentration. This same effect is encountered when mixing phosphorene with carbon nanotubes, Figure 4c [17]. Authors explained that not only phosphorene binds all polysulfides more strongly than carbon (adsorption energies range in between 2.5-1 eV from Li_2S to Li_2S_8 vs. ≈0.5 eV on graphene) but the energy balance upon adsorption is such that polysulfides prefer to adsorb on it rather than cluster on each other, thus improving the electrical contact and the redox reaction reversability. The battery delivers a constant capacity of 800 mAh g^{-1} for 500 cycles at 0.2C with a 3.3 mg cm^{-2} mass loading.

Covalent organic frameworks belong to this last strategic orientation. In the next paragraph the readers will learn more about what they are and the opportunities that their major characteristics (tailored pore size distributions, large surface area and surface chemistry) bring to the field of cathodes for PS confinement.

Covalent organic frameworks

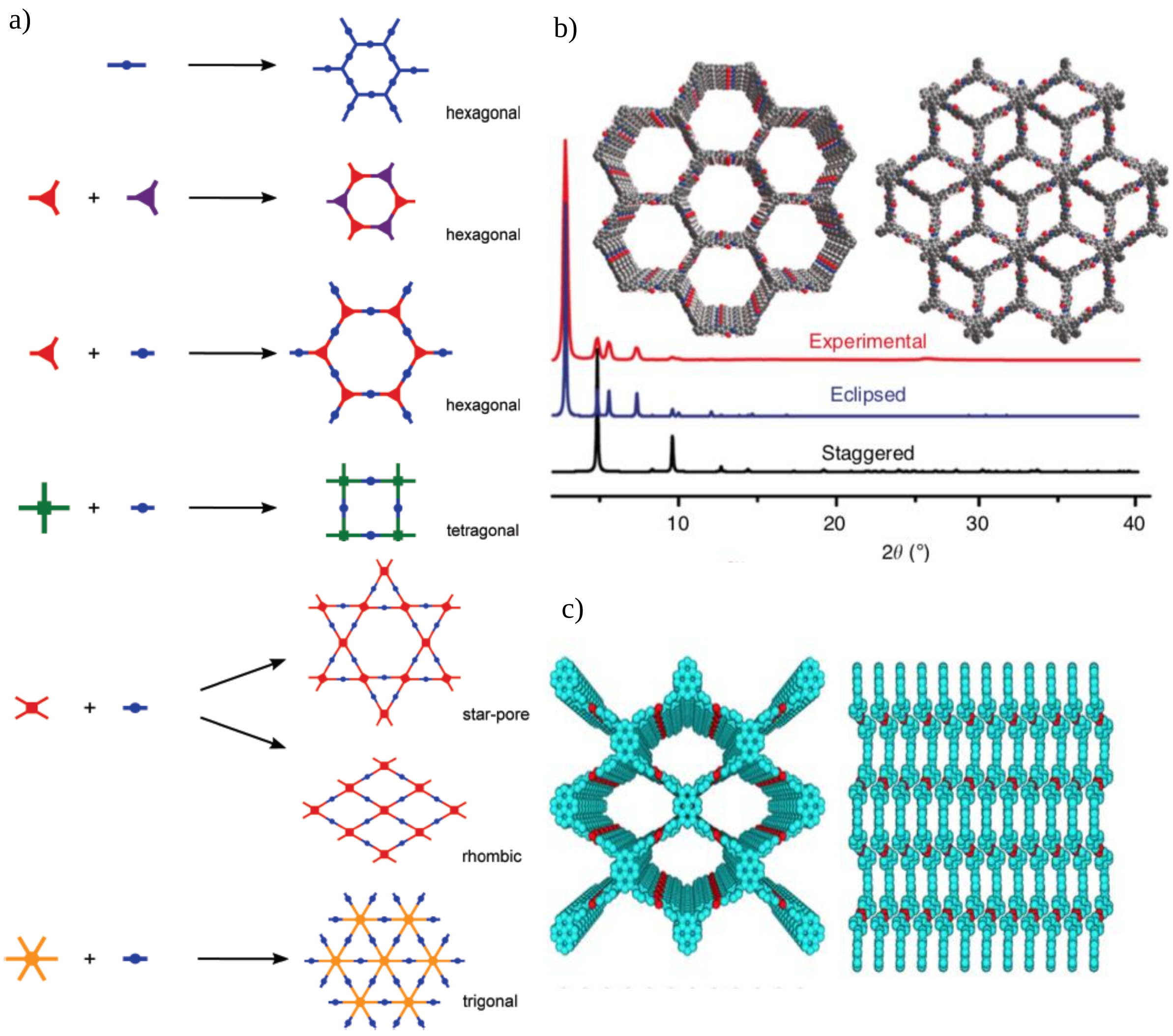

Figure 5:
Scheme picturing how choice of linkers (often tri or tetra functionalized monomers) and linkages (edge units, bifunctional monomers) determines the geometry of COFs. First reaction is a self-condensation, while others are co-condensations [22] (a). Eclipsed and staggered configurations in DhaTab 100 COF and their simulated XRD patterns [23] (b). Channel and side view of an azine based COF [24] (c)

Covalent organic frameworks (COFs) are crystalline porous networks formed by the spatial assembly of organic molecular building blocks and characterized by narrow pore size distribution and large surface areas. Their geometrical characteristics, pore size and shape, as well as composition, can be completely predetermined by the choice of the reacting bricks, Figure 5a, which can only couple with each other according to very specific condensation reactions to form covalent bonds. Among those that are frequently reported are Schiff's chemistry reactions, boronic acids self-condensations or co-condensations with boronate esters, and trimerization of cyano groups [22], [25], [26] .

Crystallinity is instead achieved by two means: (1) an error correction process made possible by the slight reversibility of the coupling with retention of water and (2) a stacking of planar sheets through conjugation of π orbitals. The latter is particularly true for 2D COFs, Figure 5c. Stacking can be helped by choosing rigid, symmetric linkers, rich in aromatic rings, which can stimulate the growth by the anchoring of identical building blocks with the same orientation on top of them. If then they are combined with flat, rigid linkages, their growth is synchronized with that of near by linkers columns

[27]. This was also confirmed by theoretical simulations of this molecules potential energy, which found that a precise conformation produces one minimum potential energy locking position for the deposition of following layers [22]. Therefore, according to the conformation of the propeller building block, two types of stacking configurations have been observed: eclipsed and staggered. Eclipsed means that every ring overlaps with those above and below it, to form channels of that diameter, staggered instead means that layers are shifted in position with respect to each other and the COF will behave as if it had pores of different sizes.

Intramolecular and intermolecular forces also play a role in making a COF more or less stable. One study investigated the ability of intramolecular hydrogen bonds to hinder rotation of linkage molecule. When hydroxide groups attached to the pore walls link to imine bonds (-C=N) in a 1,3,5-tris(4-aminophenyl)benzene/terephtalaldeyde type of COF they can produce a 4° difference in the dihedral angle towards a more planar configuration [28]. Another study proved that electrons-rich oxygen atoms can soften the intra-layer electrostatic repulsion due to the overall charge polarization produced by the heteroatoms in the ring [29].

It is important to take all this factors into consideration, because the stacking is very relevant for battery purposes, since it is the one responsible for the formation of 1D channels, which are highly desirable for the diffusion of ionic species, storage and confinement of active materials and fulfillment of surface reactions.

Synthesis conditions play a huge role in the achievement of an optimal crystallinity and porosity.

For the synthesis route that was adopted all along this thesis, called solvothermal treatment, there are 5 crucial parameters that has to be tuned to allow reversibility and deliver a stable product or, in other words, to regulate the energetic path towards the thermodynamic equilibrium of the reaction:

1. Temperature
2. Solvents
3. Reagent concentrations (and stoichiometry)
4. Catalyst
5. Water content

The relevance of each point will be discussed here, but it has to be pointed out that this is very system-specific. Since most of the COFs synthesized belong to the Schiff's base family, that's where the focus of the excursus will go.

Relatively high temperatures are necessary to trigger covalent bonds formation and break and to allow the thermodynamic formation of the chemical bond in reasonable times. For some categories of COFs (boroxine) it was observed that product precipitation does not occur at all unless the reaction takes place at a minimum temperature, while imine systems, as pictured in Figure 6a, tend to precipitate as an amorphous agglomerate at low temperatures because the activation energy required for its formation is lower [30]. At the same time, high temperatures enhance the solubility of the product in the chosen solvent mixture, which is reported to be essential to prevent pore obstruction [22].The solvent mixture is usually identified after a long trial and error process and it's often composed of a more polar and a less polar solvent. It has a role in matching the reactivity of the precursors and tuning the precipitation-dissolution equilibrium [27]. Next to this, it has to guarantee the solubility of two or more components that may have very different requirements due to their different polarity. The volume of solvents is related to the concentration of the reagents and to their subsequent ability to diffuse within the medium. In the end, the concentration of catalyst and water have been found to be crucial for the formation of a crystalline network, as investigate by [31] , see Figure 6b.

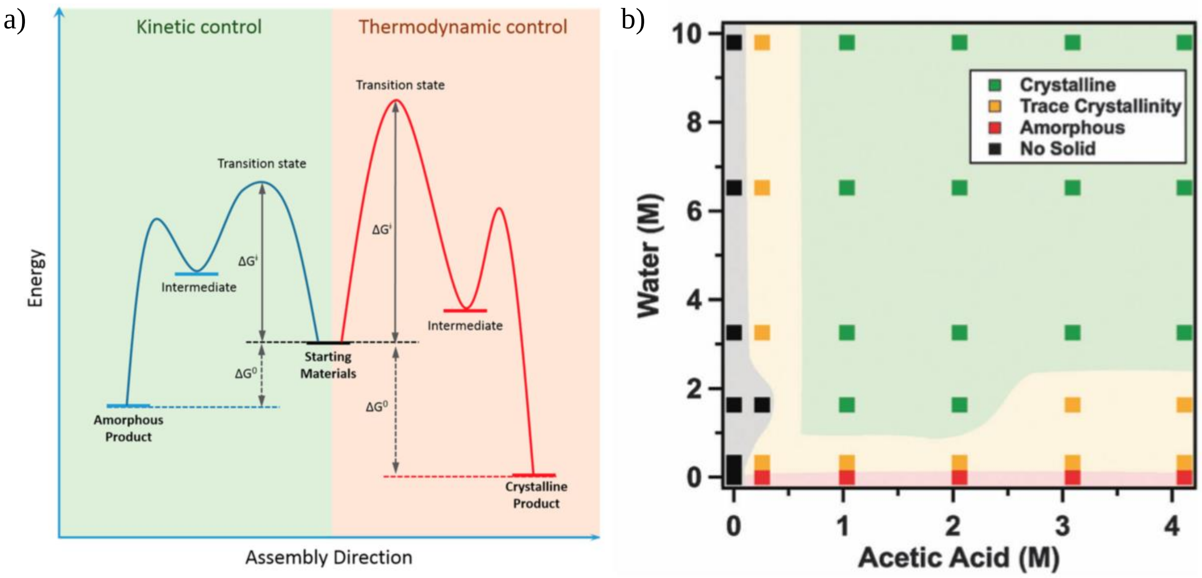

Figure 6:
Reaction coordinate diagram of a dynamic covalent chemistry (DCC) reaction showing the tendency of the system to quickly lower its energy through precipitation of an amorphous product before being able to crystallize (a) [30]. Study on the role of water and acetic acid concentrations in TPB-PDA COF (here called TAPB-DMTP COF) amorphous-crystalline phase transformation (b) [31].

As far as Schiff’s base COFs are concerned, the temperature at which the reaction is run is not as important as the concentration of water and acid in the total solution. Being below a minimum threshold can either hinder the precipitation of the product or stop the reaction at an amorphous stage. Temperature in this system becomes just a mean to control the speed of the reaction and in the green zone an equally crystalline COF can be obtained even at 25°C.

Despite the available mild synthesis conditions, COFs are know to be stable due to their strong covalent bonds network. They were tested for 7 days against many solvents, both in acidic or basic pH and proved to be insoluble and to conserve their crystallinity [29]. Nevertheless it was also observed that COFs can be destroyed in few hours when exposed to extreme pH levels [32]. On the other hand, they can resist degradation up to high temperatures, some up to 400°C according to TGA curves [23, 33, 34]. COFs can also be altered by mechanical treatment, which can break apart their π bonds, without destroying their chemical structure, as done in [35] by ball milling.

Among the many other synthesis techniques that have been explored up today, a nice review of which is given in [22] and [25], the most revolutionary is the mechanochemical method developed by Karak et al. [36] in which precursor molecules are simply ground together in sequence, with the addition of a catalyst solvent and a modulator molecule. Each step does not take more than 10 mins and only during the last one the powder is heated at 170°C for few minutes. Samples are crystalline and some also have a very large surface area. This synthetic procedure is the only one to have an industrial outlook, since the same manual steps can be replicated with an extruder.

Properties and applications

COFs are already used in a large number of applications that require high surface areas, confined volumes and diffusion pathways coupled with low density elements, such as gas storage materials [30].

However, due to their design flexibility, they have also raised a lot of expectations in the field of catalysis and sensors materials, where opto-electronic properties are demanded. Through post-synthetic modification (PSM) steps their pore size and surface chemistry can be altered in such a way to endow COF with the ability to catalyze surface reactions [29], to detect molecular species [24] or improve molecules adsorption at different concentrations [37] or pressures [38]. These post-synthetic modifications have been achieved in many ways, mostly by use of orthogonal click reactions, among which alkyne-azide cyclo-addition [29, 39], isothiocyanate (-R-N=C=S) addition to alcohol [40]and oxime formation (-R-N=C-R) [22]. Next to this, COFs can conduct electrons in the direction perpendicular to the layers, along the π system, and if building blocks are conjugated by their chemical bond electrons can also flow in the other two directions [27]. Studies have shown that they are semiconductor materials and that their ability to conduct either electrons or holes depends on the electronic properties of the building blocks. In [41], three 2D COF, with either H_2, a copper or a zinc atom in the centre of the porphyrin rings have shown respectively hole, electron and ambipolar conductivity, with mobilities as high as $\mu_h = 3.5\ cm^2V^{-1}s^{-1}$, $\mu_e = 0.19\ cm^2V^{-1}s^{-1}$ and $\mu_e = 0.032\ cm^2V^{-1}s^{-1}$ $\mu_h = 0.016\ cm^2V^{-1}s^{-1}$.

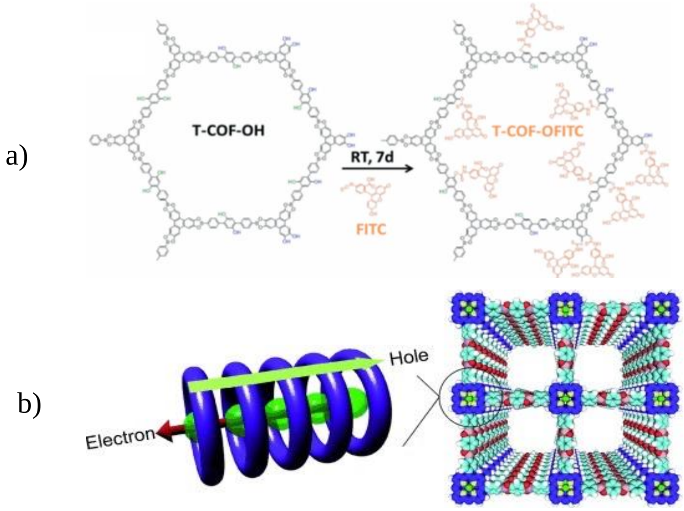

Figure 7:
Example of a post-synthetic modification, in which -OH groups have been placed especially on the walls to react further with the isothiocyanate group on a fluorescent label [40] (a). Porphyrin COF front view showing the z direction mechanism of electron and hole conduction. Holes flow in the so called “macrocycle-channel” while electrons flow along the “metal-channel” [41] (b).

COFs as sulphur storage materials

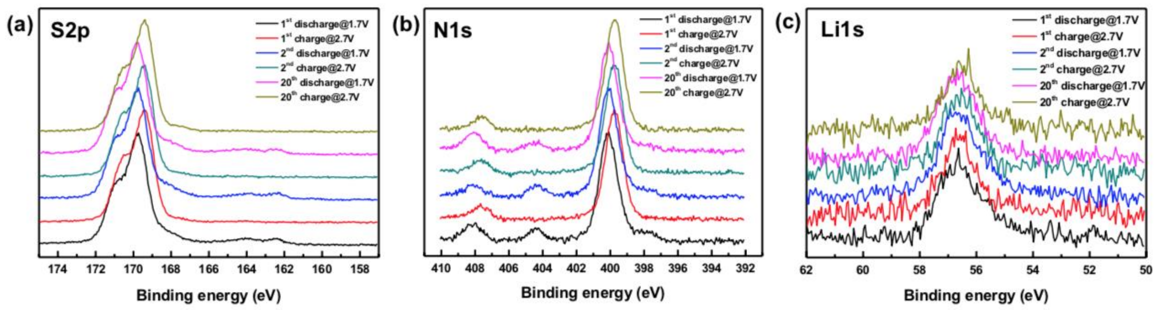

Figure 8:
Ex-situ XPS spectra of cycled CTF-S COF [42]. After the first discharge the small peak at 168.4 eV due to covalently bonded -C-S- is not visible anymore and at its place appear two minor bumps at lower energies (164 and 162 eV) that are due to sulphur new position within the framework or its bond with Li, since both disappear completely during charge(a). The same thing happen for N_{1s}, except the peak at 408 eV is still present during charge (b). Another indication that lithium does not completely leave the structure is given by Li_{1s} spectra (c).

Research on COFs as cathodes for Li-S batteries is still at an infancy stage, nonetheless since it can relay on the experience collected from all the other cited fields of study, its level of development is quite advanced. It is already a shared procedure to introduce sulphur into the structure by the so called melt-impregnation method, according to which both COF and sulphur are ground together and heated in a sealed container to 150-155 °C for at least 12 h to achieve sulphur melting and diffusion [43] It is assumed that sulfur phase once cooled down will be S_8. However, some have tried to introduce sulphur earlier, during the co-condensation reaction of the COF, in order to bind sulphur covalently to benzene carbons [42]. Once collected, the composite's crystallinity and porosity are checked, compared to the as-synthesized sample and the disappearance of reflections and adsorption is an accepted trademark for the success of impregnation. Nonetheless, there is a diffuse misconception that states that the composite is now amorphous, while the crystallinity is in fact not lost but hidden by a larger amorphous background. Additional tests, like thermal gravimetric analysis (TGA) and electron dispersion spectroscopy (EDS) are often performed to confirm the weight percentage of sulphur adsorbed and its distribution within the channels.

The most stressed aspect is the achievement of polysulfides trapping by use of the physical pore constraint and the electrostatic constraint by heteroatoms-induced ring polarization. In order to achieve that, selected COFs are usually rich in F atoms [44], triazine rings [42] [45], imine bonds [46], azide bonds [43], boroxine rings [34] or aldehyde groups [43]. This is confirmed by the analysis of these atoms' peaks by X-ray photoelectron spectroscopy, Figure 8. Usually, next to elemental sulphur peaks ($S_{2p}^{1/2}$ and $S_{2p}^{3/2)}$), curve deconvolution reveals the presence of C-S at lower binding energies, while N1s shows that its chemical surrounding has changed due charge transfer towards lithium, Figure 8b. However, it's curious that both peaks at low binding energy disappear from Figure 8a: since sulphur has moved from a covalent bond to a Van der Waals type of interaction, one would expect that the peak at 162 eV remained, as it's also found in [44].

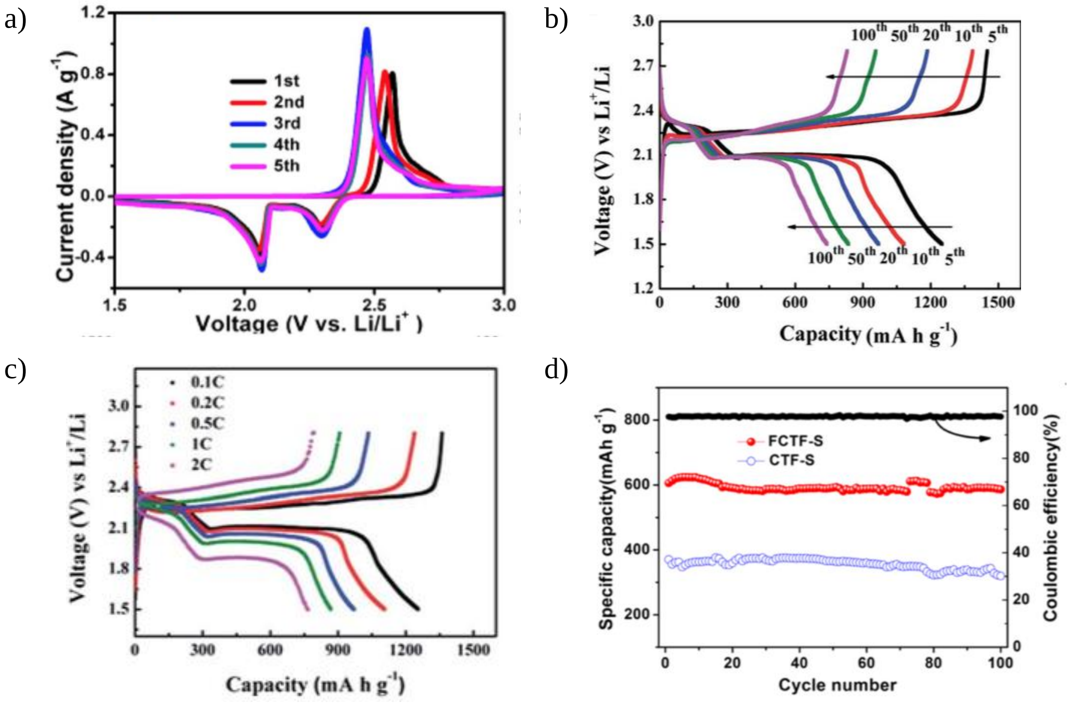

Figure 9:
Cyclic voltammetry plot showing the initial decrease of polarization due to sulphur rearrangement in TB-COF [34](a) Cycling life and rate performance of S\Azo-COF. As said in the text, polarization seems constant from the first to 100th cycle, while it increases sharply with the rate, from 148 to 547 mV [43] (b,c) Cycle life of CTF-S COFs and cycle life and coulombic efficiency of FCTF-S [44] (d)

Cyclic voltammetry studies reveal that all COFs are stable and that sometimes polarization slightly reduces during the first few cycles due to the reorganization of sulphur within the structure. CV curves always show two reduction peaks and 1 or 2 oxidation peaks, which are indications that Li-S reactions are taking place. Peaks which could be attributed to changes in the COF structure or to SEI formation are usually absent. Polarization energy, calculated as the voltage distance in between the second discharge plateau and the first charge plateau, is always of the order of hundreds of millivolts, with a minimum value obtained with FCTF-S COF (290 mV) [44] and a maximum with CTF-S (≈ 500 mV) [45] . Its value doesn't increase as much during cycling as it does when the current rate is increased. This can mean that the increased resistance is not due to deposition of Li_2S and loss of electronic contact, but it's related to electronic and ionic conduction within the COF. This is not a surprise, since none of these COFs has a high density of π orbitals, because of small linker building blocks, and since it is reasonable to say that if pores are completely stuffed with sulphur diffusion of lithium can worsen. As a consequence of this reasoning, capacity fades with cycling must instead be attributed to a progressive deposition of Li_2S on the pores surface and/or to polysulfide shuttling. It is worth noticing that during galvanostatic tests all these COFs display both sulphur peaks, during discharge and charge, even after many cycles and at high rates.

To conclude, all batteries show a quite remarkable performance. S-CTF-1 [42] delivers around ≈ 500 mAh g^{-1} after 50 cycles at 0.05C and retains 85.8 % of its initial capacity (482.2 mAh g^{-1}) when cycled at 1C for 300 cycles. F-CTF-S delivers 1132 mAh g^{-1}at 0.5C and delivers twice as much its "un-fluorinated" counterpart after 100 cycles (862 and 488 mAh g^{-1}) [44]. Quite superior are the numbers reported for those COFs which display both positively and negatively polarized areas along the same ring: as addressed by [47] adsorption is more efficient when polysulfides are trapped both through bonds with sulphur and with lithium, in particular during charge. By DFT calculations it was proved that adsorption energies for all forms of polysulfides, from long to short chains, is superior in a boroxine type COF (COF-1/S) than in a triazine type (CTF). On the same wave of thought were synthesized TB-COF [34] that can deliver 663 mAh g^{-1} at 1C after 800 cycles, which correspond to 82% of its initial capacity at that rate; COF-1/S that produces 1032 mAh g^{-1}after the first discharge at 0.5C and retains mAh g^{-1} after 200 cycles [47] and S\Azo-COF [43], which delivers 1536 mAh g^{-1} after the first discharge at 0.1C and retains 70% of it after 100 cycles.

COFs and graphene have also been combined in a unique system in which carbon nanotubes (CNT) served as a template for boroxine COF-1 growth. This cathode could combine the best of both worlds: CNT would provide diffusion pathways through mesopores, together with electrical conductivity, while COF-1 provides the necessary adsorption sites for Li_2S_x trapping and also hinders the diffusion of larger polysulfides via steric hindrance. This composite could provide 84% of its initial capacity, around 800 mAh g^{-1}after 300 cycles at 2C and could still deliver 650 mAh g^{-1}at 10 C [20].

Research Goal

In this thesis, covalent organic frameworks will be used as cathodes in lithium-sulfur batteries. The aim is to draw conclusions regarding the connection between surface area, pore volume and density of trapping groups with the storage of sulfur, battery capacity and trapping ability of the COFs. Are COFs really preventing polysulfide shuttling and how are they affecting the kinetics of the Li-S system? If yes, how? In order to answer these questions it was planned to synthesize two families of COFs, each with a different ratio of either methoxy (-OMe) or azide ($-N_3$) groups within the pores, via post-synthesis modification, as well as a group of COFs whose pore walls are intrinsically rich in heteroatom groups, such as boroxine and triazine rings. Due to time and some unsuccessful synthesis, only 3 out of 8 COFs could be synthesized and used in batteries, while 2 of them could be only characterized. Despite that, as far as my most recent bibliographic research has deepened, all the batteries that were assembled are new and have never been tested before. Unlike COFs systems for gas capture, the potential of pore post-modification on sulphur trapping is still unknown, but since it gave hopeful results in the adsorption of CO_2 [38] it was worth investigating.

Introduction to paragraphs

After the theoretical introduction has made the readers familiar with lithium-sulfur systems working principles and challenges and COFs' science, the next paragraph will introduce them to the experimental work pursued to the achievement of the already stated research goal. In particular they will start by acknowledging the methodologies with which the experiments and the analysis of the results were conducted. In the later paragraph results will be presented and discussed in the light of the possessed theoretical background. In the end, conclusions and suggestions on how the works could be improved and pursued will be given.

Experimental Methods

COFs synthesis

The solvothermal procedure that have been mentioned above is the most popular COFs synthesis technique within the battery community. It consists of mixing all reagents in a solution of one or two solvents, a catalyst, in a glass tube (either Pyrex or borosilicate), which is vacuum sealed to prevent the escape of water molecules. The followed procedure in detail was:

1. Clean the vial with gas N_2
2. Flash freeze the vial in liquid N_2
3. Turn the valve to vacuum for 5 min (or until the mixture has liquified slightly)
4. Flash with gas N_2 and repeat for 2 more times

The mixture was then sonicated, to ensure reagents mixing, and then brought to a temperature higher than both solvents boiling points to enhance solubility, for 3 days or more. This was done both in an oven or in an oil bath and differences in outcome was observed, as long as the temperature in the mixture was homogeneous and the vial was properly sealed to ensure an internal boiling-condensation cycle. All parameters mentioned are adapted to deliver an optimal crystallinity and surface area and since many trials are needed to identify even the ideal solvent ratio, i have substantially relied on COFs structures already found in literature [29],[23],[34],[48], with some minor modifications in the reagents ratio, see Table 1. The number next to the COF name stands for the ratio of linkers; for example TPB-DMTP 50 means 50 mol% of terephtalaldeyde and 50 mol% 2,5-dimethoxybenzene-1,4-dicarboxaldehyde, while in brackets is the reference article. In figures 10-12 is possible to see the drawings of all the structural formulas.

Table 1: List of the synthesized COFs together with a brief synthesis of the synthesis conditions and yield of the reaction

COF name [paper]	**Reagents and solvents***	**T(°C)/days**	**Yield (mg, %)**
IISERP-CON1 [48]	1,3,5-triformylphloroglucinol (90 mg, 420 µmol), 3,5-diamino-1,2,4-triazole (45 mg, 450 µmol) in dioxane, dimethylacetamide and mesitylene (3:1:3 vol) with 1.0 mL of 6M aqueous acetic acid	120/3	86.8, 45
TB-COF [34]	4-cyanophenylboronic acid (0.5 g) and Trifluoromethanesulfonic acid (2 ml) in CHCl3 (20 ml) mixed at 0°C	60/4 80/3	334, 25
TPB-DMTP 100 [29]	1,3,5-tris(4- aminophenyl)benzene (84.5 mg, 240 µmol) and 2,5-dimethoxybenzene-1,4-dicarboxaldehyde (69.9 mg, 359 µmol) in o-DCB/BuOH (1.5 mL/1.5 mL) and 0.3 ml of 6M aqueous acetic acid	120/3	141, 50
TPB-DMTP 50	1,3,5-tris(4- aminophenyl)benzene (84.6 mg, 240 µmol) , 2,5-dimethoxybenzene-1,4-dicarboxaldehyde (34.9 g,179 µmol) and Terephtalaldeyde (24,14 mg,180 µmol) in o-DCB/BuOH (1.5 mL/1.5 mL) and 0.3 ml of 6M aqueous acetic acid	120/3	128.1, 49.10
TPB-DMTP 17	1,3,5-tris(4- aminophenyl)benzene (84.3 mg, 240 µmol), 2,5-dimethoxybenzene-1,4-dicarboxaldehyde (12.2 mg, 63 µmol) and Terephtalaldeyde (40,5 mg, 302 µmol) in o-DCB/BuOH (1.5 mL/1.5 mL) and 0.3 ml of 6M aqueous acetic acid	120/3	115.9, 47
TPB-TP [29]	1,3,5-tris(4- aminophenyl)benzene (85.7 mg, 244 µmol) and Terephtalaldeyde (49.3 mg,367 µmol) in o-DCB/BuOH (1.5 mL/1.5 mL) and 0.3 ml of 6M aqueous acetic acid	120/3	Oven: 118, 48.5
DhaTab 100 [23]	1,3,5-tris(4- aminophenyl)benzene(30.2 mg, 90 µmol) and 2,5-dihydroxybenzene-1,4-dicarbaldehyde (21.6 mg, 130 µmol) in 1.7 ml of mesitylene, 0.3 ml of dioxane and 0.2 ml of 8.0 M aqueous acetic acid	120/3	Oven: ≈ 70, 71
DhaTab 50	c(30.2 mg, 90 µmol), 2,5-dihydroxybenzene-1,4-dicarbaldehyde (10.79 mg, 55,5 µmol) and and Terephtalaldeyde (8.7 mg, 65 µmol) in 1.7 ml of mesitylene, 0.3 ml of dioxane and 0.2 ml of 8.0 M aqueous acetic acid	120/3	Oven: ≈ 80, 85

*See papers for detailed synthesis procedures and purification steps

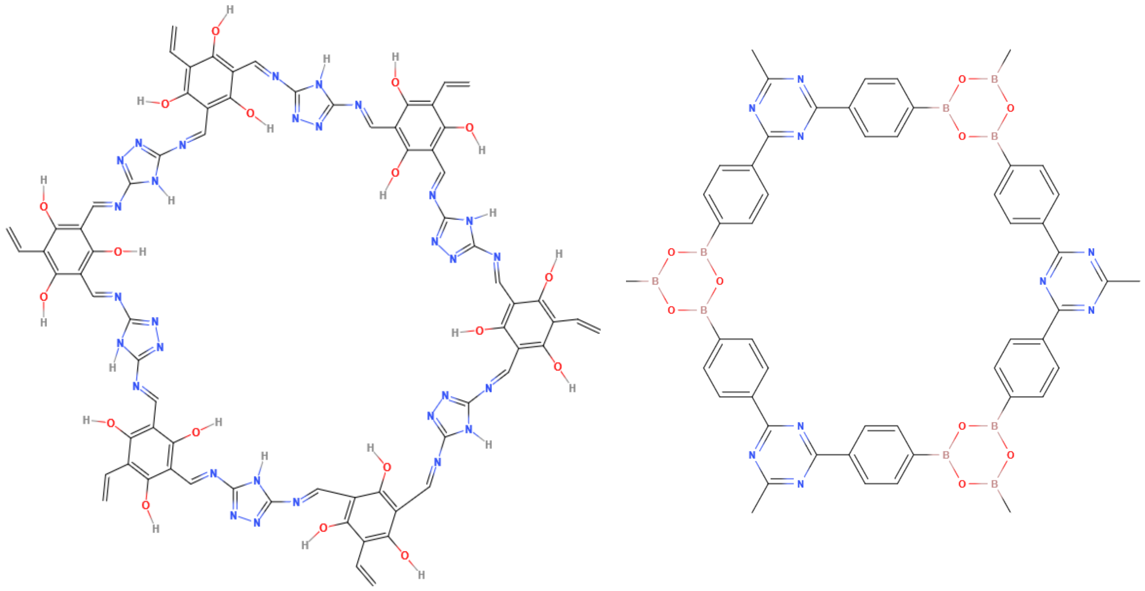

Figure 10: Structural formula drawing of IISERP-CON1 and TB-COF

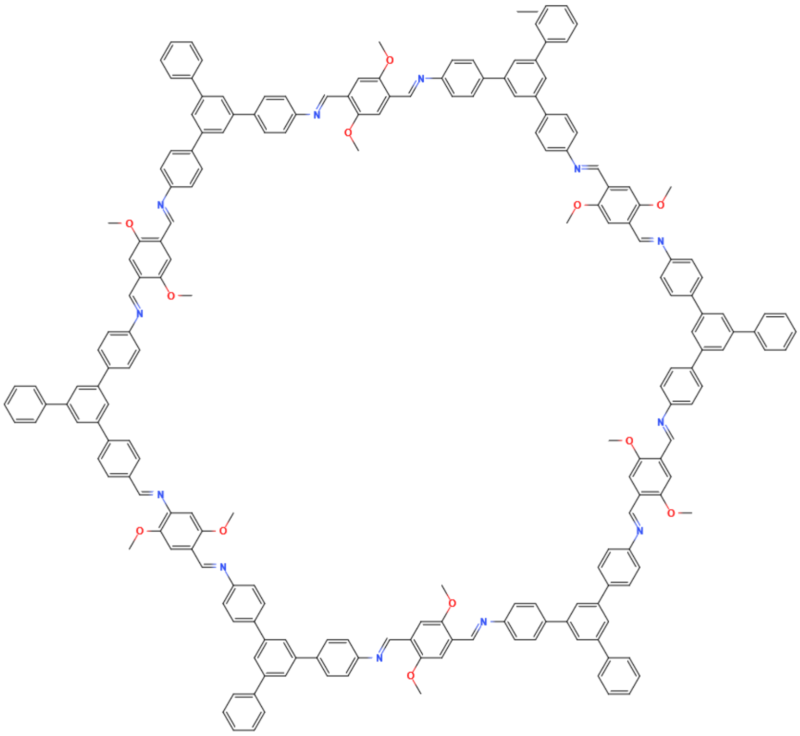

Figure 11: Structural formula drawings of TPB-DMTP 100 .

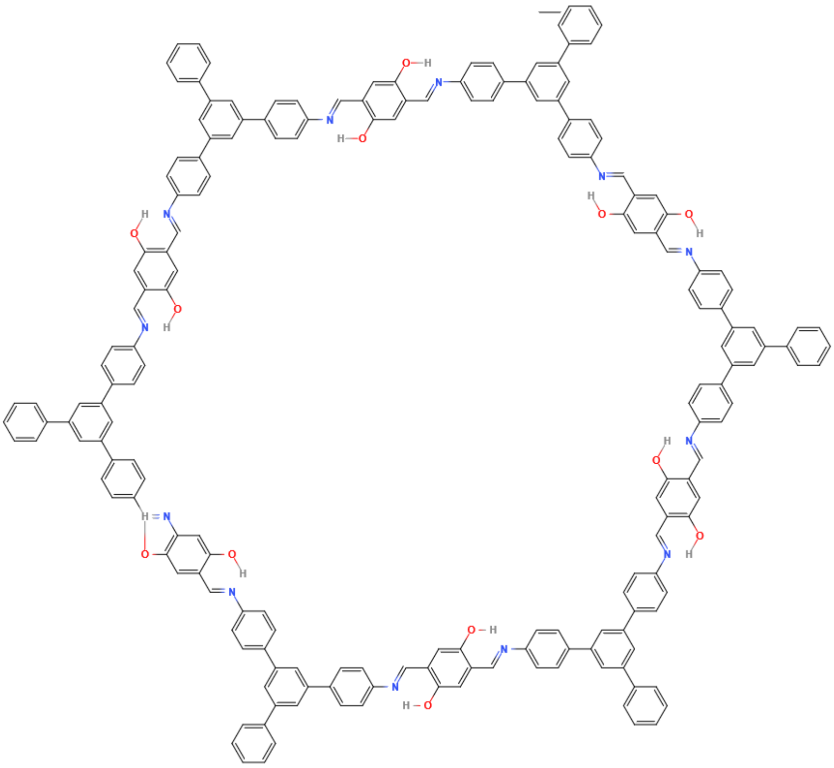

Figure 12 Structural formula drawings of DhaTab 100.

Recrystallization of TPB-DMTP 17 and IISERP-CON1

What it's called here recrystallization are two attempts to increase the crystallinity of already synthesized COFs (imine bonded).

The first was carried out by partially dissolving TPB-DMTP 17 into a very basic aqueous solution (ph 13) and then inducing the recrystallization by dropwise addition of pure HCl, in order to turn the solution slowly to ph 8. When a stable ph was reached, the mixture was sonicated for three hours to be sure that the ph of the solution was the same everywhere within the framework. The mixture was then filtered, washed with water and dried in a vacuum oven at 120°C. In [32] a similar method is used to study the dynamics of crystallization. The second attempt was carried out by placing IISERP-CON1 back into its reaction solution and adding a larger volume (3ml) of 6M aqueous acetic acid. The following steps are already described in the previous paragraph. The method is adapted from [31], where it was used to investigate the transition from amorphous to crystalline phase during COFs crystallization.

Materials

All chemicals were purchased by Sigma Aldrich, TCI Europe or Carbosynth and used without further purification.

COFs characterization

Powder X-ray diffraction

X-ray diffraction patterns were collected on a Bruker D8 Advanced Instrument using a Co $K\alpha$ (1.7889 nm) source. Most of them were acquired at a scan speed of 0.2 s/step, 0.02 step increment and fixed divergence slit of 0.3. However, to tell the [42] peak from the probe background at very small 2θ, the scan speed sometimes was reduced to 0.5, while to improve the resolution of the [49] peak at larger 2θ, often a V4 or V6 flexible divergence slit was necessary. Powders were ground beforehand difficultly, being very electrostatic, therefore sometimes asymmetric peaks are observed, due to large particles and surface roughness. A first assessment of the crystallinity was achieved by use of the Diffraction Evaluation Package applying the following in a 2θ interval of 0°-60°:

%Amorphous = (Global Peak Area - Background Subtracted Area)/Global peak area
% Crystalline = 1-%Amorphous

Since some COFs were reproduced from papers, the aim of this measurement was mostly to verify that the structures coincided. Therefore data were analyzed at first by a quick manual calculation, according to [50]. The calculation assumed an initial knowledge of the crystal system and thus could return only values for the lattice parameters, in our case with large uncertainties on c, being the number of reflections for these COF materials very limited.
The relation between the inter-planar distance, d, and the lattice parameters a, b and c, is given by:

$$\frac{1}{d^2} = \frac{4*(h^2 + hk + k^2)}{3a^2} + \frac{l^2}{c^2}$$

Pawley refinement was performed on the more crystalline samples, using the software provided by the Cambridge Crystallographic Data Center, Dash, for ab-initio structural solution and refinement.

Fourier transform infrared spectroscopy (FT-IR)

IR spectra were obtained using a Nicolet 8700 Research FT-IR Spectrometer with attenuated total reflectance (ATR). Spectra were collected in the range of 100-4000 cm-1 and were indexed according to [51]. The reflection at 2359 cm-1 visible in all spectra is due to CO2 present in the atmosphere.

Scanning Electron Microscopy (SEM)

Imaging of all samples was performed on an Analytical Scanning Electron Microscope JEOL JSM-6010LA by detecting secondary electrons. On the same instrument was carried out also EDS: elemental detection was done both by collecting electrons coming from a large surface and by spot analysis. The technique proves its validity if electrons are collected from a surface as flat as possible. Samples were hold on a carbon tape.

Transmission Electron Microscopy (TEM)

TEM images were obtained on JEOL JEM1400 Plus Electron Microscope. Samples were ground and transferred onto a graphene micro drum.

Nitrogen adsorption measurement

Nitrogen adsorption isotherms were acquired with Micromeritics 3Flex Surface Characterization Analyzer. Before measuring, samples were weighted in a flat bottom vial and heated up under N2 pressure at the temperature at which they were dried previously, for at least 12 hours.
From each measurement the BET surface area was calculated interpolating linearly the isotherm curves in a pressure range of 0.05-0.25 p/p°, specific to the sample. It was chosen to rely on the pore

size distribution and cumulative volume obtained by non linear DFT calculations (NLDFT), using as simulation model either carbon slit (CS) or carbon single wall nanotubes (SWNT). The BJH method was discarded since it is known to underestimate the width of pores below 10 nm of 20-30%. [52]

Confocal Raman Spectroscopy

Raman spectra were obtained using a Renishaw inVia confocal Raman microscope with a light probe of 785 nm and collecting at least 25 acquisitions for each sample. Again Raman gave information on the chemical structure of the COFs, but in particular it was used to detect the bonds in between S, or Li_2S and the COF network.

X-ray photoelectron spectroscopy (XPS)

XPS spectroscopy was carried out using a Thermo Scientific™ K-Alpha™ XPS spectrometer.
Elemental scans were acquired at 0.1 eV/step. Spot size 400 um, analyzed depth 10 nm. All peaks positions for all elements have been shifted accordingly to a standard reference that in this case was decided to be the C1s sp2 band at 284 eV. The deconvolution and peak indexing was performed with the help of the software Avalanche.

COFs impregnation

*Disclaimer: due to the scarce amount of powders and their electrostatic nature, they have been often mixed and ground in a glass vial with a metallic spatula. This means that inhomogeneities in the cathode composition are likely. This was accounted for by favoring the equilibration and the diffusion of species within the sample.

Stoichiometry

To quantify the real trapping ability of the COFs, the amount of S and Li2S have been esteemed for each network according to the expected number of bonding sites, thus assuming that each mole of Li_2S bonds only once to the framework. For S batteries this was done by making the ideal assumption that all sulphur would react into Li_2S by the end of discharge. Nevertheless, the amount of S/ Li_2S was reduced, if the calculated BET surface area was lower than reported, as well as the number of exposed trapping sites, because it was accepted that adsorption would take place only within the pores.

Sulphur cathodes

Impregnation with sulphur was achieved by the described method of melt diffusion as described in [43] and [45]. Each COF was mixed with sulphur in a borosilicate vial, flushed with nitrogen and vacuumed before being sealed. The tubes were then placed in the oven at 155°C for at least 12 hours.

Li_2S cathodes

Impregnation of COFs with Li_2S was achieved by dropping a solution of 0.55 M Li_2S in ethanol on the COFs powders, as described by [53]. The mixtures were agitated and let in the glove box overnight, so that the solution could penetrate into the pores. Subsequently, precipitation of Li_2S was achieved by evaporating ethanol on a heating plate, at 100°C and then by forcing the evaporation of the last drops by vacuum drying in the anti-chamber of the glove box. In the cited paper, mixing and precipitation were taking place at the same time and at higher temperatures (250°C) to achieve a rapid nucleation and restrict the growth of the Li_2S particles. With COFs this was not possible since the solution needed to diffuse into the pores and because COFs may start to display mass loss at temperatures higher than 200°C according to their TGA curves [29], [48]

Electrochemical testing

Electrolyte

The selected electrolyte formula is among the most used in literature and it consists of a solution of 1M LiTFSI in a 1:1 volume ratio of DOL/DME with 1 wt% of LiNO3.

Cathode composite

The final cathode composition consisted into a mixture of COF, sulphur or Li_2S, and Super P Carbon (SPC), which was always 30% of the total weight.

Cells preparation

Figure 13:
Picture of a lab cell where are visible the two metal plates (1), the o-ring (2), the spring within the cavity where one metal plate is placed (3) and the external sealing screw (4)

The tested lab cells have the configuration shown in Figure 13. They were all assembled according to an equal stacking, which consisted of, from plus to minus:

1. Cathode composite
2. First solupor separator (d = 19 mm)
3. Second glass fiber separator (d = 16 mm)
4. Electrolyte (100 µl)
5. Metal lithium anode

Since a more efficient coating procedure was hindered by the scarce amounts of synthesized COFs, the cells were assembled by mixing the cathode composite with some drops of 1:1 DOL/DME solution, distributing and leveling the suspension with a spatula on the metal plate and laying the further layers on top. Despite being probably an unconventional method, it was still possible to know the amount of sulphur in each cell, distribute the powder homogeneously on the plate and guarantee the electrical contact by tightly pressing the counter metal plate on the stack.
However, some of the first batteries have been assembled without solvent addition and they can be recognized because usually electrical contact is lost right after the first discharge curve, see Figure 25a.
The tested battery systems are summarized in details in Table 2. Those made without addition of solvent, will be distinguished with an asterix * next to their code in the following paragraphs.

The surface specific capacity was set to 1 mAh cm^{-2} in a first stage, but since this was equivalent to 10-12 mg of composite mixture and powders were very volatile, I decided to reduce it to half, in order to make the handling easier and more accurate. This couldn't be changed till the end for consistency. On the contrary, Li_2S batteries could be loaded with the established amount, being the composite more dense.

Table 2: Summary of the battery made with the number of adsorption sites for Li-PS in each COF and the amount of sulphur that is in each battery.

Battery code	**Cathode Composition**	**Trapping sites (mole/unit)**	**Amount of S/Li_2S (mg,umol)**	**Surface specific S/Li_2S (mg/cm^2,wt%) ****
B1	Li_2S/SPC	NA	NA	NA
B2	TPB-DMTP 100/ S/SPC	12 mol/unit	(6.7 mg, 209 µmol)	0.298,17
B3	TPB-DMTP 50/S/SPC	9 mol/unit	(6.7 mg, 209 µmol)	0.298,17
B4	TPB-DMTP 50/ Li_2S /SPC ***	9 mol/unit	(23.95 mg, 532 µmol)	0.857, 79.8
B5	IISERP-CON1/SPC	21mol/unit	NA	NA
B6	IISERP-CON1/S/SPC	21mol/unit	(9.89 mg, 308 µmol)	0.298, 24
B7	IISERP-CON1/ Li_2S /SPC ***	21mol/unit	(29,5 mg, 655.72 µmol	0.857, 63

** Assuming a metal plate diameter of 1.9 cm and a surface specific capacity of 0.5 mAh cm^{-2}. ***Based on 1 mAh cm^{-2}

Maccor

All batteries were cycled on a Maccor 4000 automated test system.

Cyclic voltammetry

All batteries where tested on an Autolab System at 0.1 mV/s rate.
Reduction goes from right to left and has negative currents.

Results and discussion

Synthesis outcome

Success in the the formation of a crystalline COF is provided by observation of FT-IR spectra, elemental analysis by EDS and XRD patterns.

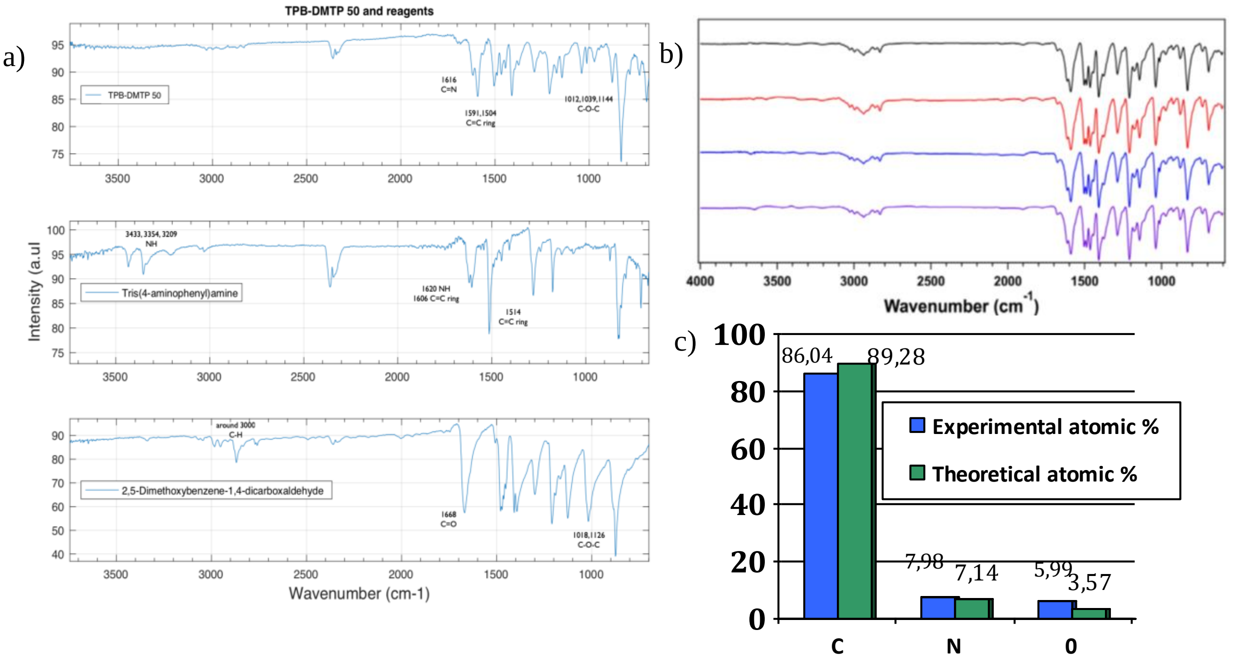

Figure 14

Experimental FT-IR spectra of TPB-DMTP 50 and reagents (a). Experimental FT-IR spectra of as-synthesized TPB-DMTP 100 from [29], black curve (b). Experimental and theoretical atomic percentages obtained by EDS elemental mapping (c)

In Figure 14 one can observe that the experimental vibrations (a) coincide quite well with those found by the authors of the paper (b) [29]. In particular, the vibrations produced by the amine (3433, 3354, 3209 cm-1) groups disappear from the product, while the aldehyde (1668 cm-1) group stretching band is replaced by vibration frequencies for -N=C bonds (1616 cm-1) and -C=C bonds (1591,1504 cm-1), whose bands change shape in the same fashion in both TPB-DMTP 50 and 100 (Sup. Info), due to the accomplishment of the reaction.

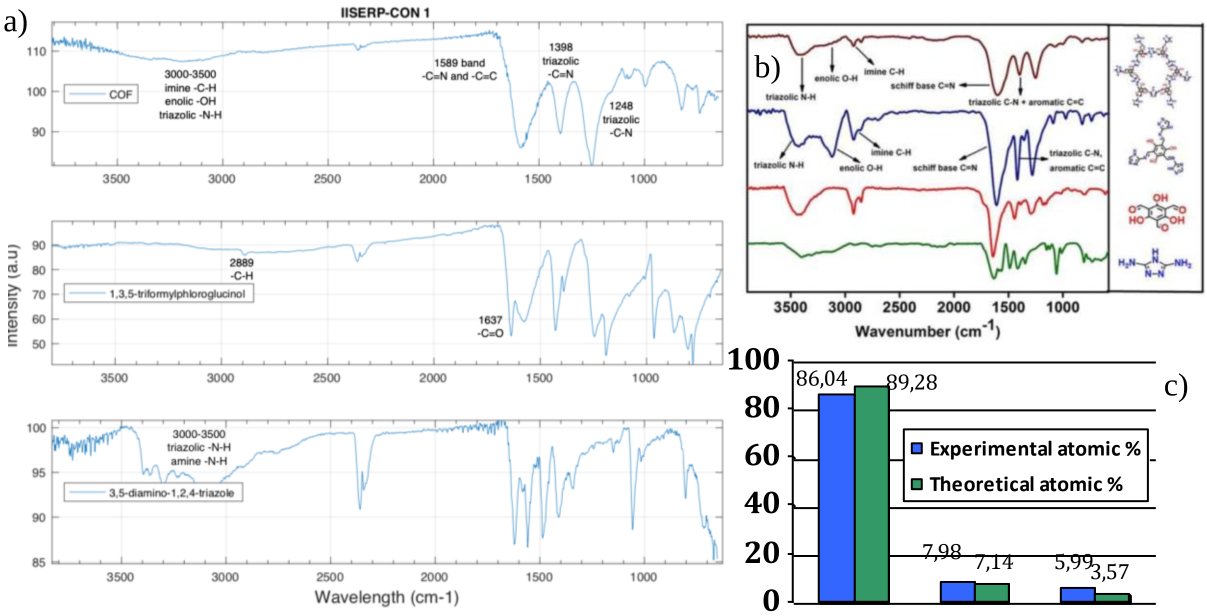

Figure 15:
Experimental FT-IR spectra of as-synthesized IISERP/CON1 from [48], bordeaux (b); experimental and theoretical atomic percentages obtained by EDS elemental mapping (c)

IISERP-CON1 vibrations are very close to those reported, Figure 15b as well: in particular, in Figure 15a, stand out the three main bands assigned to -C=N (1589 cm-1), - C=N (1398 cm-1) and -C-N (1248 cm-1) and amine vibrations that have disappeared, despite it is hard to distinguish selective transmission bands in the 3000-3500 cm-1 range.

The FT-IR spectra of the other COFs can be found in the Supplementary Information section and was analyzed according to the same criteria.

Due to band overlap it is hard to judge whether total conversion has taken place and, as observed, in [48] it is difficult to confirm just by FT-IR analysis whether one is looking at the designed network or to an incomplete version of it. In Figure 15b, the spectra of the COF and what called by the authors its monomer coincide, except for intensities, which don't give any information, and except for a few bands below 1000 cm-1, which could be due to some additional vibrations of the monomer but that are also very close to the instrument limit.
Additional information come from EDS analysis. The composition in atomic percentage, measured from collection of electrons from a large area, was compared to the theoretical atomic percentage esteemed by summing all the atoms in a unit cell, except for hydrogen atoms, which are not detected by the instrument. Figure 14c and 15c show for both COF that there are still some aldehyde groups unreacted, since the oxygen percentage is higher than that expected in a molecular unit. TPB-DMTP 17 (Sup.Info) and DhaTab 50 (Sup.Info) show both excess of nitrogen and oxygen, while TB-COF EDS spectra instead (Sup. Info) has detected few percentages of fluorine and sulphur coming from the reaction catalyst, a higher oxygen content and a lower boron content. Nevertheless, boron low levels could be attributed to the instrument low sensitivity, since nitrogen detection meets the theoretical amount and since they can't have been washed away separately during purification being part of the same building block, 4-cyanophenylboronic acid.

EDS results were not surprising given the reaction yields listed in Table 1 The TPB-DMTP series, IISERP-CON1 and TB COF synthesis all yielded around 50%. A low yield means that the expected moles of product were not obtained, and if some reagents have not reacted, it also means that the structure expected from the weighted ratio of starting compounds may not have formed. For COFs this implies that a product may not not have reached its ideal porosity distribution and maximum degree of crystallinity. In terms of performance, a large amount of amorphous phase and a smaller crystallite size decrease the adsorption capacity of the COF. This was true for most of the networks and will be explained in the next paragraphs.

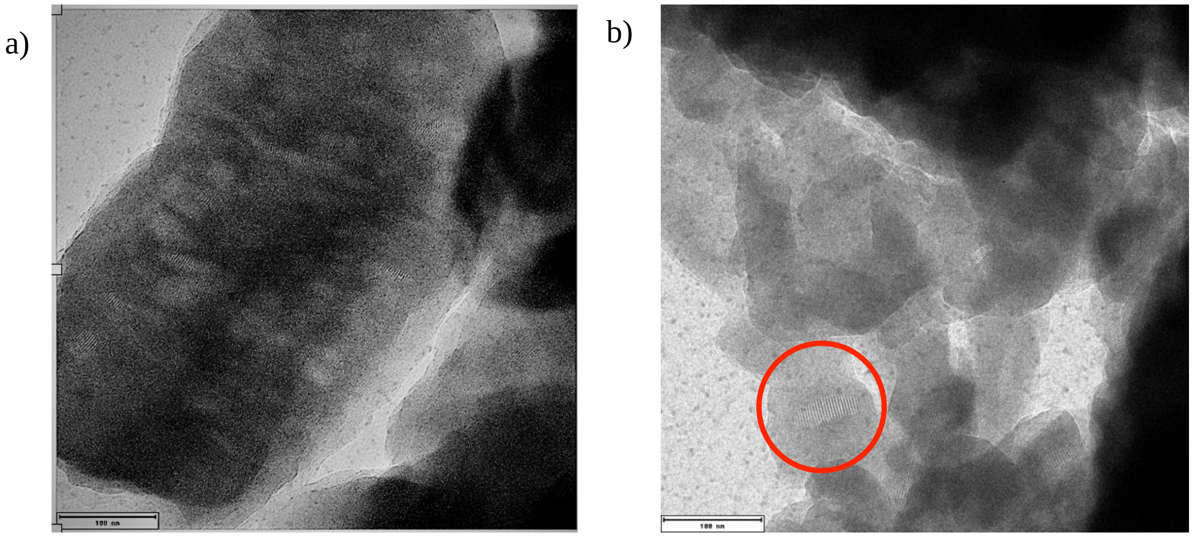

Figure 16:
TEM picture of DhaTab 100 showing many scattered crystalline areas, 60 nm long and few nm high (a); TEM picture of TPB-DMTP 17 where 50x10 nm crystalline area embedded in an amorphous globe is circled in red (b)

To get insight on how an incomplete reaction looked like at the atomic level, TEM pictures were taken. Figure 16a and 16b from DhaTab 100 and TPB-DMTP 17 show scattered crystallite areas whose shape and size are hard to identify since they seem embedded within an amorphous matrix. This fact agrees with what stated by [31] according to which a COF structure pass through an amorphous stage before reaching its crystalline form. This also tells that nucleation occurred but that growth was hindered. According to the classical nucleation theory, growth depends on both the rate of the reaction and the rate of diffusion of the molecules to the surface of the nuclei. These crystalline phases are very small, so it is safe to say that the reaction was reversible. On the other hand, the amorphous phase surrounding the crystalline phase makes one think that molecules couldn’t diffuse back and forward from and to the reaction site. Another possible occurrence is that layers belonging to the same crystal grew with different speeds, the diffusion of molecules towards the slowest layers was hindered, the π system did not form and so the phase remained amorphous.

By making the ratio among the area underneath the curve and the calculated background, it was found that, two imine COFs are predominantly crystalline, with a percentage of 95% and 97% respectively for TPB-DMTP 50 and 100, Table 5. The crystallinity is lost when the number of -OMe groups is reduced to 1/pore and 0/pore (Sup. Info). In literature the crystalline degree of TPB-TP is not reported [29], but it is supposed to be lower due to a poorer stability of the stacking. As far as TPB-DMTP 17 is concerned, instead, the poor crystallinity is due to the molar ratio of the two linkers: being only 1 OMe/pore, the formation of a π system becomes less probable and therefore the molecule can still rotate on its axis and assume a non planar configuration which destabilize the layering in the c direction [22]. However, COFs with 1.5 and 0.3 ratio of substituents have been synthesized, even when the functional group was very electron rich (azide N_3)[39]. Therefore I conclude that either the functional group is enough negatively charged to polarize the whole ring, and the energy balace has to include an ionic contribution, or the functional group is bulky or has bonds (double, triple backbone bonds) that can hinder the rotation [27]. In addition to this, the composition of TPB-DMTP 17 appears to be very inhomogeneous, since by elemental mapping the atomic percentage matches what i should be as long as a spot analysis is carried out. Different particle with a different ratios of N and O are found, which suggests the formation of different phases in the same material (Sup.Info).

On the basis of the trend observed for the TPB-DMTP group, DhaTab COFs were synthesized only in the 100 and 50 linkers ratios. The crystallinity degree was not as high as wanted, but in this case the poor dissolution of the reagents can be accounted for it.

IISERP-CON1 produced a diffraction pattern very similar to what found in literature, (Sup.Info), and the low crystallinity was a predictable fact, given the small size of the linkage molecule, that does not provide enough π electrons, and the out of plane conformation of the edge building blocks. From TEM it was not possible to make hypothesis on the growth mechanism of this COF because no crystalline region was observed.

TB-COF poor crystallinity can also be attributed to the little number of π electrons per unit cell, Nevertheless, it is difficult to make hyphothesis on the reason why this was the case, since the reaction chemistry is very different from the other COFs and in literature there are no examples in which boroxine and trizine rings are used together. What is known is that the two rings are usualtty obtained at very different temperature (120 ^{o}C and ≥ 400 ^{o}C) and diffusive medium (organic solvent – ZnCl salt) conditions. Moreover it was studied that according to temperature –CN groups can react together to form very different and unpredictable pore shapes and sizes [54].

Crystalline structure

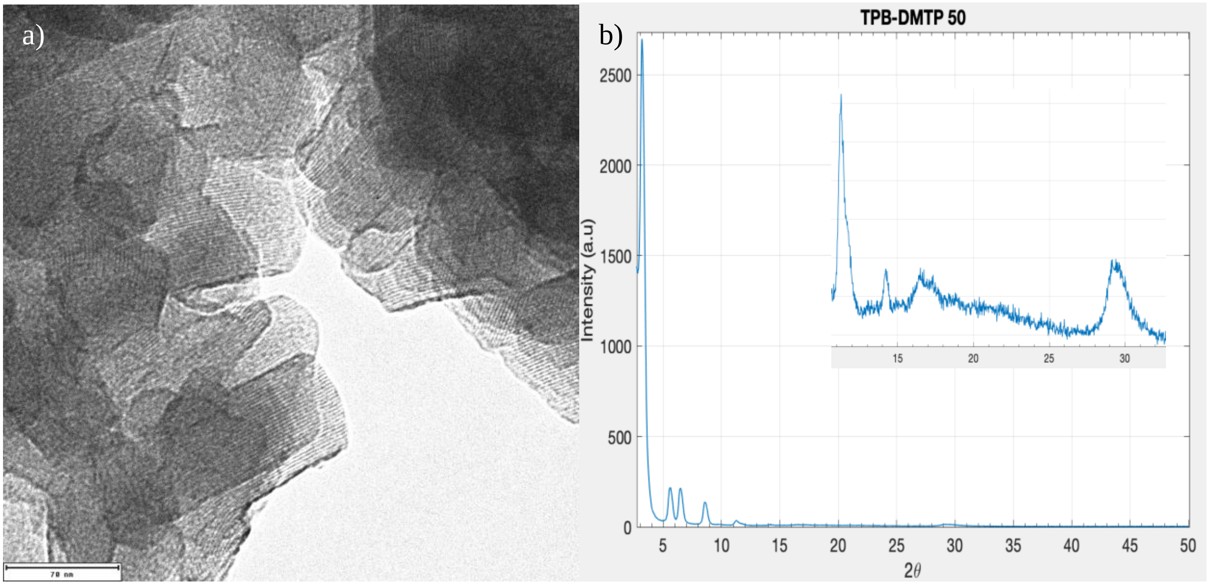

Figure 17: TEM picture of TPB-DMTP 50 (scale bar is set to 70 nm) (a). Diffraction pattern of the same COF showing 4 major peaks, of which the first most intense one is associated with 100 planes, and a series of minor peaks, of which the one at 2θ=30^{o} degrees is used to determine the interplanar distance in between two layers, c. (b).

According to literature, COFs of the TPB-DMTP and DhaTab groups display a pattern characterized by an intense reflection at very low 2θ and reflections towards larger angles progressively less intense, as shown in Figure 17b. It is hard to detect the reflection at low theta, due to the probe intensity entering the detector directly, unless it is very intense. Otherwise it is visible only after background subtraction. This repetitive trend reveals information over the preferred particle shape: since a larger intensity is produced by a larger density of planes reflecting and viceversa, one can expect that the crystallite shape will have a predominant dimension and that it is 2 dimensional. This is indeed confirmed by TEM imaging, Figure 17a, where are visible thin stacked rectangular platelets ≈ 70-80 nm wide and ≈ 100 nm long. Looking closer it is also possible to recognize the layering of the platelets, which confirms the 2D nature of the material.

As one can read from Table 3 and 4, peak positions were converted from cobalt to copper source with Bragg's law to compare them with the reported values of 2θ. As a second step, the hand calculation was performed according to [50] and the equation below, assuming the same reported Bravais lattice to get a first confirmation of the cell parameters and to assign a crystal family to each peak. As assumed in the papers, the a and b parameters were found from the lowest 2θ reflection, while c was found from the highest value, although there is some uncertanty in the identification of this last one since it could correspond to either 100 or 101 planes. Family of planes that have been reported differently appear in two colums of the table, some peaks instead could not be indexed due to the little number of reflections. This methode coud be applied only because I had reason to assume that I would have obtained the same crystalline lattice. At the same time it was easy to use as long as the crystal cell was not Monoclinic or Triclinic, which is the case of DhaTab 100. An hexagonal lattice was also assumed for this COF with reasonable agreement, Table 4. Lattice parameters found with this methode are listed in Table 5.

Table 3 TPB-DMTP 100

2θ Experimental (Cobalt)	2θ Experimental (Copper)	2θ Paper []*
3.2028	2.7582	2,76 (100)
5.5888	4.8127	4,82 (110)
6.4564	5.5596	5,6 (200)
8.5663	7.3757	7,42 (210)
11.2480	9.6830	9,7 (220)
29.2115	25.0858	25,2 (001)

Table 4: Dha Tab 100

2θ Experimental (Cobalt)	2θ Experimental (Copper)	2θ Paper []*
3.253	2.801	2.8 (100)
5.659	4.873	4,9 (110)
6.527	5.620	5,6 (200)
8.676	7.470	7,4 (210)
11.81	10.166	9,8 (220)
29,83 ?	25.613	26.3 (001)

Equation for hexagonal lattice:

$$\sin^2\theta = \frac{\lambda^2}{3a^2}*(h^2+hk+k^2)+\frac{\lambda^2}{4c^2}l^2$$

Pawley refinement was done on the most crystalline samples (TPB-DMTP 100, 50 and DhaTab 100). The smallest fit error was achieved when the crystal cell of both TPB/DMTPs was hexagonal and when DhaTab 100 was trigonal with edges of the same length.

Calculations of the atomic percentages, molecular weights and of the number of trapping sites relied on the molecular bases drawn in Figure 18. Each red line that breaks in half triazoles and aromatic rings is there to mark the edges and to determine the content of a unit cell. For example, in this way, each IISERP-CON1 cell there will contain 3 triazole rings. This model works for all TPB-DMTP and DhaTab COFs, just by substituting group varying the degree of occupancy according to the ratio of terephtalaldeyde and 2,5-Dimethoxybenzene-1,4-dicarboxaldehyde or terephtalaldeyde and 2,5-dihydroxybenzene-1,4-dicarbaldehyde, which changes the number of -OMe and –OH groups.

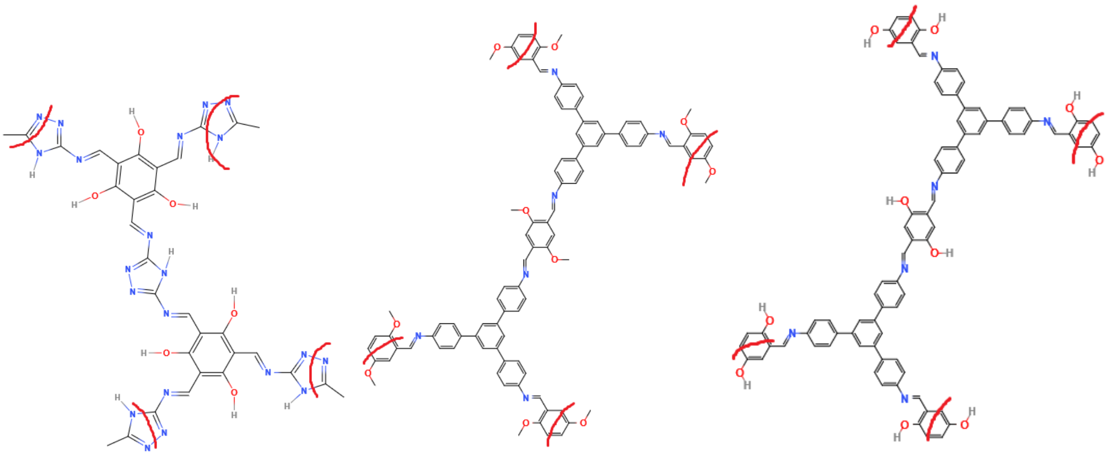

Figure 18: Molecular bases of of the unit cells of IISERP-CON1, TPB-DMTP 100 and DhaTab 100, from left to right.

Table 5: Nitrogen isotherm results for various COFs

COF name [paper]	**Molecular Weight (g/mol)**	**Crystallinity (%)**	**Hand calculation of lattice parameters (Å)***	**Pawley refinement (Å)**	**Paper (Å)**
IISERP-CON1 [48]	610	60-70	(100) reflection not found	NA	a = b = 19,78 c= 3.47-3.26
TB-COF [34]	393	≈ 54	a = b = 14.997 c = 3.9023 (3.479)	NA	a = b = 15.03 c = 3.48
TPB-DMTP 100 [29]	1177.34	≈ 97	a = b = 36.956 c = 3.546 (3.568)	Hexagonal a = b = 36.16454 c =3.60576	a =b = 37.2718 c = 3.5215
TPB-DMTP 50	1087.26	≈ 95	a = b = 37.417 c = 3.554 (3.575)	Orthorhombic a = 31.2409 b = 18.0297 c=6.5755 Hexagonal a= b= 36.46266 Å c= 3.6413	NA
TPB-DMTP 17	1027.81	≈ 37	NA	NA	NA
TPB-TP [29]	997.19	≈ 8	NA	NA	NA
DhaTab 100 [23]	1093	≈ 56	(Hexagonal) a = b = 31.336 c = 2.992(3.011)	Trigonal a=b= 36,2 c = 3.4	a =b = 36.2 c = 3.4
DhaTab 50	1045	≈ 47	NA	NA	NA

*The second value of c is obtained assuming the the largest 2θ reflection comes from the 101 family of planes

Recrystallization

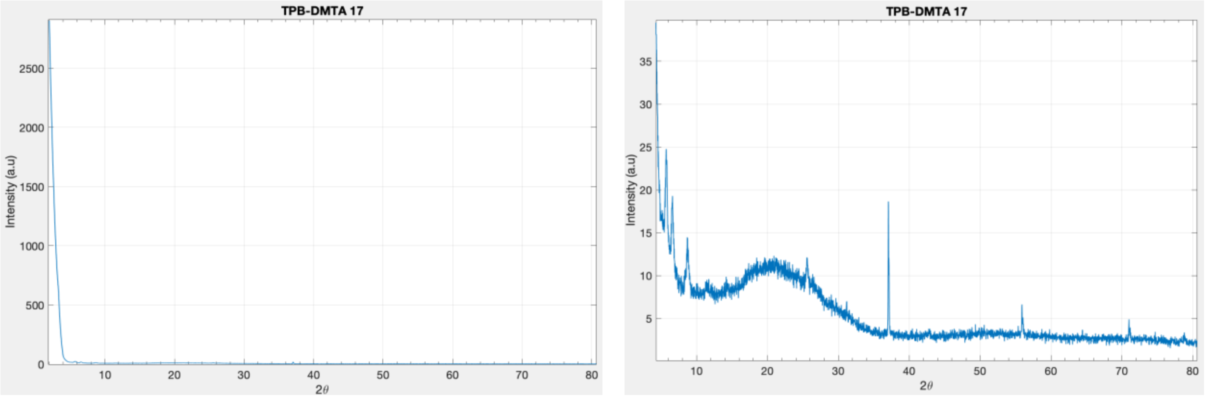

Figure 19 : XRD diffraction pattern of TPB-DMTP before and after recrystallization

In Figure 19, one can observe that despite the amorphous curve at intermediate 2θ (10°-30°) has not flattened, peaks that were already present are sharper and new ones have appeared. From FT-IR instead it appears that the vibration bands with respect to the as-synthesized COF have not been altered: therefore the material is still the same as the one at the beginning. However, SEM pictures show a clear presence of an unknown phase, which is probably NaCl, which wasn't washed away properly during the purification step and to that have to be assigned the peaks at $2\theta \geq 30°$. There is no evidence to say that a rearrangement have occurred.
The same conclusion can be drawn for IISERP-CON1. There is no change in the XRD pattern that can be connected to a rearrangement in the structure and an improved crystallinity.

Adsorption isotherms

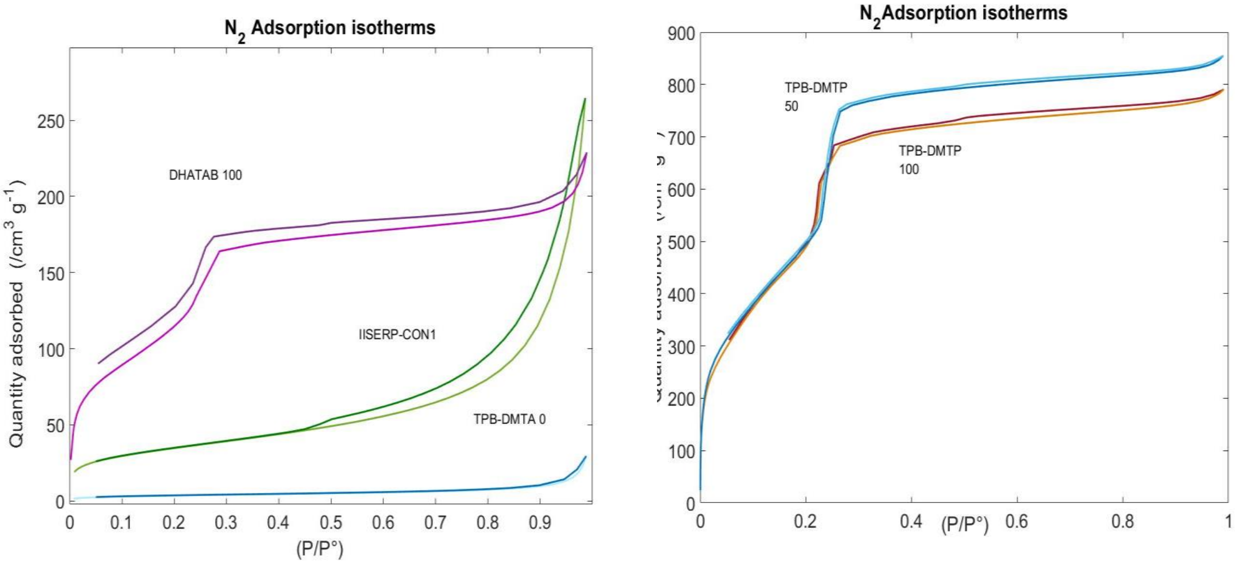

Figure 20: N_2 adsoprtion curves of some of the COFs. Shades of th same colour stand for adsorption (lighter) and desorption (darker) curves.

An achieved porous structure is what eventually determined whether a COF was suitable to be used in a battery or not. Porosity is what allows sulphur to be stored, therefore it determines the capacity, and facilitates lithium diffusion; if the structure is not porous, all reactions would take place at the surface in direct contact with the electrolyte, without any restriction to polysulfide shuttling. A large surface area instead should improve the kinetics of the process, since more adsorption sites are available for chemical reactions.

A first visual description of the shape of the isotherms can already tell a lot about the porous structure that is analyzed, Figure 20. According to the recently updated IUPAC classification [52], COFs from the TPB-DMTP and DhaTab group had a Type IV isotherm, typical of mesoporous materials, while IISERP-CON1 had a Type II. Both TPB-COF 17 and 0 adsorbed very litttle, therefore their calculations were limited to BET surface area, which was respectively 31.5 m^2 g^{-1} for the first one and 13.3 m^2 g^{-1} for the second one, in agreement with literature (16 m^2 g^{-1}) [29]. None of the TB-COFs batches adsorbed a significant amount of N_2 .

Type IV is characterized by a not very steep uptake at low pressures and saturation at high pressures, which means that the adsorbate is first forming multilayers and then is condensing. The fact that the second adsorption knee is at low-intermediate pressures and that the condensation plateau is quite long is characteristic of porous dimensions that are in between the micro and meso range.

COFs from the DhaTab group also display a hysteresis loop spanning a wide range of pressures, which resembles an H5 type. However, since the hysteresis spans from high to very low pressure, it is likely that during adsorption the COF had experienced some sort of expansion and the consequence of this is an overestimation of the fluid adsorbed during desorption. Indeed by looking at its data set its visible that equilibrium pressure for the first few points was reached after a very long time, a sign that the structure was enlarging and the gas was diffusing at the same time.

Type II is the fingerprint of macro-porous materials with an unconstrained adsorption. Unlike what literature suggests, the synthesized IISERP-CON1 misses the sharp knee at very low pressures which should be due to micropore filling. It also displays a hysteresis of type 3 which is usually due to adsorption of fluid in between layers of non-rigid aggregates.

Table 6: Nitrogen adsorption results for all COFs

COF	**BET (m^2 g^{-1}) and t-plot (cm^3 g^{-1})**	**BJH (cm^3 g^{-1})**	**NLDFT**
IISERP-CON1 []	125 (C = 115.79; n_m = 28.72 cm^3 g^{-1})	0.401 (ads) 0.407 (des)	54.592 m^2 g^{-1} 0.334 cm^3 g^{-1}
TPB-DMTP 100 []	1906 (C = 29.30; n_m = 438.0894 cm^3 g^{-1})	1.282 (ads) 1.258 (des)	1387.843 m^2 g^{-1} 1.155 cm^3 g^{-1} 3.167 nm
TPB-DMTP 50	1952 (C = 27.63; n_m 448.49 cm^3 g^{-1})	1.486 (ads) 1.460 (des)	1470.410 m^2 g^{-1} 1.250 cm^3 g^{-1} 3.239 nm
DhaTab 100 []	437 (C= 34.43; $n_{m=}$ 100.39 cm^3 g^{-1})	0.370 (ads) 0.352 (des)	331.001 m^2 g^{-1} 0.262 cm^3 g^{-1} 3.31 nm
DhaTab 50	466 (C=56.02; $n_{m=}$ 107.15 cm^3 g^{-1})	0.359 (ads) 0.332 (des)	351.013 m^2 g^{-1} 0.22340 cm^3 g^{-1} 3.167 nm

The application of the BET method for most samples was always far from being trivial and a bit improper, specifically for those COFs whose condensation was shifted towards lower pressures. Despite BET surface area is always presented as a standard attribute in the characterization of COF, these measurements brought me to think that its accuracy should be evaluated case by case. BET is determined by plotting the isotherm data according to following equation:

$$\frac{\frac{p}{p^0}}{n(1-\frac{p}{p^0})} = \frac{1}{n_m C} + \frac{C-1}{n_m C}\frac{p}{p^0}$$

n = specific adsorbed amount, p/p° = relative pressure
and interpolating the data in a linear interval to obtain n_m, the specific monolayer capacity, and C, a parameter related to the shape of the isotherm at low relative pressures. To be applicable, C should be at least larger than 50, otherwise the evaluation of n_m is questionable, because it’s not possible to identify a monolayer unit due to multilayering at low pressures. As a consequence, also the micropore volume calculation by the t-plot method, may be inaccurate, since it relies on BET.

What is never mentioned in papers is the possibility to use density functional theory to simulate the adsorbent/adsorbate system and obtain values for micropore volume, pore distribution and surface area, that is potentially more reliable, as long as the chosen model is as close as possible to reality.

The available software models were Carbon Slit, Single wall carbon nanotubes and Cylindrical oxide pores. It’s reported that all three models have been used to simulate MOFs or COFs [55], therefore here the model chosen to simulate the pore size distribution will be the one whose sizes matched better with crystallographic results. For all cells it was assumed to have a rhombic 2D unit cell with a = b and internal angles equal to 60° and 120° degrees and eventually the a size found with the refinement is also the pore diameter.

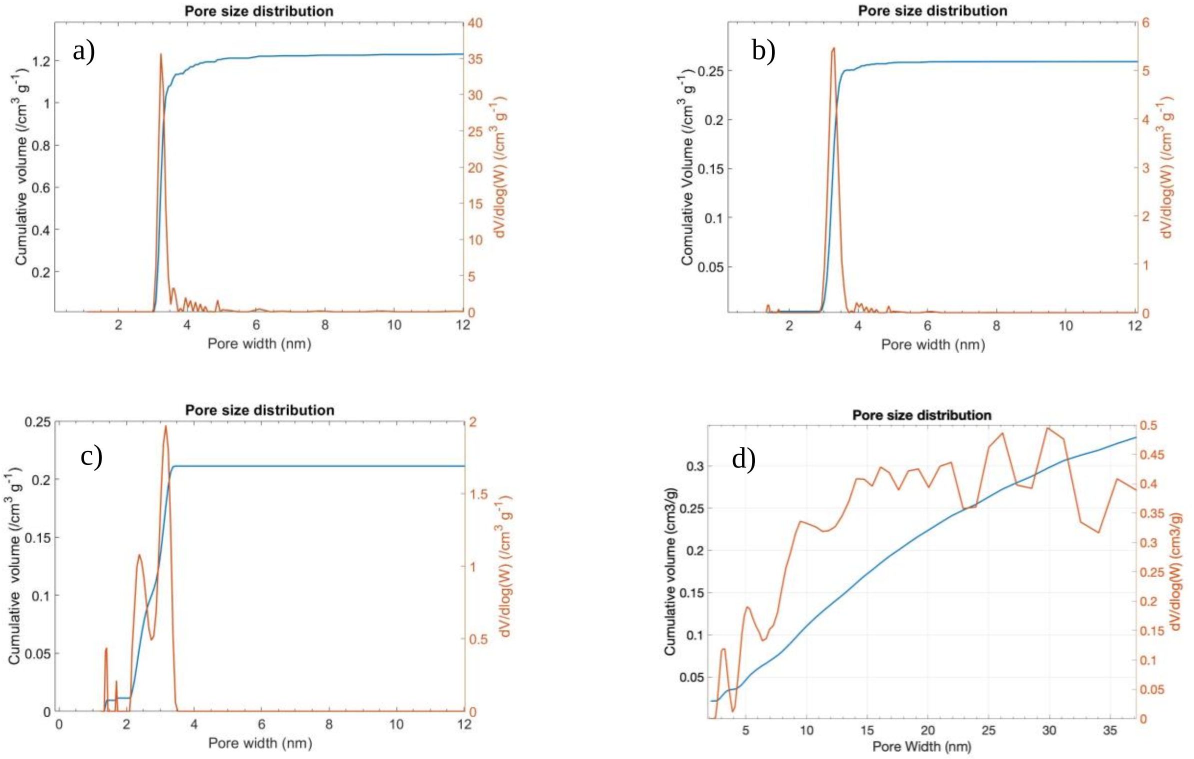

Figure 21: Pore size distributions of TPB-DMTP 50, d = 3.239 nm (a), DhaTab 100, d = 3.31 nm (b), DhaTab 50 and IISERP-CON1 (d).

COFs from the TPB-DMTP group and the DhaTab had in general a narrower pore size distribution and a larger surface area. In particular TPB-DMTPs values for the BET surface area are close to match those reported (2105 vs 1906.81 m^{2}g^{-1}, d = 3.167 nm vs 3.26, v = 1.15 vs 1.28 cm^3 g^{-1} for TPB-DMTO 100) while DhaTab synthesis was not as successful. Figure 21b, as already foreseen by XRD patterns, since DhaTab 100 adsorbed 3 times less that what predicted (437 vs 1480 m^{2}g^{-1}, d = 3.31 vs 3.7 nm). Almost complete pore condensation takes place for a very precise pore size, in fact there are only few small peaks at larger diameters, except for DhaTab 50, Figure 21c, which shows smaller pores at 2.381 nm, 1.702 nm and 1.416 nm and IISERP-CON1 which failed to have an organized porous structure. According to literature it should display two peaks corresponding to 1.3 and 1.7 nm pore size [48]. For each COF can be calculated the maximum amount of sulphur that could be adsorbed, based on an average of bulk sulphur density (2 63 g cm^{-3}) and on Li_2S density (1.63 g cm^{-3}), as well as the surface density of trapping sites, based on BET and NLDFT values.

Impregnation

To understand how sulphur connects to the structure at the beginning and end of discharge, TPB-DMTP 50 and IISERP-CON1 were impregnated with both sulphur and Li_2S.

As predicted by its adsorption measurement, the first COF absorbed the solution quickly and it was necessary to add more drops to distribute Li_2S homogeneously, so eventually 1 ml volume was added. For the future it should be reminded to add only ethanol. However, there were no visible traces of Li_2S that was not absorbed after ethanol had evaporated. The second COF instead, being it's surface area 4 times smaller than reported, had less open pores, thus less available trapping sites: some white traces of Li_2S were present on the surface after drying, therefore the procedure was repeated by adding COF powder and ethanol, heated at 100°C to help solubilization, mixed, ground with a metal spatula, let rest and dried again.

Eventually TPB-DMTP 50 COFs contained more Li_2S than required by its number of trapping sites, while IISERP-CON1 contained as much Li_2S as if only half of its trapping sites had been accessible

To achieve these results, it was calculated that in 40 mg of starting compound (for example IISERP-CON1), there are 65.57 umol. Every mole unit contained 10 possible trapping sites for Li, 655.73 umol. Since the solution has a concentration of 0.55 M, the COF has to be impregnated with 1.19 ml of solution.

Identify COF-S/Li_2S bonds

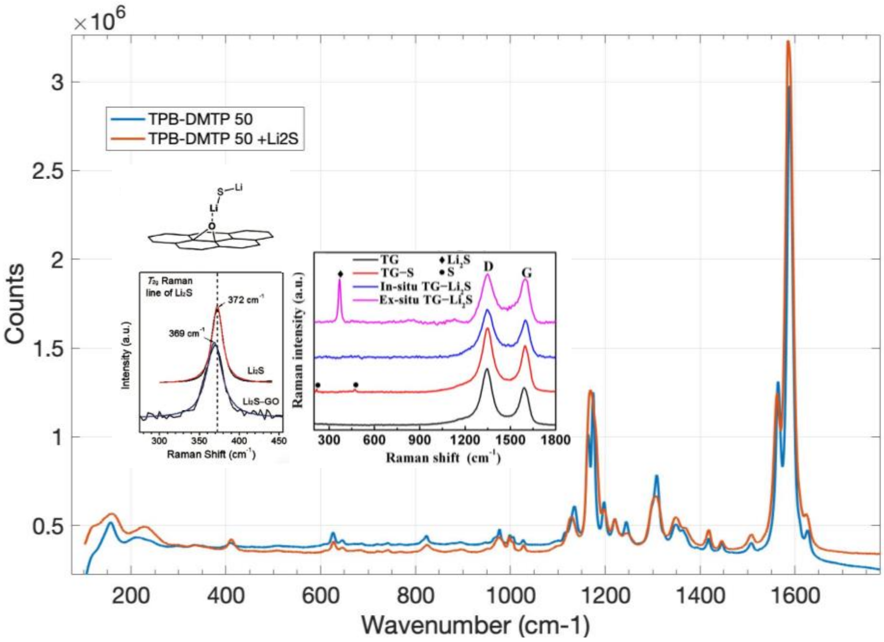

Figure 22

Experimental Raman spectra of TPB-DMTP/Li_2S composite. Inserted picture: Raman spectra of pure Li_2S and Li_2S adsorbed on graphed oxide (GO) [56] or on thermally exfoliated graphed (TG) [57]

All COFs-S/Li_2S compounds were studied with Raman spectroscopy in the attempt to observe how Li_2S and sulphur are binding to the structure. All IISERP-CON1 samples produced a too high photoluminescence background to be analyzed with this technique at the available wavelengths, while among the TPB-DMTP group, both COFs could be studied with Raman in the as-synthesized form and in the presence of Li_2S. The composites that contained sulphur were highly photo-luminescent.

In the Raman spectra of TPB-DMTP 50, Figure 22, can be identified the peaks related to the aromatic rings vibrations, the so called G band at 1589 cm^{-1} and the D-band at 1309 cm^{-1}, as well as the vibration due to -C=N bonds at 1627 cm^{-1} and the asymmetric vibration due to the ether groups at 822.3 cm^{-1}.

The spectra of TPB-DMTP 50 with Li_2S totally resemble the previous one, except for some peculiar frequency shifts that could be attributed to the presence of Li_2S. These are the -C=N shift to 1624 cm-1 and the -C-O-C shift to 824.6 cm-1, together with shifts in the low frequency region, which could be as well related to the -S-Li-O. However, it has to be pointed out that there is not trace of the finger print of -Li-S-Li bonds in the spectra, which should be found at around 369 cm^{-1}[56] . Because of all the shifts that distinguish one material to another, Li_2S is connected to the structure, but its vibration is somehow obscured. It can’t be excluded that some vibration shifts are also due to the interaction among sulphur and carbon, such as those involving peaks that can be attribute to -C=C bonds in aromatic rings (G-band, D-band, -C=C at1564 cm^{-1}).

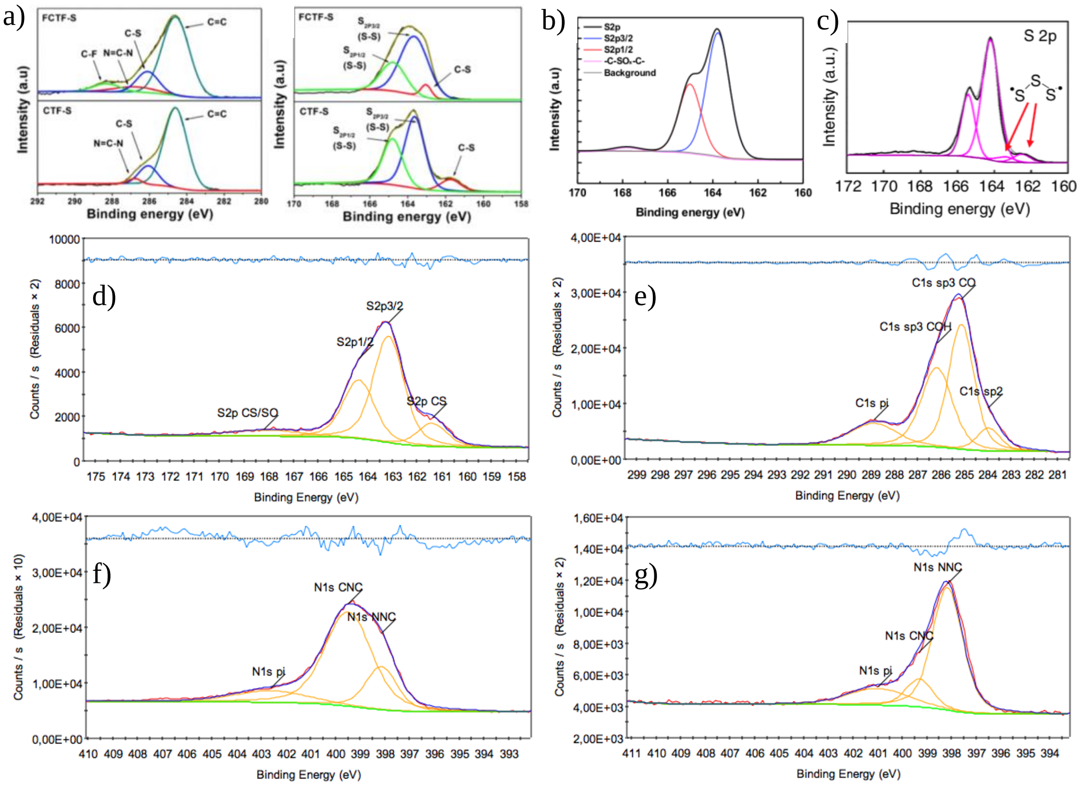

Figure 23:
C1s and S2p Raman spectra of FCTF COF [44] (a), S2p spectra of S-CTF-1 [42] (b) and S2p spectra of CMK-3/S@PAN [58](c). Experimental XPS spectra of S2p of TPB-DMTP 50/S composite (d), C1s spectra of IISERP-CON1/Li2S (e), N1s spectra of prison IISERP-CON1 (f) and IISERP-CON1/Li2S composite (g). See Supplementary Information for the complete tables of spectra.

Once Raman results proved unsatisfactory, the same samples were analyzed by XPS.
All carbon peaks for the three samples in the pure form are characterized by a similar fitting, which includes an sp^2 peak at 284 eV, two sp^3 peaks at slightly higher energies for -C-O and -C=N bonds and a broader not very intense peak at around 290 eV which was attributed to the COFs π system. This analysis is supported by the fact that indeed the sp^3 peak is slightly more pronounced for TPB-DMTP 100 than TPB-DMTP 50, because of the larger number of -OMe groups, the intensity of sp2 and sp3 is reversed in IISERP-CON1 because carbon is hybridized sp3 more than it is sp^2. However, the π band is equally intense for all COFs, despite i would have expected it to be stronger for the TPB-DMTP group.
When sulphur is added, it is very hard to detect a -C-S bond because its binding energy (BE) is very close to that of the -C-O and -C=N. This is also evident from other XPS tests performed on triazine COFs [42, 44]. When Li_2S is added, the sp^3 peak in IISERP-CON1 shifts slightly to lower energies and becomes less intense. I think that this is possible only if the electron density near the triazole rings has rearranged due to lithium adsorption.

S2p regions are characterized by the two typical sulphur peaks at 163 eV ($sp^{3/2}$) and 164.5 eV ($sp^{1/2}$). Towards higher binding energies can be found a broad low peak that is attributed to -S-O (≈169 eV) interactions while the shoulder at lower BE (≈ 161 eV) is linked to -C-S interactions, in agreement with results from [18]. In [42] the 169 eV band is assigned to -C-SO_x-C- but here sulphur and carbon are covalently bonded in the pristine COF.
When Li_2S is in the structure, all curves are shifted towards lower BE. The two main sulphur peaks are found at 160.5 eV and 162 eV, the shoulder at low BE (159 eV) could be due to Li, as observed in [58], while the now more intense band at high BE shifted to 165 eV could be either due to -C-S interactions or -S-O. The first should be more plausible, but the COF is very crowded by heteroatoms

and i don’t see how S could make so many bonds with C. On the hand, Li_2S decomposition in air, is know to form sulfuric acid and lithium oxides, not sulphates, unlike what is suggested by [18] for pristine Li_2S.

Nitrogen peaks in the presence of sulphur don’t shift, unlike observed by [34, 47], but their intensities rearrange. The same can be concluded for oxygen in both TPB-DMTP samples. In IISERP-CON1 instead lithium is for sure interacting with the imine groups because the N1s peak shifts of 1 eV towards lower energies. The same shift is found for the oxygen peaks at the lower BE peak assigned to -C-O-H in the pristine sample.

It can be concluded that, despite S2p spectra may suggest that there is a connection in between TPB-DMTP COFs and sulphur after impregnation, the polarization seems to be weak, since signs of this interaction are missing from both C1s, N1s and O1s. Bonds in between carbon structures and sulfur straight after impregnation had already been observed in other studies [18].
In IISERP-COF1 it is clear that there is interaction in between lithium, nitrogen and oxygen. However, it can’t be concluded as easily that also sulphur is attached to the positively polarized carbons. In addition it can’t be excluded that some Li_2S has decomposed into lithium oxide, since lithium band can be fitted quite precisely by one peak which is shifted towards lower energies when compared with other lithium sulfides XPS spectra [34, 42].

TPB-DMTP batteries

Cyclic voltammetry

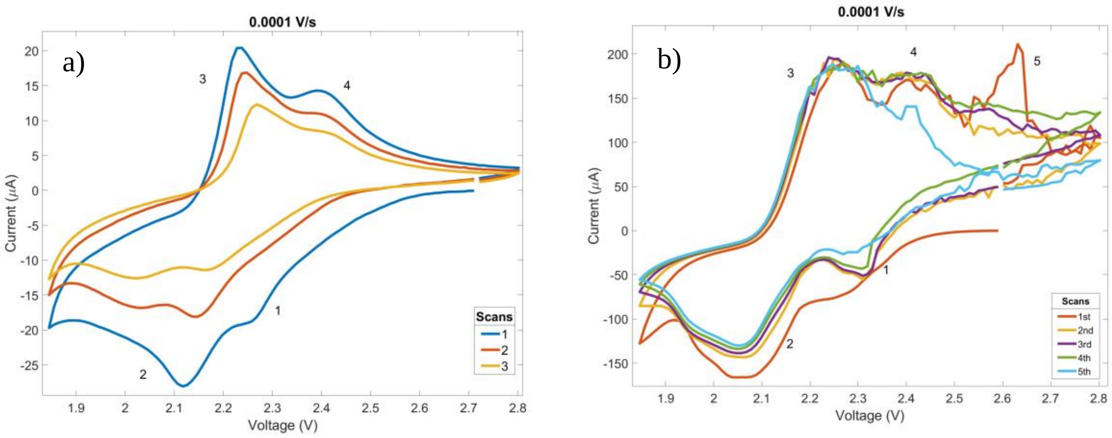

Figure 24: TPB-DMTP 100 composite (a) and TPB-DMTP 50 composite (b) cyclic voltammetry curves. Both batteries display the two sulphur reduction peaks, at around 2.1 and 2.3 V, and the two oxidation peaks, at 2.2 and 2.4 V.

Although the cathode materials are very similar from a molecular point of view, the two batteries show distinctive behaviors. B2 displays only the four peaks that are indication of the reaction of sulphur with lithium, Figure 24. Currents are not very high and their intensity decreases scan after scan, while peak positions shift, in particular on the reduction side, which means that polarization doubles from an initial value of 111 mV to 242 mV, which is more in line with what found in literature [42, 44, 46]. B3 scans are instead unstable towards higher voltages. These spikes could be produced by local charge accumulations that increase the resistance to the current flow. Once the charge has redistributed, the reaction takes place again. In addition, the first scan shows an irreversible peak at the end of oxidation, which could be due to a rearrangement of sulphur in the structure [48] or be a sign that lithium sulfides have not reacted back to S_8.

Nevertheless, despite these irregularities, B3 stabilizes earlier, since polarization seems to level at 202 mV during the four following scans, and can deliver a larger capacity, since currents are 10 times higher than in B2. It seems that TPB-DMTP 50 provides a better electric contact since reactions are more reversible.

However, the presence of wide peaks in both systems points out that the cathodes structures are far from being homogeneous and that different particles oxidize and reduce in different moments, because they have a different size and different composition.

Voltage-capacity curves

B2* and B3* cycling performance, despite the low imposed currents, confirms that the two COFs behave indeed very differently, Figure 25 Characteristic sulphur peaks at 2.4V and 2.2V are visible in both cells. This means that, at least during the first cycle, electrical contact in the composite is actually achieved.

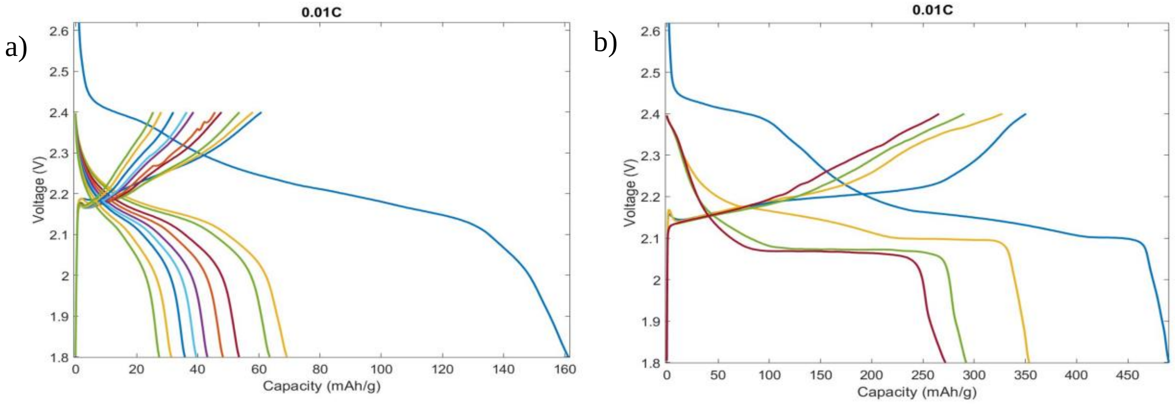

Figure 25: TPB-DMTP 100 (a) and TPB-DMTP 50 (b) tested in a sulphur battery. The voltage window was cut too early and as a consequence, after the first cycle, the first discharge plateau and the equivalent charge plateau at 2.4V are not visible. Some of the charge fading can be therefore be attributed to this inaccuracy. Cycle life of B2 (c).

However, capacity fades with time quite quickly, B2* in particular loses 42.88% of its initial capacity after the first cycle only, internal resistance increases sharply and lithium-sulfur plateaus disappear. B3* capacity fading is milder, being 6.7 % per cycle. The voltage was cut off too soon therefore the capacity associated with the last charge plateau is not recovered. A substantial fraction of the capacity lost in B3 must be accounted to that.

In the attempt to isolate the contributions to the internal resistance that are due to the COF and those that are due to electronic conductivity and lithium conductivity in the electrolyte, both batteries were cycled according to the program pictured in Figure 26.

In between every discharge and charge step at constant current (CC) were introduced two intervals at constant voltage (CV) and a rest step. The CV duration was set for as long as the current didn't reach values 5/10 times smaller the initial one. The rest step duration was set instead to 30 mins.

From the voltage curves one understands that despite both batteries are given the time to completely discharge and charge, during the rest step their voltages increase or decrease towards a new equilibrium value.

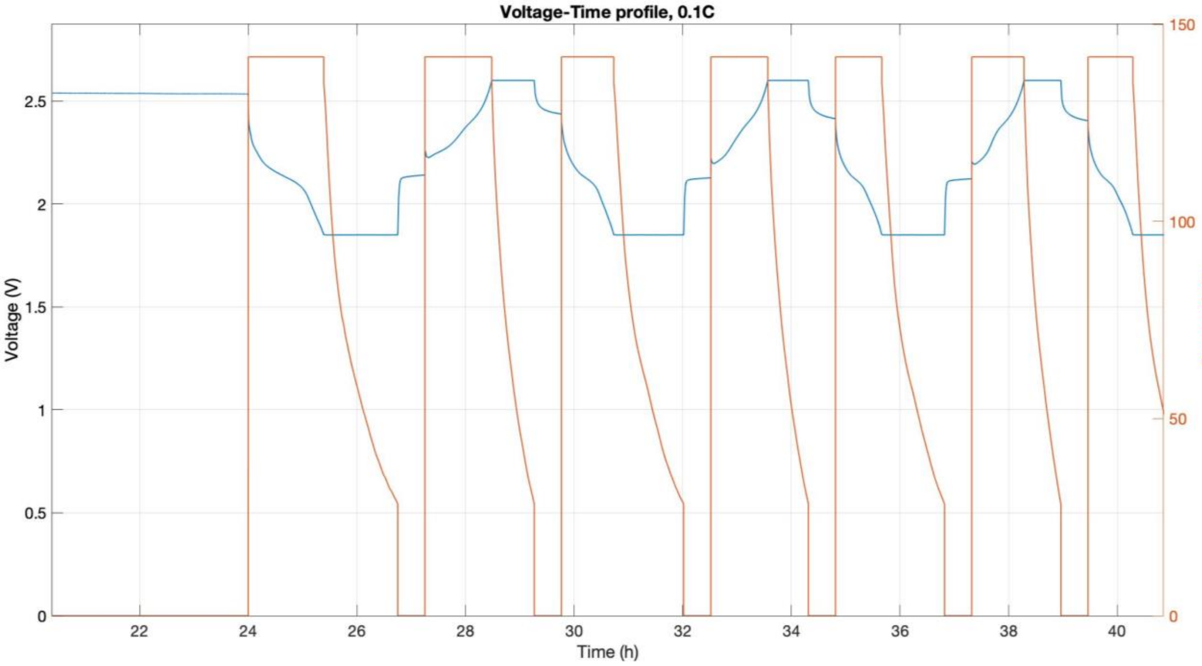

Figure 26: Current control and Voltage control program (CCCV). Each battery was discharged and charged to a cut of potential at constant current. Then the voltage was kept at that level as long as the current didn't fall to a value ten times smaller. After that, the battery could rest for 30 min without any current or voltage applied

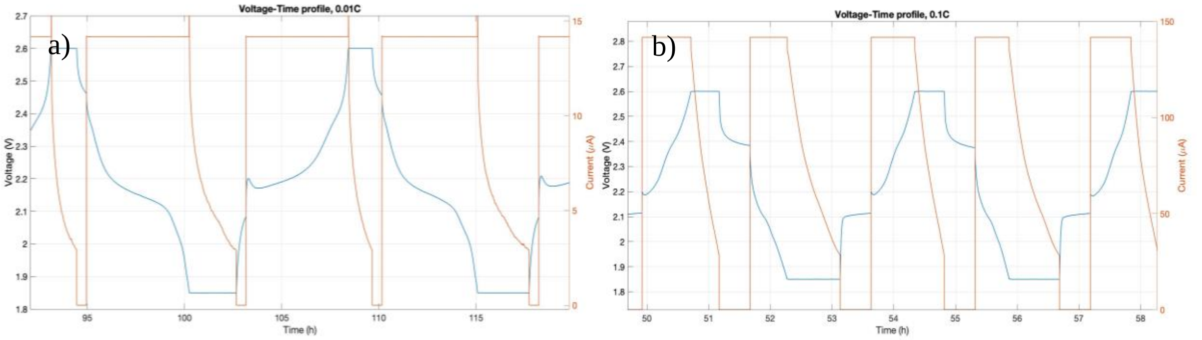

Figure 27: Details of the voltage-time curves of B2 (a) and B3 (b) showing the relaxation steps. In both batteries the voltage tends to stabilize due to relaxation of lithium or reactions in between polysulfide species.

This means that when the current at the end is very small, because the resistance is high, the system is at an unstable state and therefore once lithium is not forced in the cathode anymore, the structure and chemical species within the cathode particle can rearrange and relax towards equilibrium. It is possible that lithium was not able to react with all the sulphur contained within the pores and that it now can diffuse through them and react with the most internal reserve of sulphur. By the end of relaxation a predominant form of short chain polysulfide is probably reached, whose formation is expected at that voltage. It is curious to see how their relaxation behavior also differs, Figure 27: B2 voltage increases slowly and smoothly and hasn't reached a plateau yet, while B3 reaches an equilibrium voltage within few seconds, which means that reversible reactions in between polysulfides take place more rapidly.

This behavior could have been predicted also by looking at the cyclic voltammetry plots, since the current is 0 not at the beginning or end of the voltage ramp, but at intermediate values. This intermediate voltage range is where the battery is most stable.

The two batteries behave similarly when looking at their voltage profile, but again from the cycle plot it appears that they deliver a very different capacity, Figure 28. This test actually gave a more optimistic result for B2, since the capacity fading was reduced to 4.1 % per cycle, from the previous 8.4%, despite the same current was running, which means that something must have gone wrong previously in the manufacturing of that battery. Moreover the capacity fade is slightly reduced in B2 with respect to B3 at the same rate. Despite that, the capacity is still twice as small (129 vs 353.7 mAh g^{-1}).

The fact that the voltage is constant for some time helps the battery extracting 30-50% of the total capacity of each ramp that would be otherwise wasted due to kinetic losses, this is predominant in B4 because it is cycled at an higher current.

It was difficult to find the reason for such a disparity in the capacity in the material chemistry and structure, since both COFs were close to be optimally synthesized and they had a very similar pore size and surface area. Also, the two batteries were made in the exact same way: they contained the same amount of sulphur (quite low) and were wet with the same amount of electrolyte. It is know from literature that this factors could contribute to return unfair performance comparisons [59].

The truth was discovered when both samples were studied under the SEM microscope to check for sulphur homogeneous distribution with EDS and the difference was compelling.

Figure 29 shows that the morphology of the COF and the COF with sulphur are very similar in TPB-DMTP 50 (b): we still see the same globular shapes that are visible in the as-synthesized sample (Sup.Info) and that are reported in literature [29]. In TPB-DMTP 100 these globular units are still visible, even if some seem to have agglomerated in larger particles, but next to them are some long needle shaped particles that were completely absent before. There is reason to think that those sticks are sulphur that has solidified out of the pores and EDS performed on two different spots in the same sample indeed confirms that the chemical composition of the material is not homogeneous anymore and that sulphur concentration is higher in Particle 2 than in Particle 1. The mapping on TPB-DMTP 50 instead shows a well distributed sulphur.

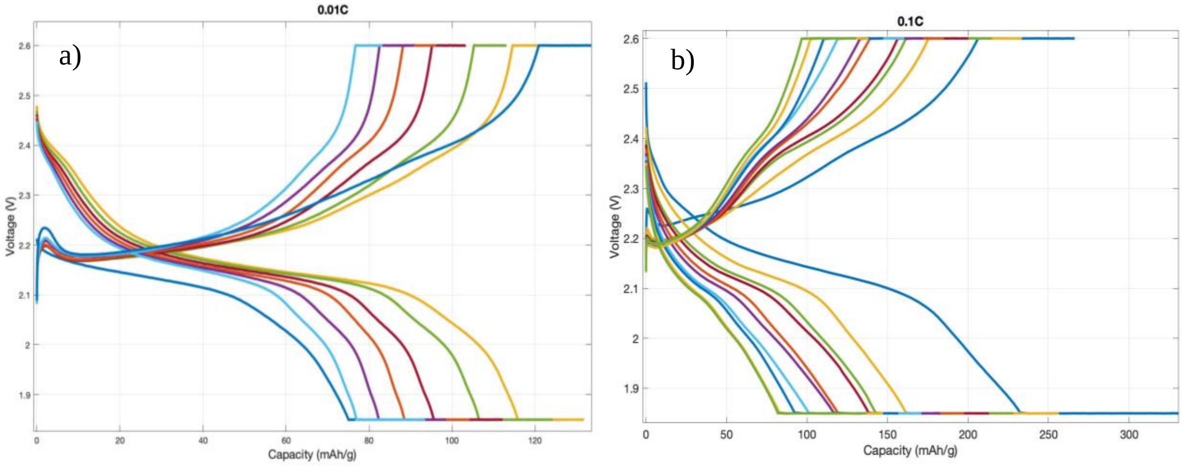

Figure 28: B2 voltage-capacity curves (a) and the same plot for B3 (b). Discharge and charge curves from the same cycle are in the same color. Both batteries have been tested according to the program depicted in Figure#. B2 rate was kept at 0.01C, while B3 rate was increased to 0.1C, since cyclic voltammetry confirmed that the battery could be run at higher currents.

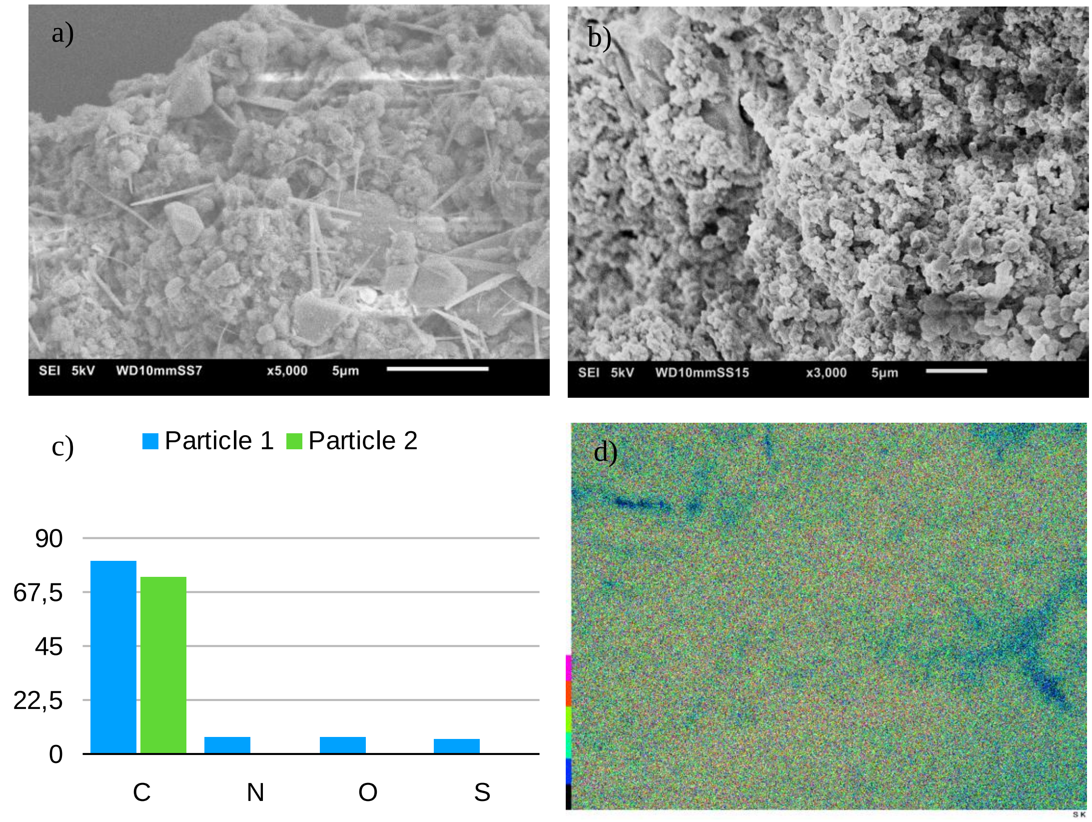

Figure 29: SEM image of TPB-DMTP 100 (a) and 50 (b) impregnated with sulphur. The COF morphology seems to have changed drastically and needle like sulphur particles are observed on the surface . EDS analysis chart that confirms the presence of sulphur (c). EDS elemental mapping of TPB-DMTP 50 after impregnation (d). Sulphur distribution looks homogeneous.

IISERP-CON1 batteries

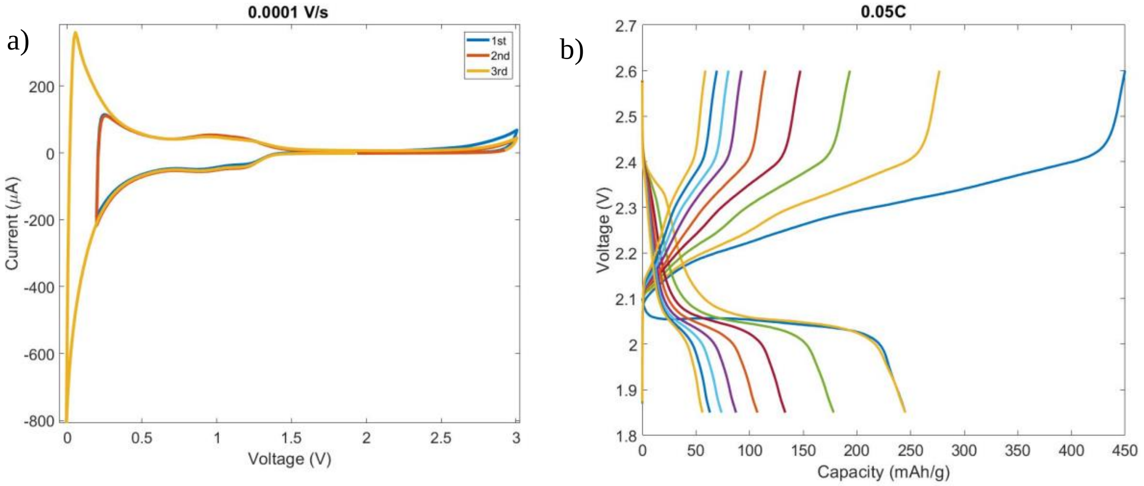

Figure 30: Cyclic voltammetry of B5 against lithium (a); voltage-capacity profile of B6 (b). Discharge and charge curves from the same cycle are in the same color. The first discharge curve should be shifted towards higher capacities, since the battery self-discharged during the initial rest step.

The IISERP-CON1 batteries were studied because of their large density of trapping sites and with the scope to evaluate the effects of a different distribution of charge within the structure on polysulfides trapping. In addition, since this COF was studied as an anode material against lithium, the intent was also that to clarify if a COF can be adequate to be both a cathode and an anode material.

As reported in [48] and pictured in Figure 30a, when the COF alone is tested against pure lithium, the battery displays three oxidation peaks and two reduction peaks at voltages below 1.5V. This fact is important because it means that lithium ions are not going to bind directly to the surface sites on the pore walls, instead of reacting with sulphur, as long as voltages are above that threshold. I think that this should be a test to perform at the very beginning whenever a COF battery is tested, to check for the presence of competitive reactions.

As expected, B6 voltage curve, Figure 30b, displays the sulphur plateaus at 2.3 and 2 V during discharge and 2.2 and 2.4 V during charge. Much can't be said about the capacity, since the battery almost completely self-discharged during the 24h rest step at the beginning of the test. Therefore capacity at the end of the first discharge curve should be at least double. Capacity at the end of charge is always larger and the coulombic efficiency as calculated is more that 100%. This is probably due to the self-discharge which produces a second current within the battery that discharges it twice as fast. Capacity fades very quickly and also polarization increases sharply ≈ 200 to 290 mV from the first to last cycle.

It is likely that capacity fade in this case depends strongly on deposition of Li_2S on the COF pore walls, since it's missing the typical overvoltage bump at the beginning of charge ramp that stands for a sudden increase and decrease of resistance within the material, probably due to Li_2S decomposition, which is instead clearly visible in B2 and B3.

The battery was aslo cycled according to the program explained above, Figure 31, and self-discharged slightly again, nevertheless, electrical contact must have improved because B6 could deliver close to 1000 mAh g^{-1} after the first discharge. Next to that, sulphur plateaus are plesently well visible and are still there even when discharge capacity falls to half of the initial one. It is interesting to notice that the second discharge plateau seems to settle at the same voltage (2.1 V) for the whole cycling, while the main contribution to polarization is given by the first discharge plateau, that drops of more or less 100 mV.

The fact that high capacities are achieved is a sign that sulphur particles are in contact with the COF pore walls, the capacity losses which cannot be recovered by keeping the voltage constant must be due to polysulfide shuttling.

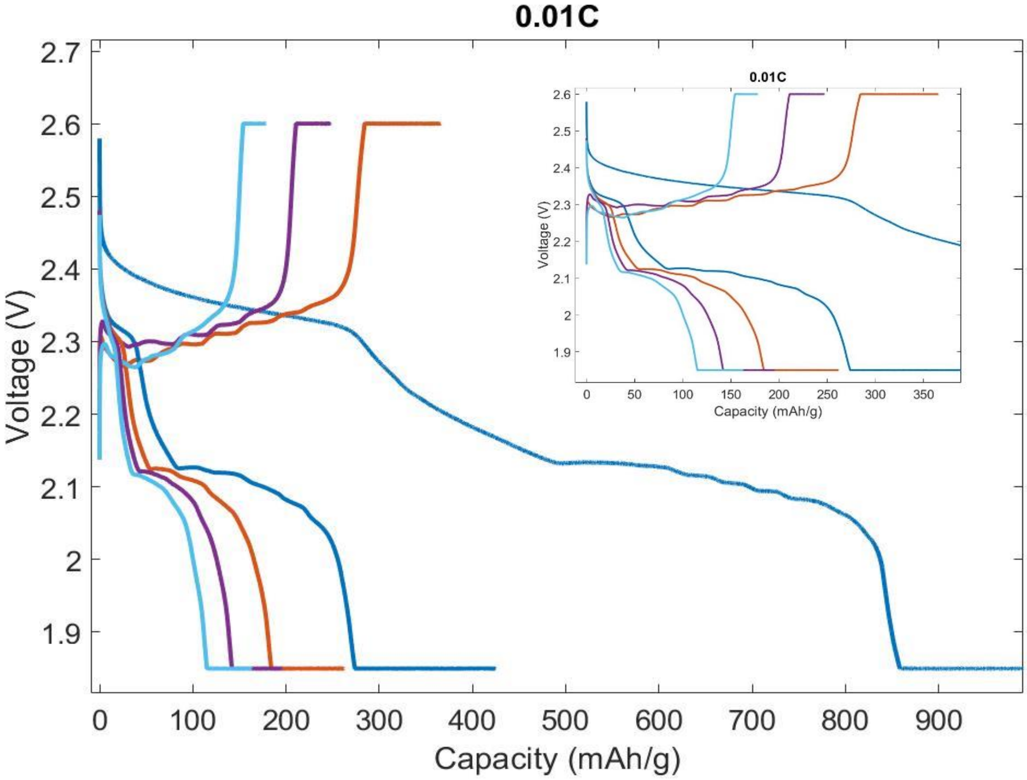

Figure 31: Discharge and charge curves of IISERP-CON1 (B6) when cycled accoarding to the Costant Current and Costant Voltage program (CCCV). B6 delivers a capacity of 991 mAh g^{-1} at 0.01C. The little CV inteval suggests that most of the sulphur in contact with the pores is successfully turned into Li$_2$S.

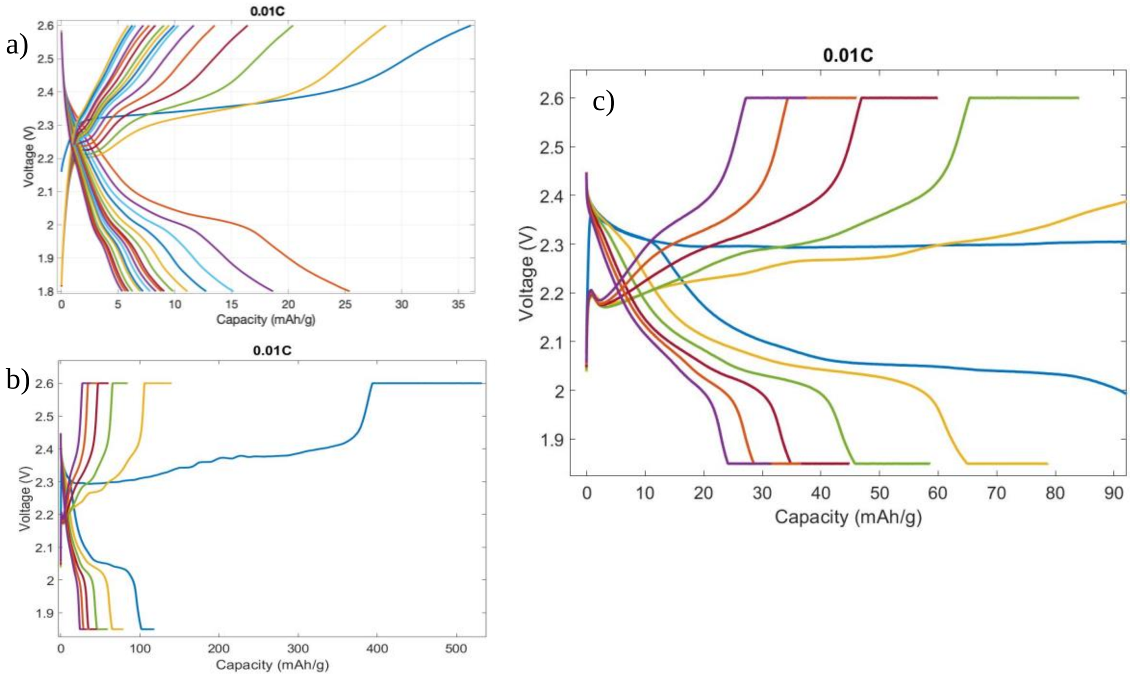

Figure 32: B4* (a), B4 (b) and detail of B4 curves (c) at low voltages showing the overvoltage at the start of charge, the progressive disappearance of the first discharge plateau, while the second discharge plateau moves from 2.1 V to 1.95 V.

Li_2S Batteries

TPB-DMTA 50 Li_2S battery (B4*) was characterized by high resistances since the first charge and could not be cycled for more than few cycles, even at low currents, as it can be observed in Figure 32a. Since one sulphur plateau is visible both in charge and discharge, probably some Li_2S in contact with the pore surface has reacted, but then dissolution into short chain polysulfides separated Li_2S particles from the carbon network and more oxidation could not follow. The first discharge peak at 2.3-2.4 is not present, which means that oxidation stops before long chain polysulfides are formed and the overvoltage bump at the start of charge is ill defined, which means that the activation energy necessary to oxidize Li_2S was not provided.

Both Li_2S batteries show a very unstable behaviour of the current when cycled accoarding to CCCV during the charge rest step. This discloses the fact that charge accumulates and diffuses, making the resistance increase and decrease.
In B4 capacity has increased, see Figure 32b, but still it drops heavily within the first cycle. Moreover the first discharge plateau is still not visible, which means that polysulfides are likely to be in the form of short chains. It is very important to notice that, despite the voltage is kept constant, the fraction of capacity that can be recovered by slowing down the kinetics is very little.

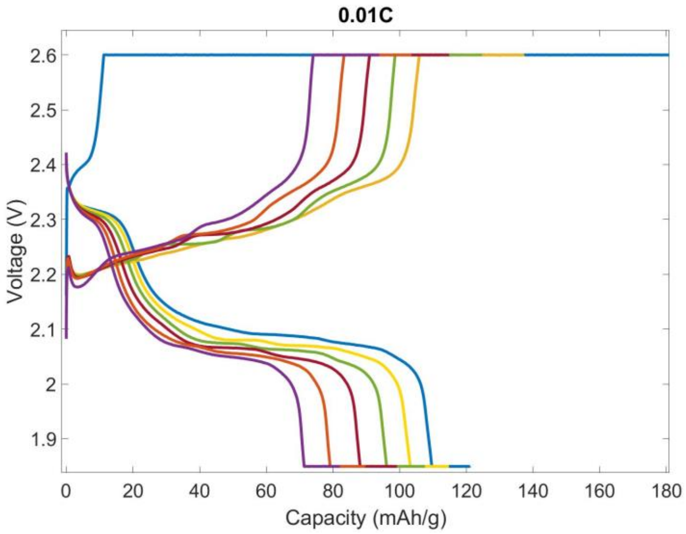

Figure 33: Charge and discharge curve of B7 cycled at 0.01C. The long CV interval during the first discharge means that Li_2S solid state reaction is indeed kinetically difficult to achieve. According to the curves plateuas reactions are reversable.

B7 is another case in which sulphur is probably found out of the pores: the maximum achieved capacity is around 180 mAh g^{-1} but there is no reason why it should deliver a much lower capacity than B6. In the experimental methods setion it was mentioned that in the attempt to dissolve Li_2S better, the process of impregnation was repeated: it probably was not enough to improve the adsorption. Nevertheless the voltage curve is very well defined, therefore reactions are quite reversible.

It was not worth plotting the cycle life and the coulombic efficiency (CE) of none of the batteries until now since they never cycled properly for more that 20 cycles and since coulombic efficiency was always well bellow 100%, except for when batteries were drained. Nonetheless CE took advantage of the CCCV program and it levels at around 90% much faster than it did before, Figure 34b.

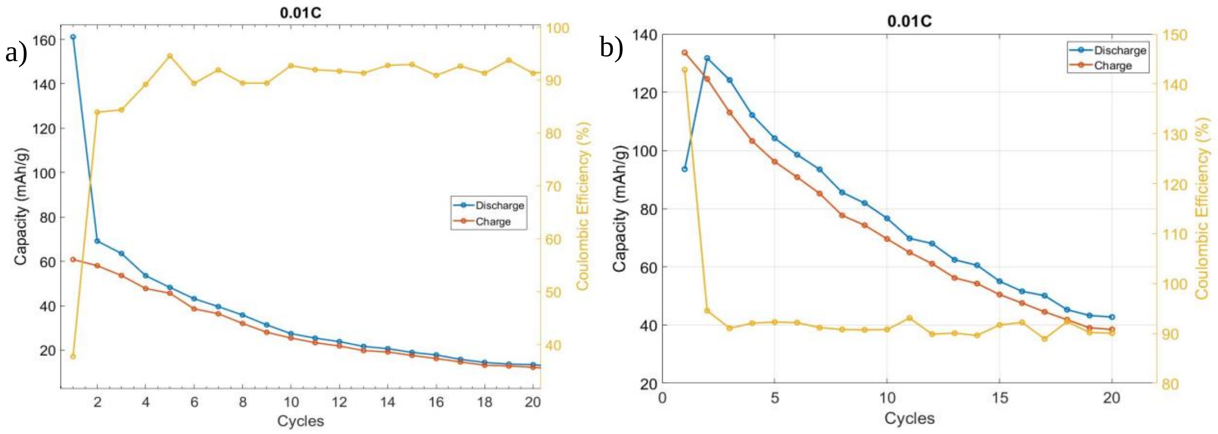

Figure 34: Cycle life of B2 before (a) and after (c) it was cycled according to CCCV

Conclusions

Three imine bonded covalent organic frameworks (COFs) have been studied as cathode materials for Li-S batteries, two of which have been assembled both in dischage (S) and charge (Li_2S) configuration.

All the batteries showed to support the reactions in between lithium and sulphur, two in particular, B6 and B7, produced discharge and charge curves with very well defined and persistent plateaus. This have been anticipated by the strong peak shifts observed with XPS spectrocopy on IISERP-CON1 with Li_2S. It seems that their heteroatom-rich nano-environment (21 trapping sites/unit cell) creates better adsorption conditions for polysulfides (PS) and promotes the progress of the reaction. Among these two, B6 delivered the maximum observed capacity of 991 mAh g^{-1} after the first discharge at 0.01C. Nevertheless, a 100 mV lower polarization was observed in B2 and B3 when cycled at the same rate.

The best capacity retention is observed in B2. Despite it was found out that its low capacity is due to sulphur particles out of the pores, capacity fades quite slowly and with a costant decay rate, unlike other batteries (B4,B6,B7) whose capacity falls sharply after the first half a cycle. This behaviour has to be attributed to either a broad pore size distribution (B6) or a not very efficient impregnation method (B4, B7). Nevertheless, B4 delivers more than 500 mAh g^{-1} after the first discharge without overcharging the battery, which is quite a success being a Li_2S cathode. This is a second sign that the TPB-DMTP COFs environment is favouring the reaction. However, clear proofs that the larger surface area of the TPB-DMTP's COFs is improving the rection kinetics cannot be observed and polysulfides shuttling is the dominant degradation mechanism in all systems.

Recommendations

A lot of work remains to be done in order to clarify the influence of pore surface chemistry and pore surface area of COFs on the Li-S chemistry. In particular, I believe that is worth to continue what was planned in the Research section and study the effects of a tailorable number of hetoratoms sites on the storage capacity and cycling performance. It would be valuable to arrive at a stage in which the chemistry of the surface is designed to favour a pre-determined specie of PS, similarly to a PS-formation by-pass strategy, that can be easily trapped by a known pore size and a chosen trapping group. Once this aspect is controlled, it may be possible to design COFs whose surfaces are catalytic for Li-S reactions. To this scope it is crucial to obtain full control over the synthesis, otherwise structure-properties relationships are difficult to identify.

For the scope of studying the correlation in between number of trapping sites, sulphur maximum storage capacity and PS retention, I think it would be interesting to test COFs adsorption properties with a molecular probe like water, whose characteristics (chemical formula, molecule geometry, polarity) are closer to that of PS. To get instead more insight on whether the pore level of occupancy can hinder lithium diffusion and sulphur utilization, one could combine depth profiling with XPS spectroscopy, not only to identify which PS species are formed, but also to check if all the sulphur contained in the cathode is being consumed.

In the end, as far as COF design choices are concerned, I think it is advisable to move towards COF species that are more stable and conductive than those experimented until now, which usually don’t have a wide π conjugated structure, and molecules in which both negative and positive polarized atoms are exploited to achieve PS adsorption. Until now, the only known positively polarized atoms used in COFs are carbon and boron, but little is clear about the extent of the ring polarization.

Supplementary Information

TB COF

a)

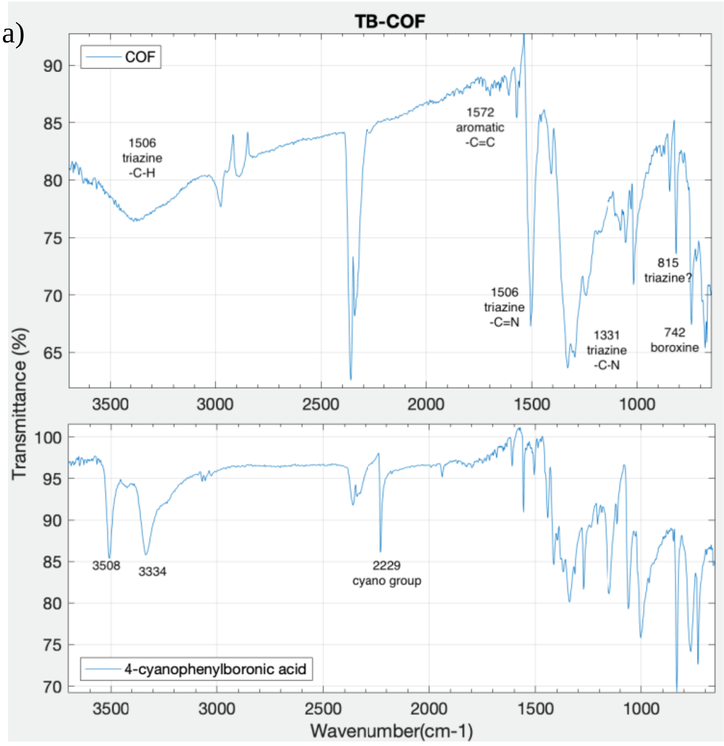

b)

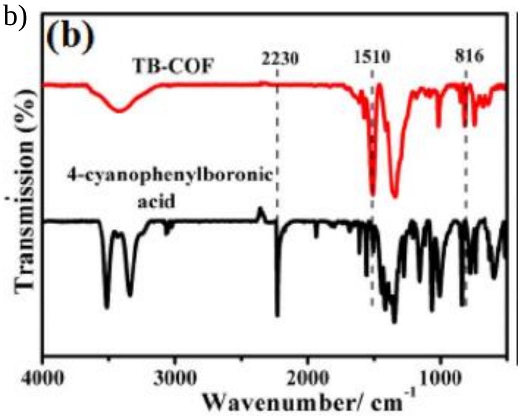

c)

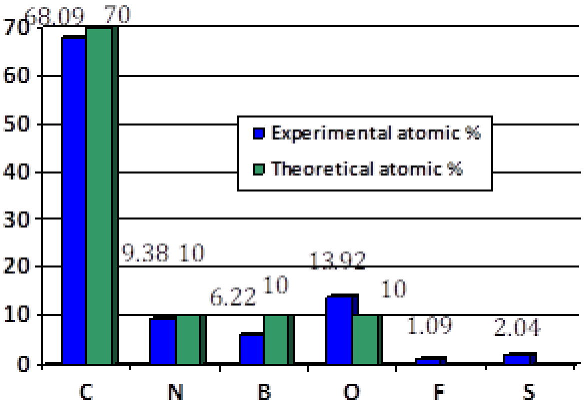

d)

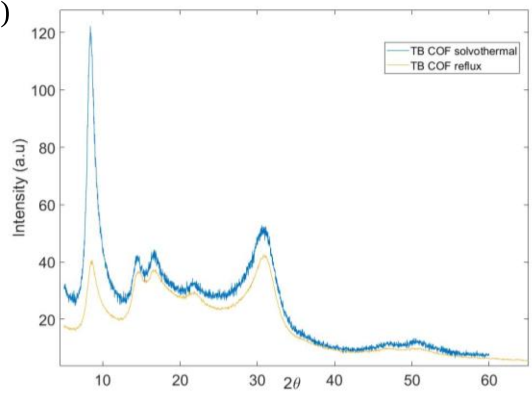

e)

2θExperimental (Cobalt)	2θExperimental (Copper)	2θPaper
8.5888	7.3950	6.8 (100)
14.6621	12.6183	12.3 (110)
16.6734(200)	14.3462	14.3 (210)
20.8142(210)	17.8999	18.8 (201)
30.5946(001/101)	26.2661	26.5 (001)

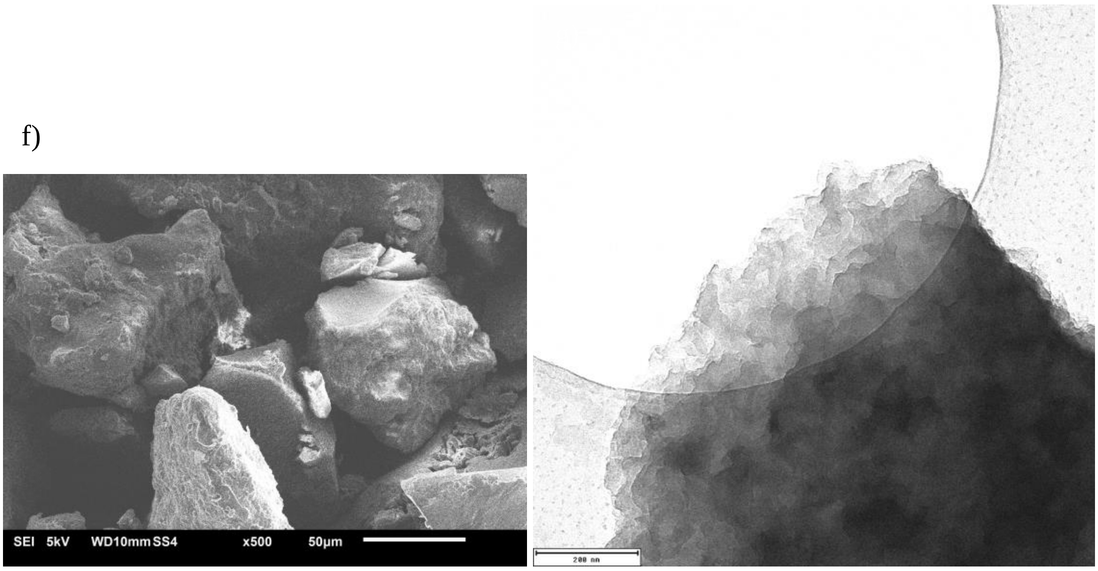

Figure 35: FT-IR spectra of TB-COF and it’s reagents (a). FT-IR spectra from [34] (b) EDS elemental analysis chart (c). XRD diffraction pattern (d) and table with peak comparison (e). SEM image (f) and TEM image (g), scale bar is 200 nm.

IISERP-CON1

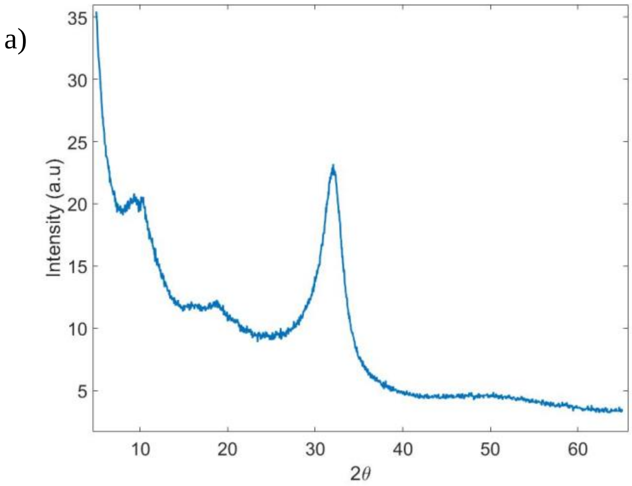

b)

2θ Experimental (Cobalt)	2θ Experimental (Copper)	2θ Paper
Not Found	NA	5 (100)
9.0226	7.7684	9 (110)
16.52	14.17	14 (020)
18.3297	15.7684	15.5 (210)
32.2115	27.6446	27.3(003)

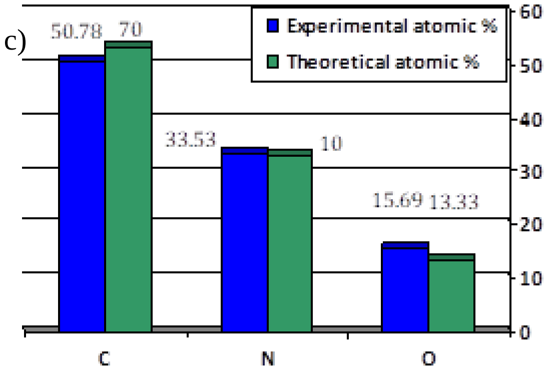

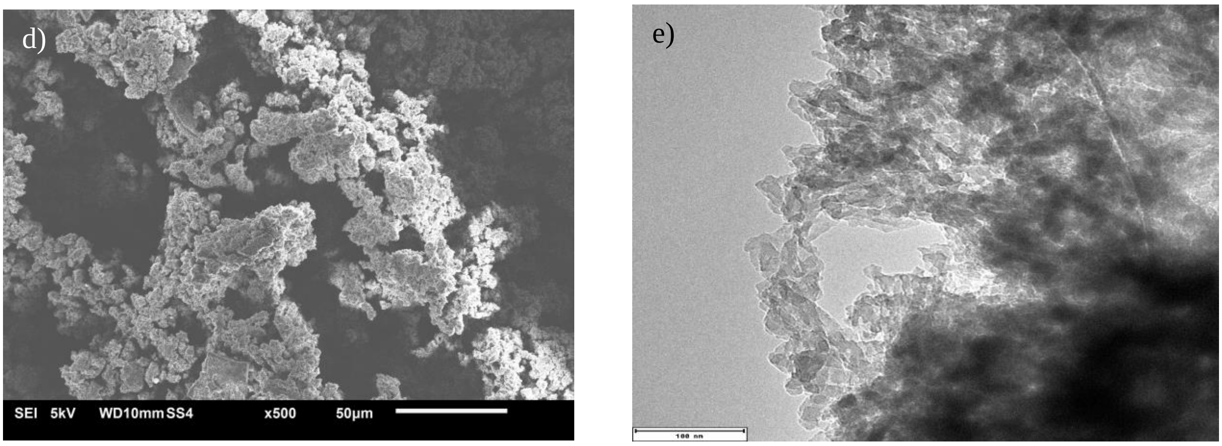

Figure 36 XRD diffraction pattern (a) and table with peak comparisons (b). EDS elemental analysis chart (cSEM image (e) and TEM image (d), scale bar is 100 nm.

TPB-DMTP 100

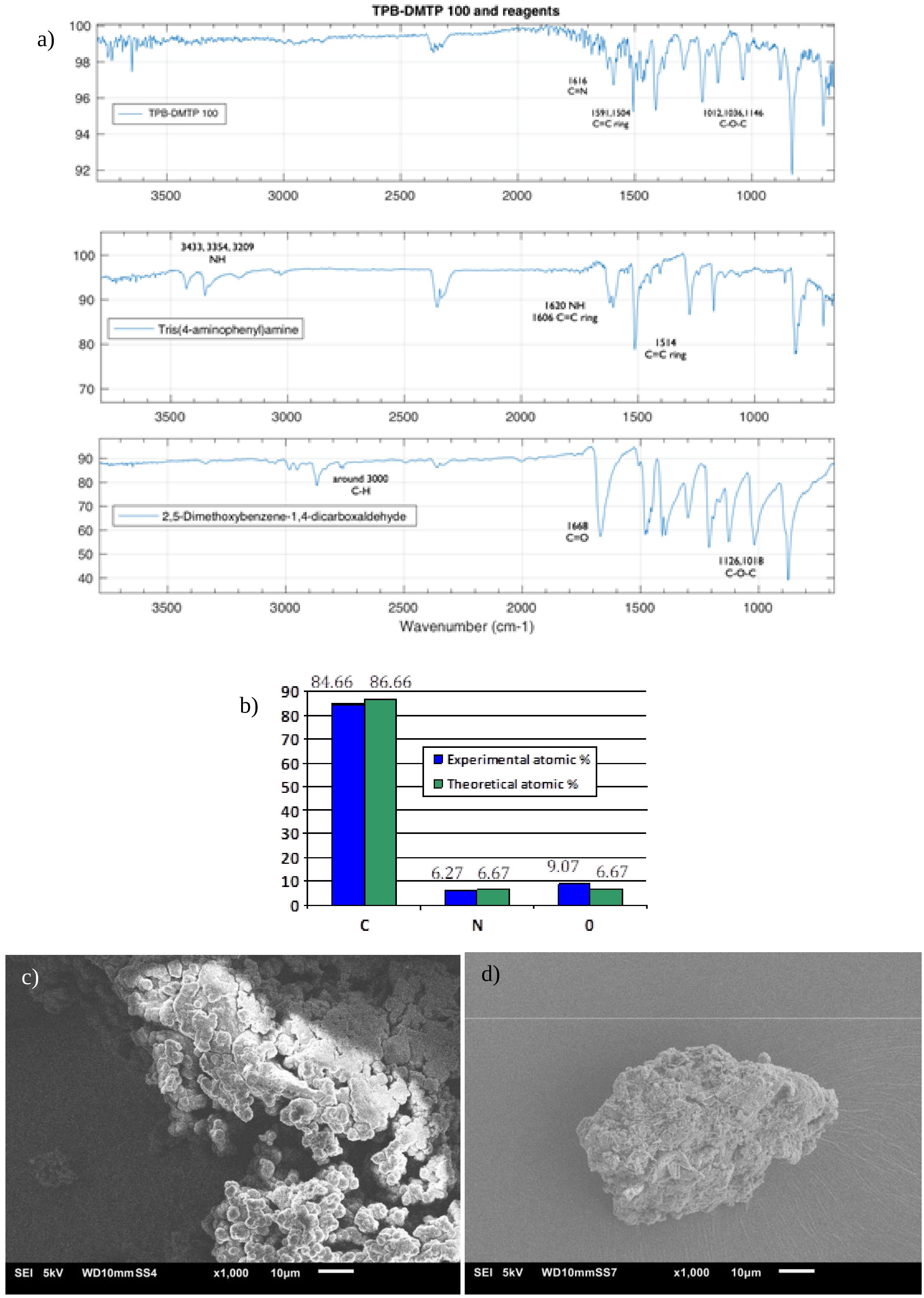

Figure 37: FT-IR spectra of TPB- DMTP 100 and it’s reagents (a). EDS elemental analysis chart (b). SEM image (e) and TEM image before (d) and after sulphur impregnation..

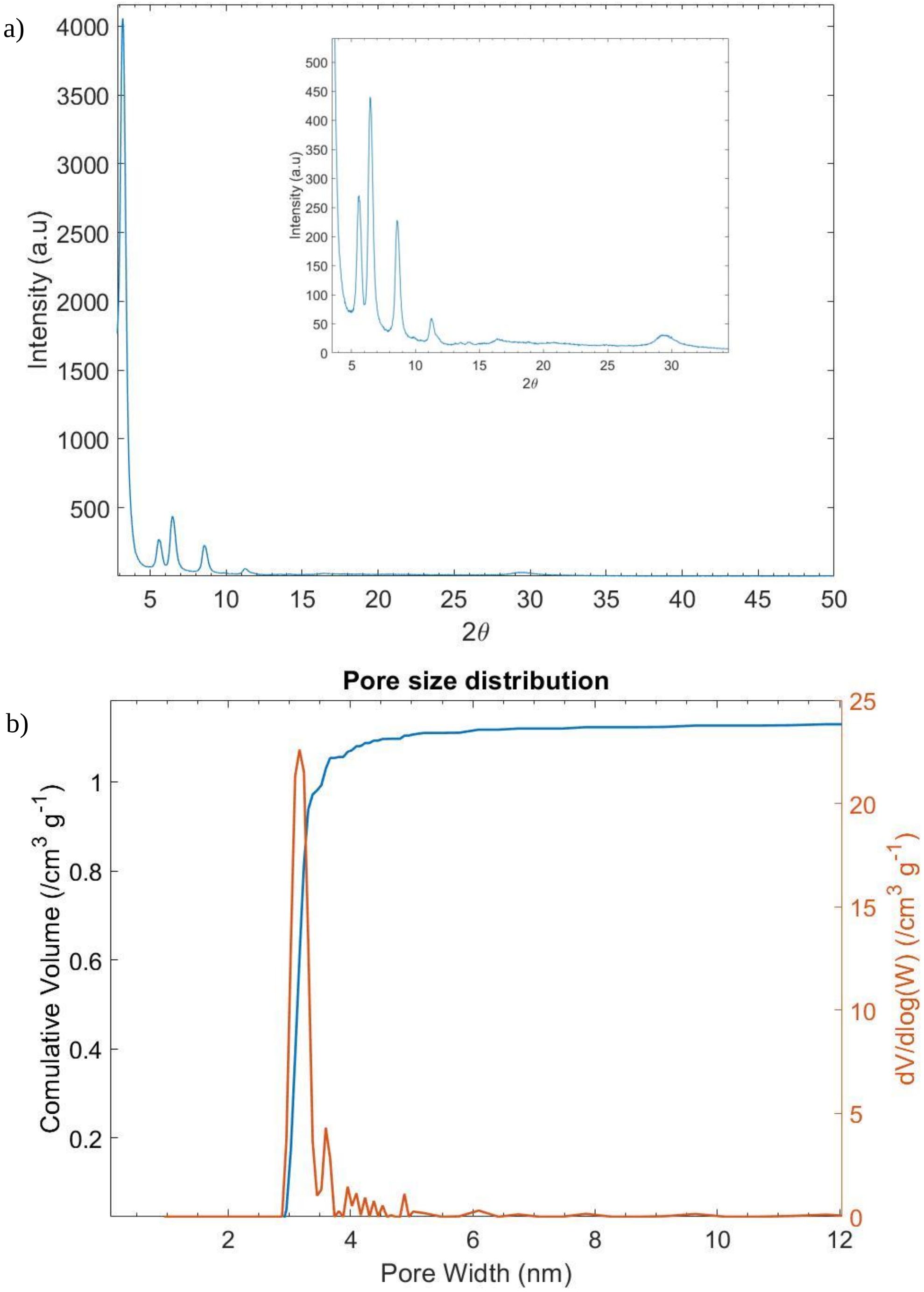

Figure 38: XRD diffraction pattern (a) and pore size distribution (b) .

TPB-DMTP 50

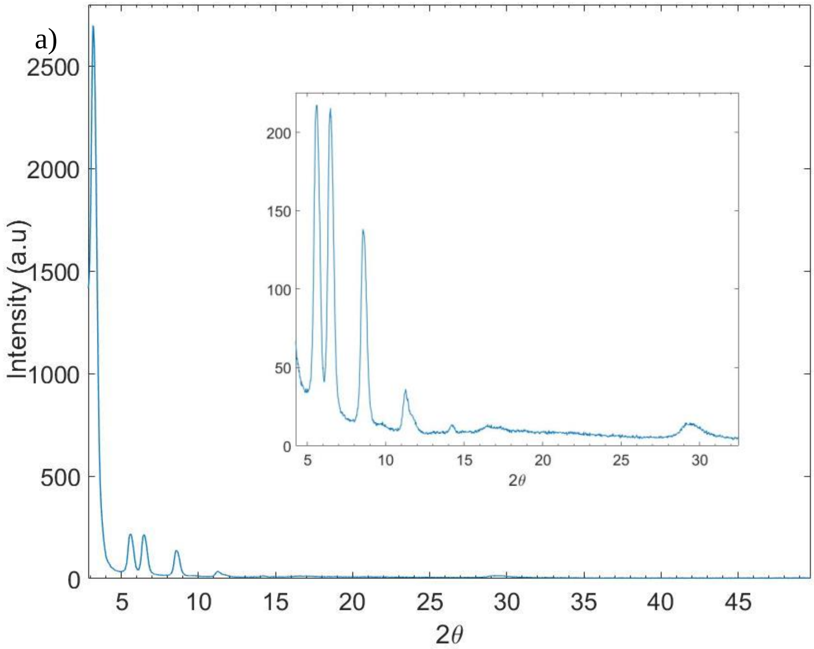

b)

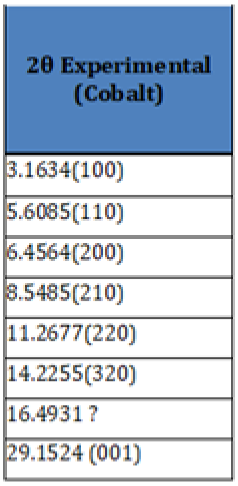

2θ Experimental (Cobalt)
3.1634(100)
5.6085(110)
6.4564(200)
8.5485(210)
11.2677(220)
14.2255(320)
16.4931 ?
29.1524 (001)

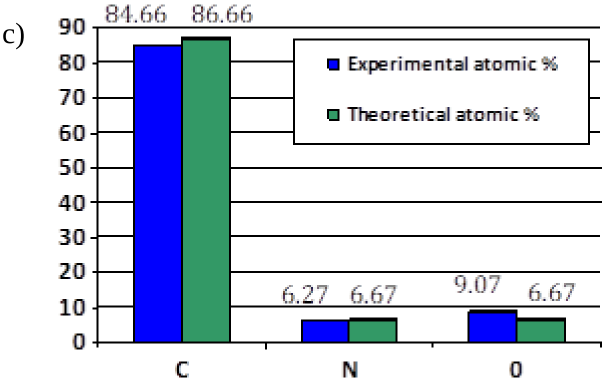

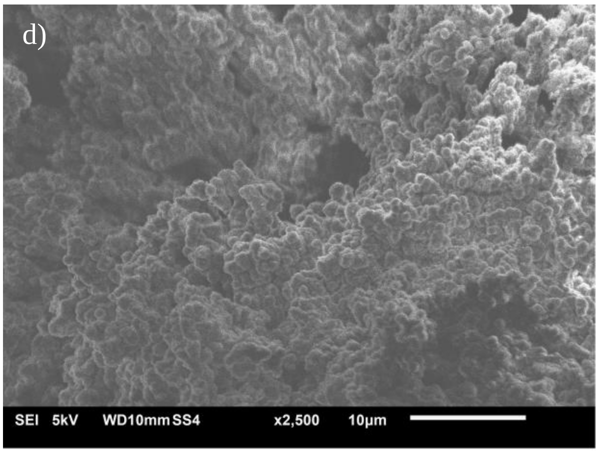

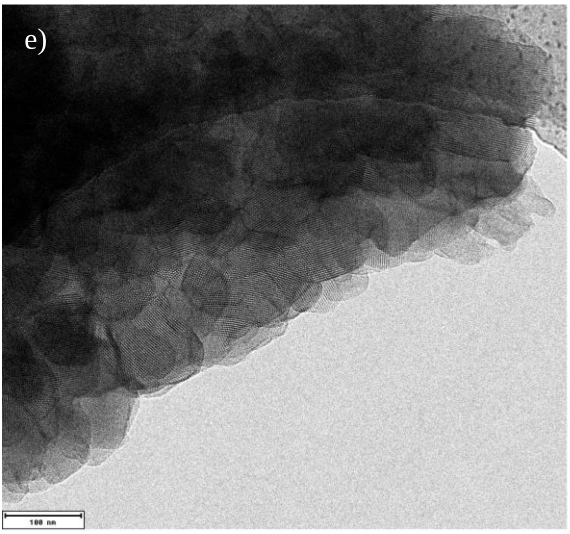

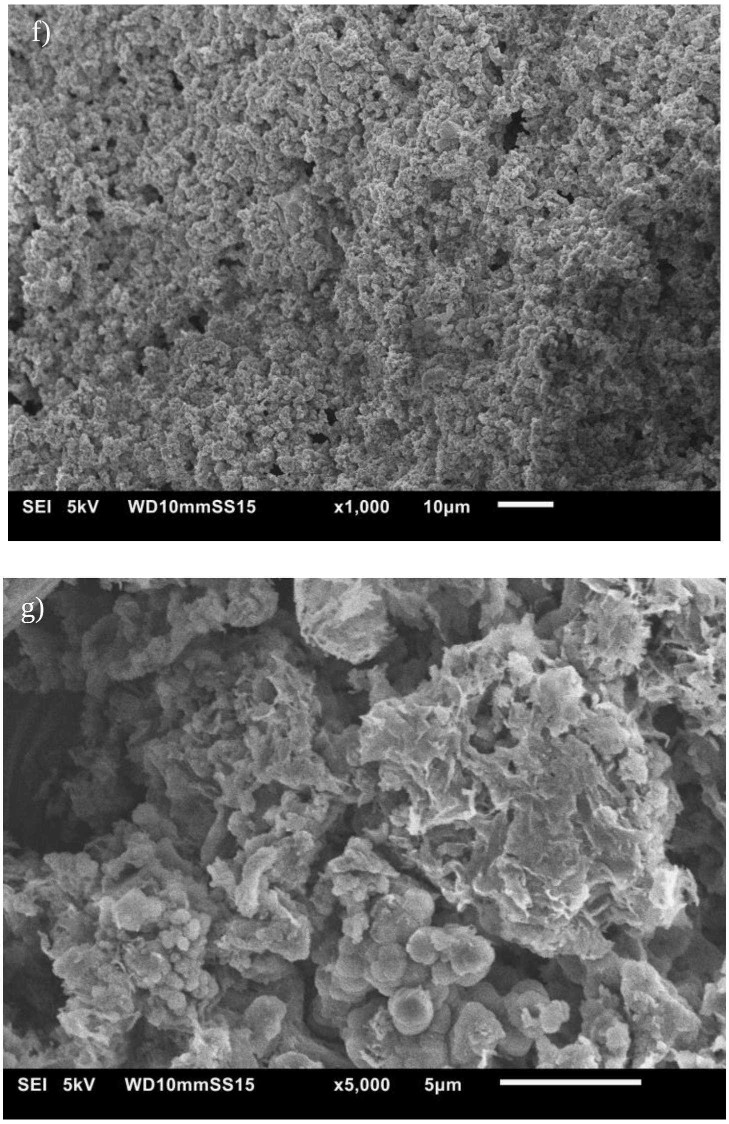

Figure 39: XRD diffraction pattern (a) and table with peak positions and associated crystal planes (b). EDS elemental analysis chart (c)/ SEM image (d) and TEM image (e), scale bar is 100 nm. SEM image of TPB-DMTA 50 after sulphur (f) and Li_2S (g) impregnation.

TPB-DMTP 17 and 0

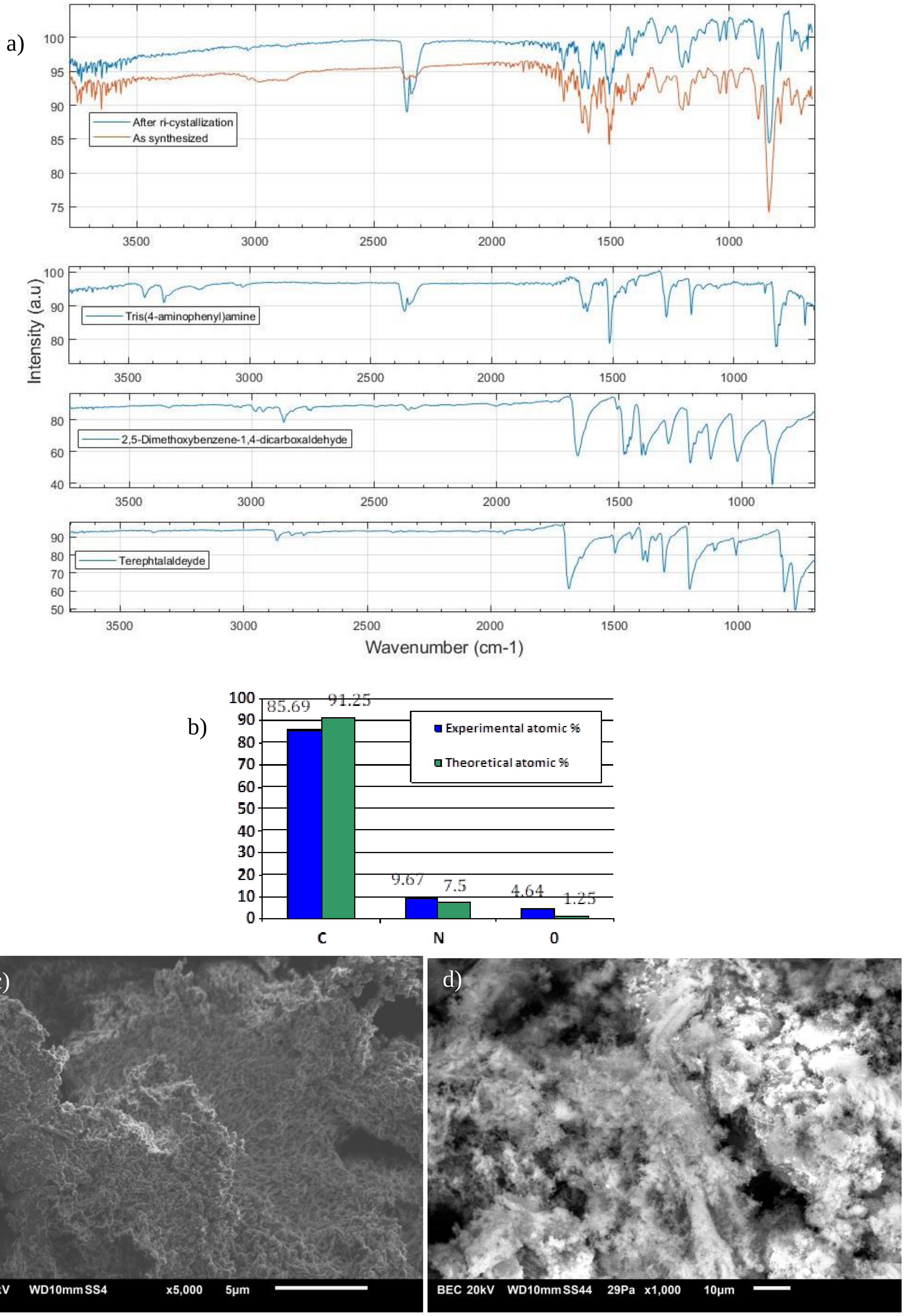

Figure 40:FT-ir spectra of TPB-DMTP 17 and it’s reagents (a). EDS elemental analysis chart (b). SEM images of the as synthesized COF.

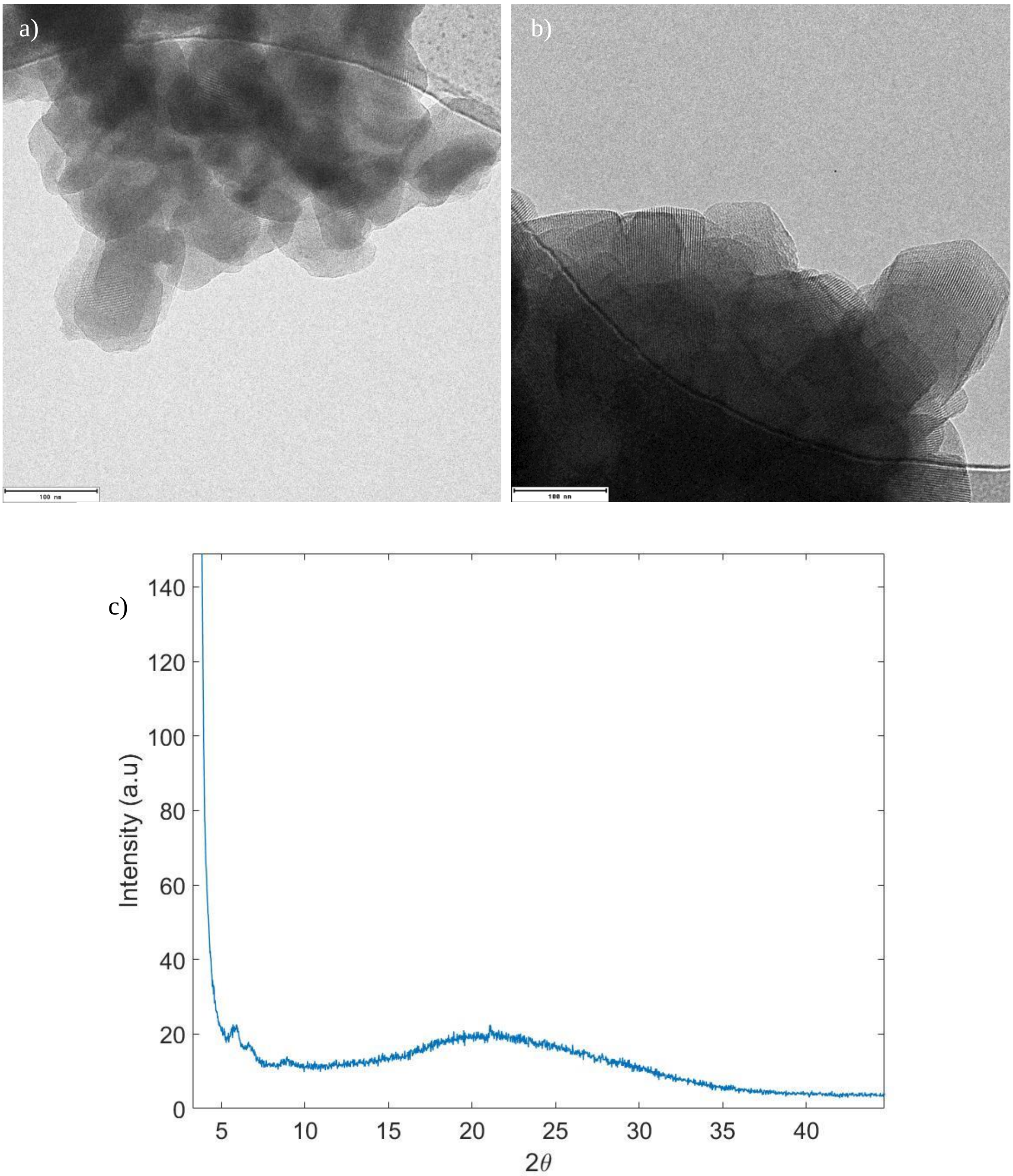

Figure 41: TEM images (a,b) and XRD diffraction pattern of the as synthesized COF (c).

Dha Tab 100

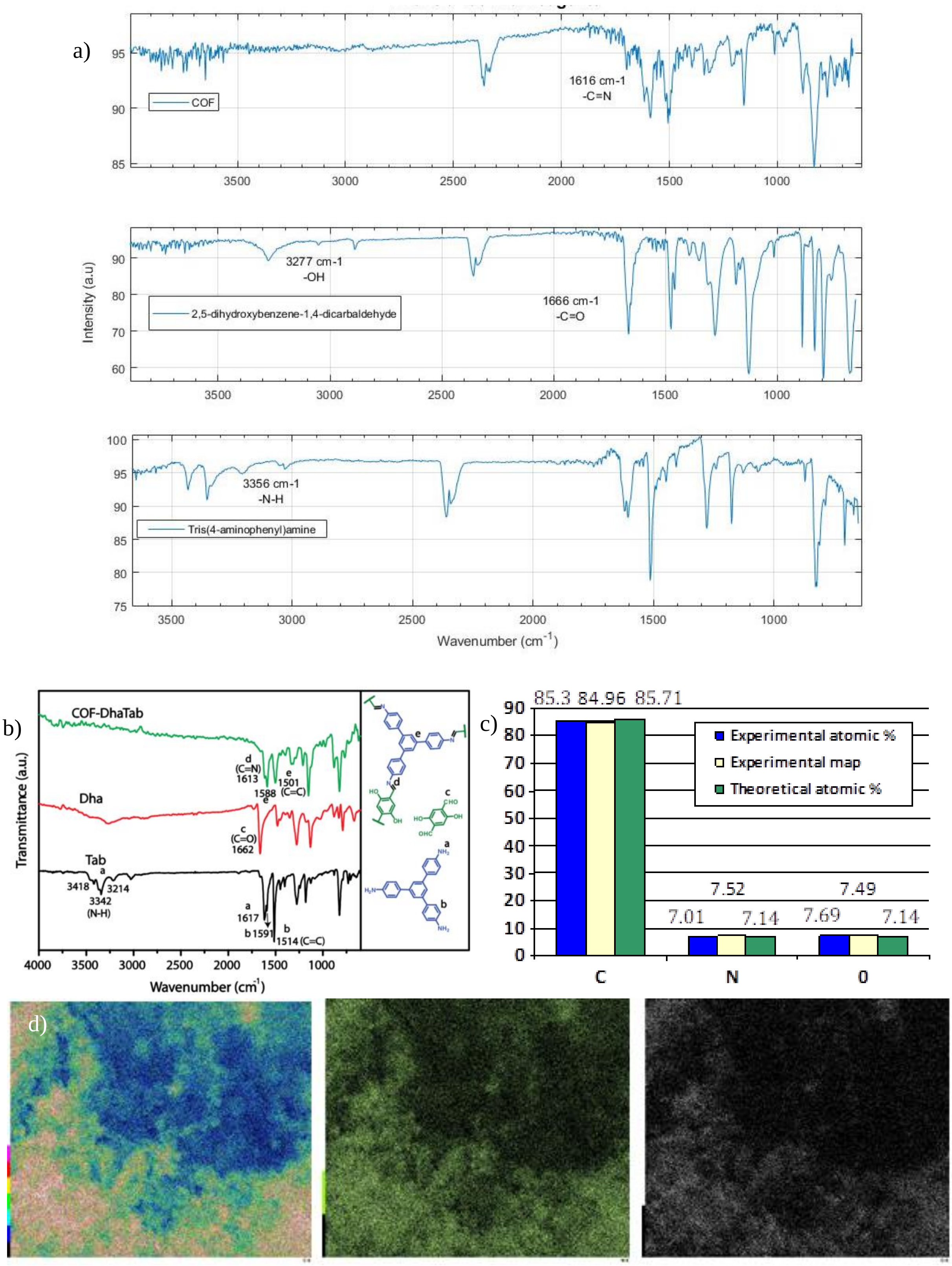

Figure 42: FT-IR spectra of DhaTat 100 and its reagents (a), : FT-IR spectra from [23] (b). EDS elemental analysis chart (c). Elemental mapping (C,N,O) (d).

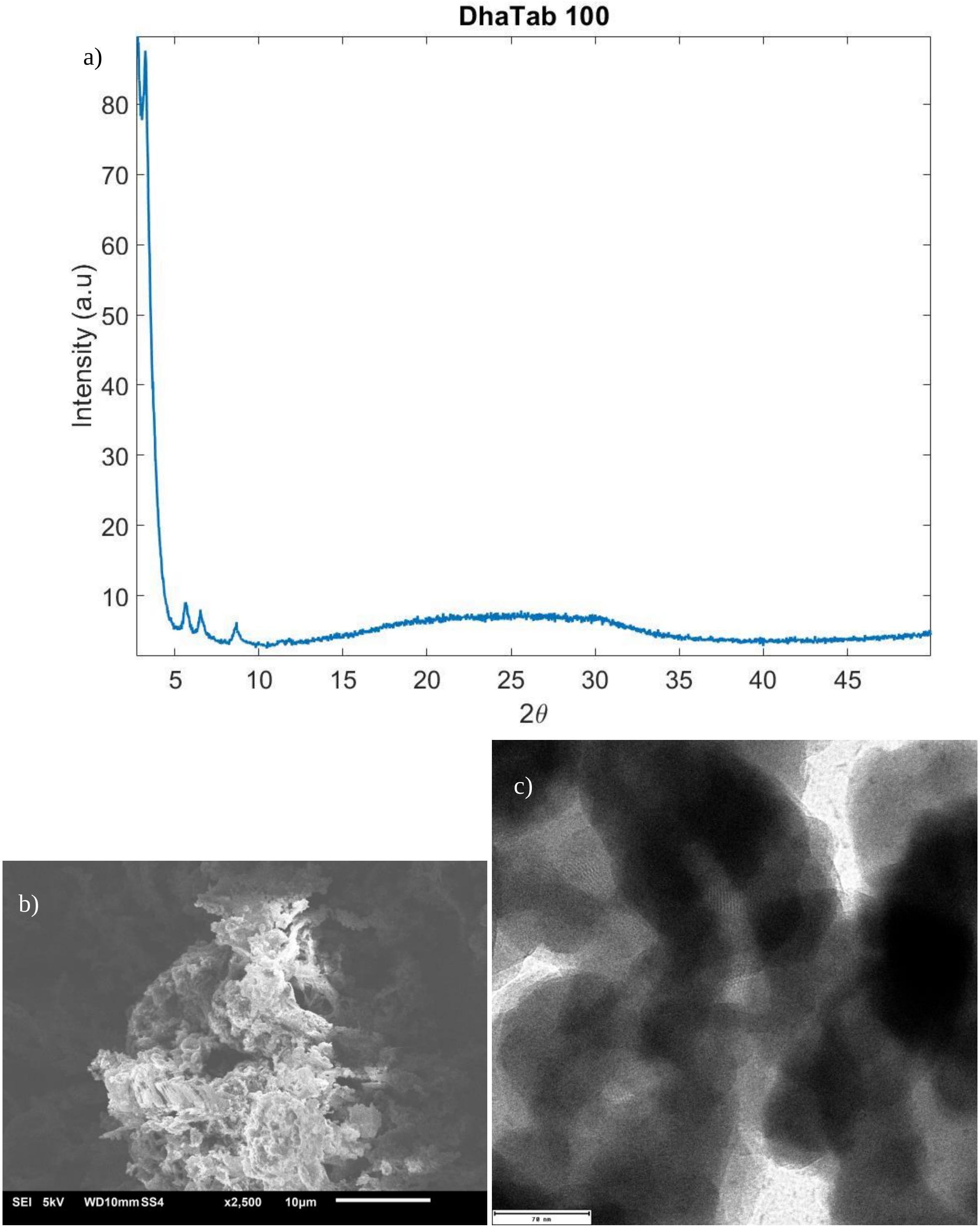

Figure 43: XRD diffraction pattern (a). SEM image (b) and TEM image (c), scale bar is 70 nm.

Dha Tab 50

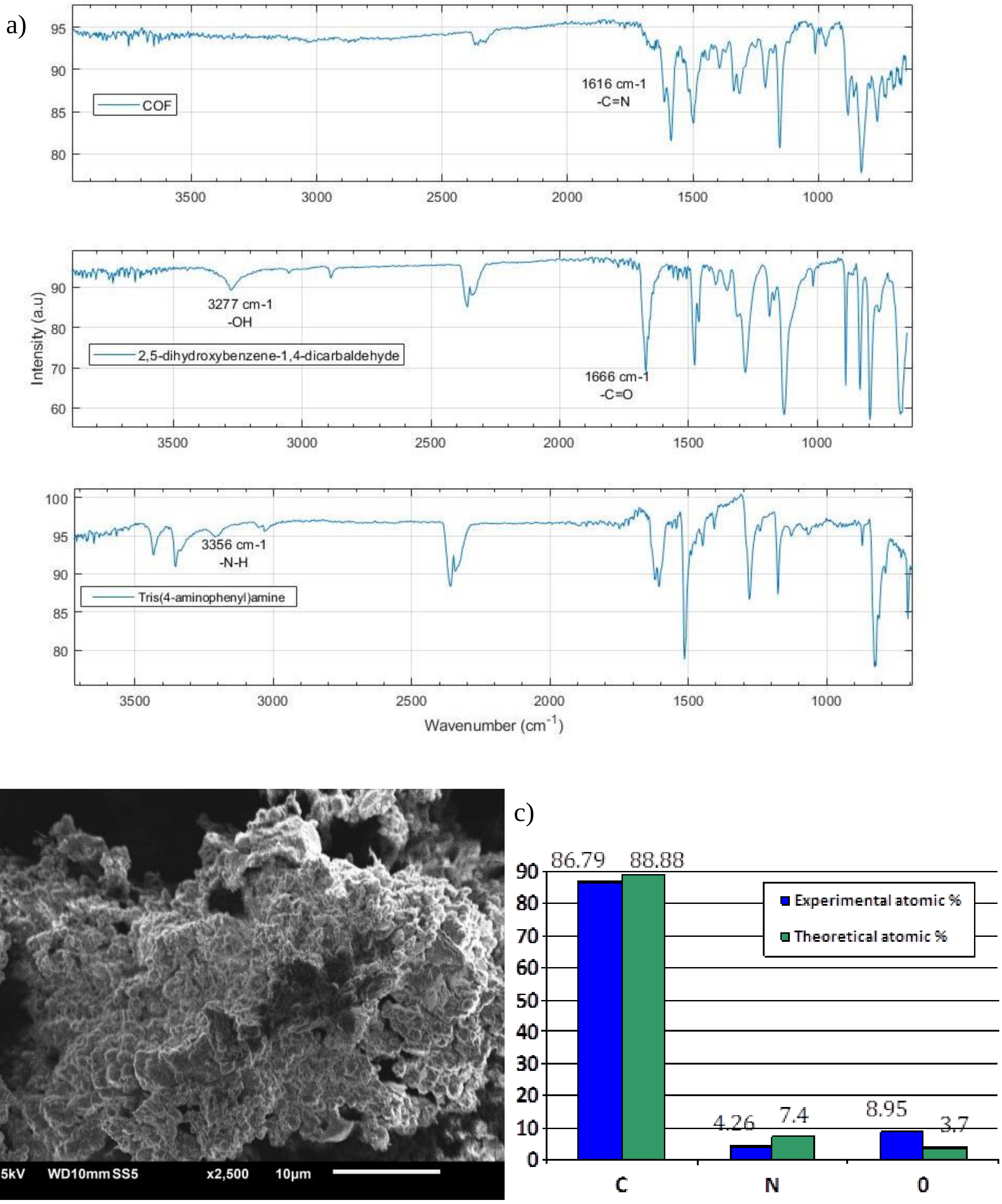

Figure 44:FT-IR spectra of DhaTab 50 and its reagents (a). SEM image (b). EDS elemental analysis chart (c).

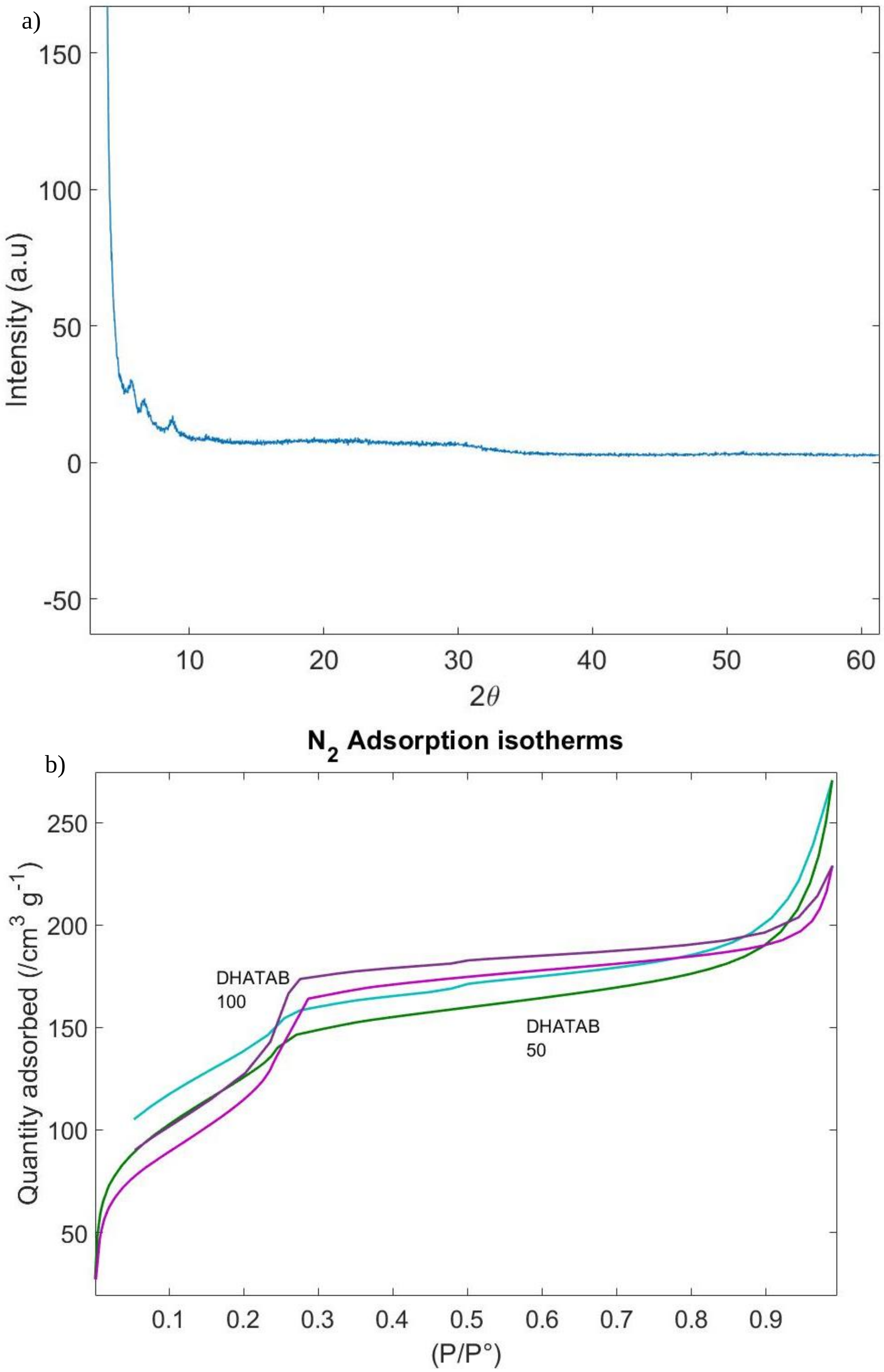

Figure 45: XRD diffraction pattern (a) and Nitrogen adsorption isotherms of both DhaTab 100 and 50 (b).

XPS results

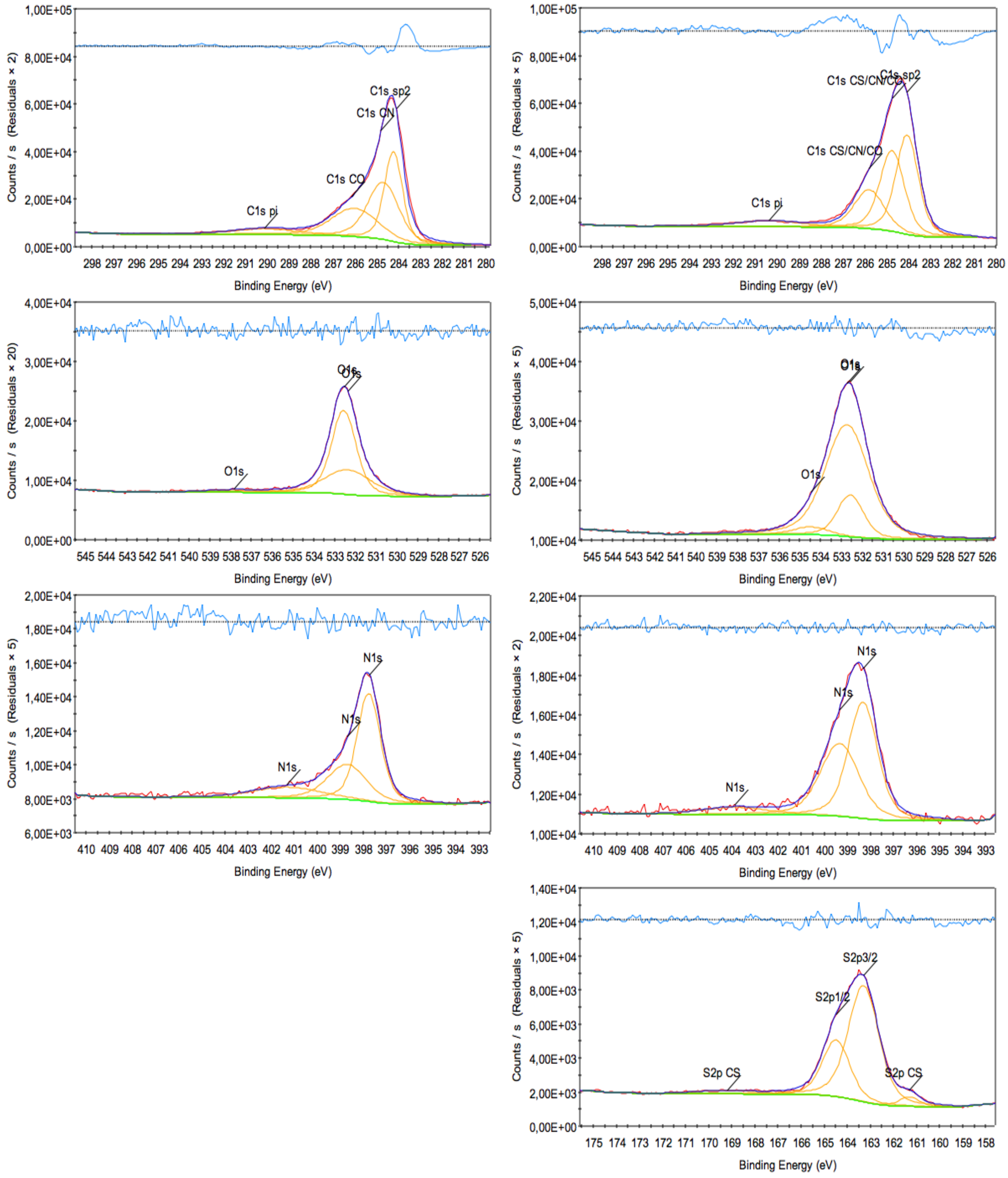

Figure 46: XPS spectra of TPB-DMTP 100 as synthesized (left) and with sulphur (right).

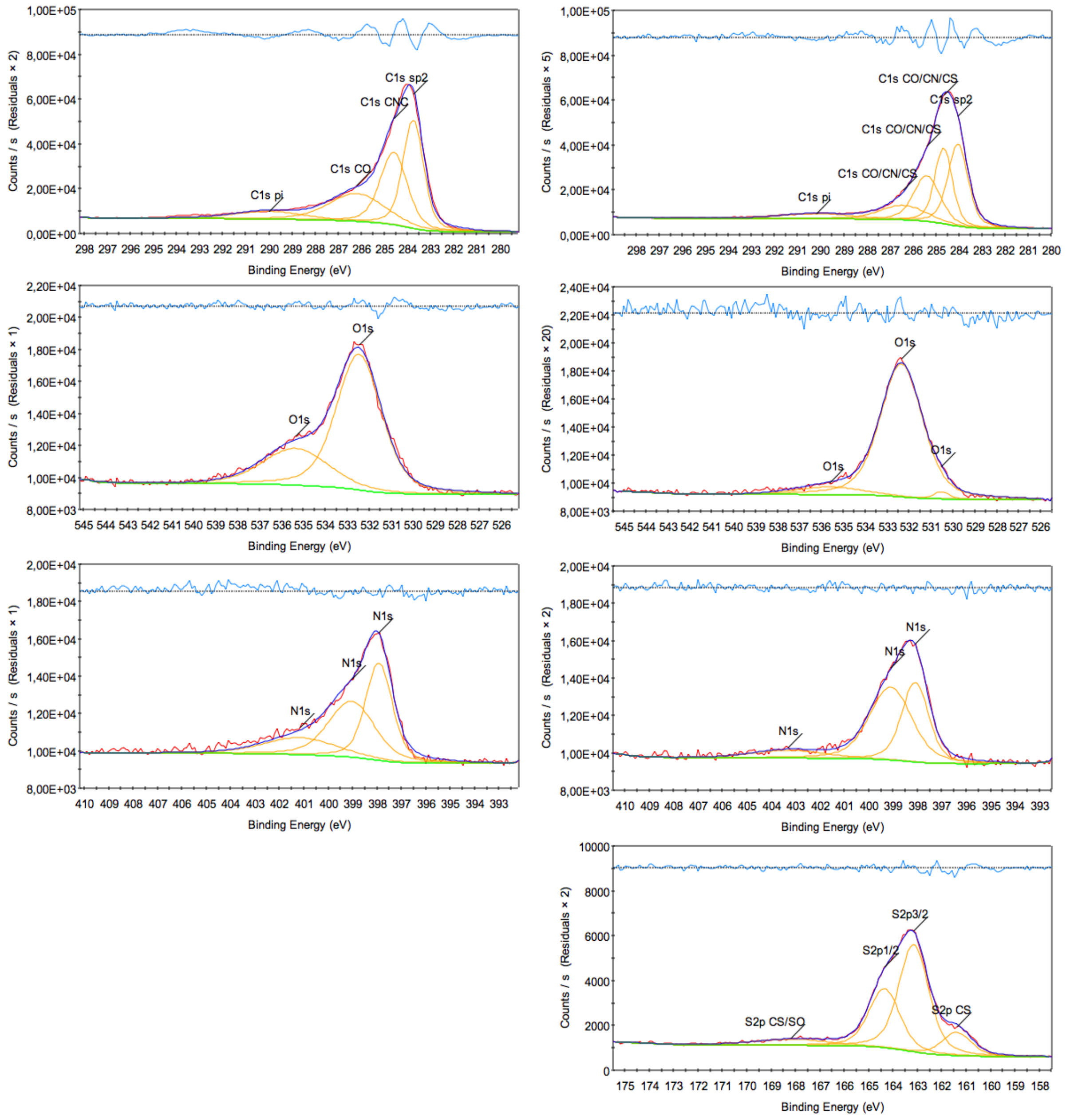

Figure 47: : XPS spectra of TPB-DMTP 50 as synthesized (left) and with sulphur (right).

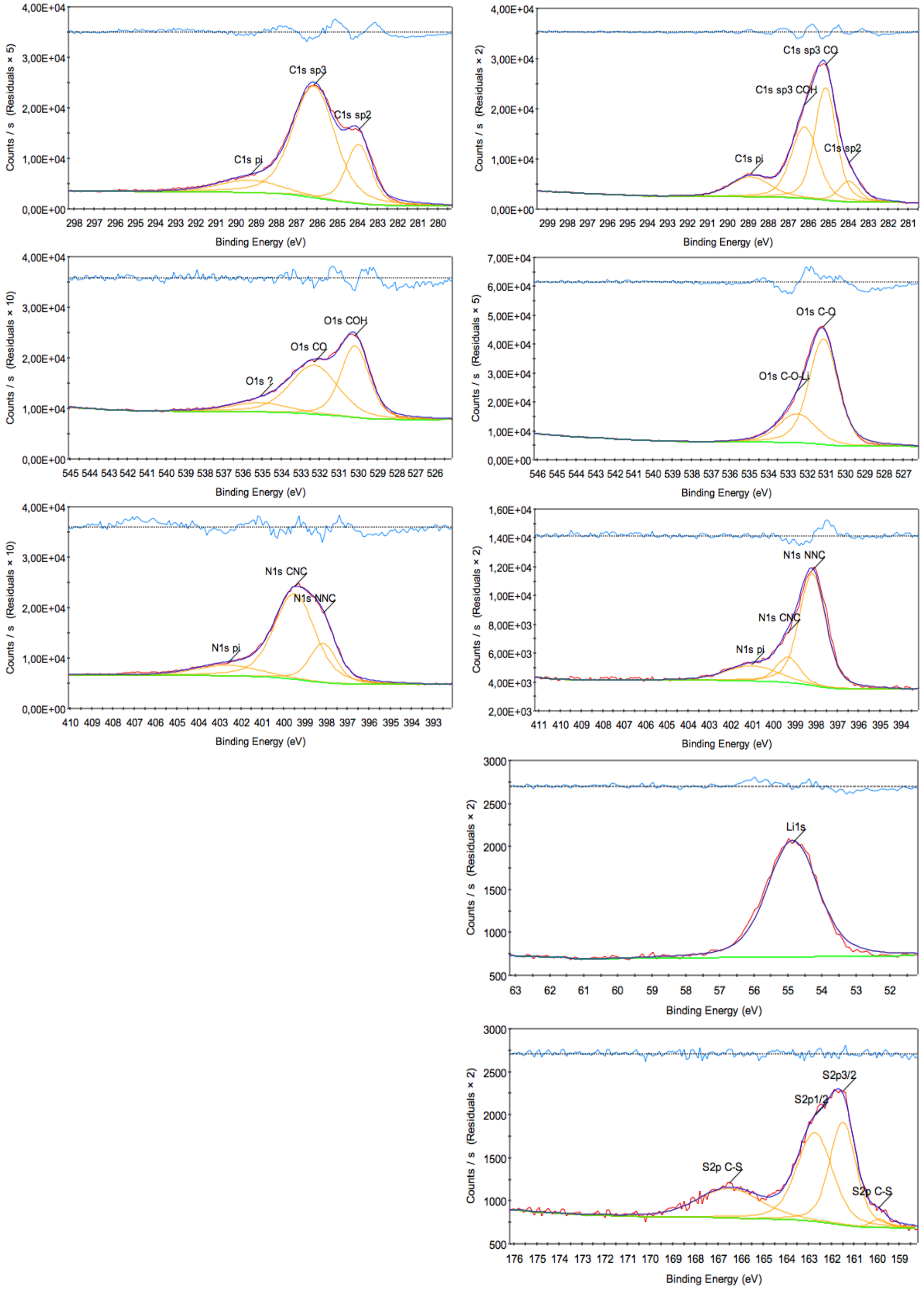

Figure 48: XPS spectra of IISERP-CON1 as synthesized (left) and with Li$_2$S (right).

Bibliography

1. Volta, A., *Sull'elettricitá eccitata dal semplice contatto di sostanze conduttrici di natura diversa*. 1800.
2. D. Larcher, J.-M.T., *Towards greener and more sustainable batteries for electrical energy storage.* Nature Chemistry, 2015. **7**: p. 19-29.
3. Liu, C., *Understanding electrochemical potentials of cathode materials in rechargeable batteries.* Materials Today, 2016. **19**(2): p. 109-124.
4. Li, G., *Revisiting the Role of Polysulfides in Lithium–Sulfur Batteries.* Advanced Materials, 2018: p. 1705590-1705609.
5. JohnB.Goodenough, K.-S., *The Li-Ion Rechargeable Battery: A Perspective.* Journal of Americal Chemical Society, 2013. **135**: p. 1167-1176.
6. Kring, D.A., *Compositions of earth's continental crust as inferred from the compositions of impact melt sheets* Lunar and Planetary Science XXVIII, 1924.
7. *U.S. Geological Survey - National Minerals Information Cente*.
8. Dean, J.A., *Lange's Handbook of Chemistry*. 3rd ed. 1985: McGraw-Hill Professional.
9. *Springer & Material Phases Data System (MPDS), Switzerland & National Institute for Materials Science (NIMS), Japan, 2016*.
10. Caixia Li, L.Y., *Chemical Immobilization Effect on Lithium Polysulfides for Lithium–Sulfur Batteries.* Small, 2018. **14**.
11. Harks, P.-P., *The Significance of Elemental Sulfur Dissolution in Liquid Electrolyte Lithium Sulfur Batteries.* Advanced Energy Materials, 2017. **7**: p. 1601635-1601640.
12. Xiulei Ji, L.F.N., *Advances in Li–S batteries.* Journal of Materials Chemistry, 2010. **20**: p. 9821–9826.
13. Zheng, D., *Investigation of the Li−S Battery Mechanism by Real-Time Monitoring of the Changes of Sulfur and Polysulfide Species during the Discharge and Charge.* ACS Applied Materials and Interfaces, 2017. **9**: p. 4326-4332.
14. Frank Y. Fan, Y.M.C., *Mechanism and Kinetics of Li2S Precipitation in Lithium–Sulfur Batteries* Advanced Materials, 2015. **27**: p. 5203−5209.
15. Zhen Li, Y.W., *Insight into the Electrode Mechanism in Lithium-Sulfur Batteries with Ordered Microporous Carbon Confined Sulfur as the Cathode* Advanced Energy Materials, 2014. **4**.
16. Yuan Yang, Y.C., *Improving the Performance of Lithium Sulfur Batteries by Conductive Polymer Coating.* ACS Nano, 2011. **5**(11): p. 9187-9193.
17. Lu Li, N.K., *Phosphorene as a Polysulfide Immobilizer and Catalyst in High-Performance Lithium–Sulfur Batteries*
Advanced Materials, 2017. **29**.
18. M. Helen, M.F., *Single step transformation of sulphur to Li2S2/Li2S in Li-S batteries*
Scientific Reports, 2015. **5**.
19. Alen Vizintin, R.D., *The mechanism of Li2S activation in lithium-sulfur batteries: Can we avoid the polysulfide formation?*
Journal of Power Sources, 2017. **344**: p. 208-217.
20. JongTae Yoo, S.-Y.L., *COF-Net on CNT-Net as a Molecularly Designed, Hierarchical Porous Chemical Trap for Polysulfides in Lithium−Sulfur Batteries.* Nano Letters, 2016. **16**: p. 3292−3300.
21. Felix Hippauf, S.K., *The Importance of Pore Size and Surface Polarity for Polysulfide Adsorption in Lithium Sulfur Batteries*
Advanced Materials Interfaces, 2016. **3**.

22. Maria S. Lohse, T.B., *Covalent Organic Frameworks: Structures, Synthesis and Applications*
Advanced functional materials, 2018. **28**.
23. Kandambeth, S., *Self-templated chemically stable hollow spherical covalent organic framework.* Nature Communications, 2015. **6**(6786).
24. Sasanka Dalapati, D.J., *An Azine-Linked Covalent Organic Framework.* Journal of Americal Chemical Society, 2013. **135**: p. 17310-17313.
25. José Segura, M.M., Feliz Zamora, *Covalent organic frameworks based on Schiff-base chemistry: synthesis, properties and potential applications.* Chemical Society Review, 2016. **45**.
26. Lijuan Zhu, Y.-B.Z., *Crystallization of Covalent Organic Frameworks for Gas Storage Applications.* Molecules, 2017. **22**: p. 1149
27. Florian Auras, T.B., *Synchronized Offset Stacking: A Concept for Growing Large-Domain and Highly Crystalline 2D Covalent Organic Frameworks*
Journal of the American Chemical Society, 2016. **138**: p. 16703−16710.
28. Mo, Y.-P., *The intramolecular H-bonding effect on the growth and stability of Schiff-base surface covalent organic frameworks*
Physical Chemistry Chemical Physics, 2017. **19**: p. 539-543.
29. Hong Xu, J.G.a.D.J., *Stable, crystalline, porous, covalent organic frameworks as a platform for chiral organocatalysts.* Nature Chemistry, 2015. **7**: p. 905-912.
30. Lijuan Zhu, Y.-B.Z., *Crystallization of Covalent Organic Frameworks for Gas Storage Applications.* Molecules, 2017. **22**: p. 1149.
31. Smith, B.J., *Insight into the crystallization of amorphous imine-linked polymer networks to 2D covalent organic frameworks.* Royal Society of Chemistry Communication, 2016, . **52**: p. 3690-3693.
32. Gao, Q., *Reconstruction of Covalent Organic Frameworks by Dynamic Equilibrium.* Chemistry European Journal 2015. **21**: p. 16818-16822.
33. Vyas, V.S., *A tunable azine covalent organic framework platform for visible light-induced hydrogen generation.* Nature Communications, 2015. **6**.
34. Xiao, Z., *Covalent organic frameworks with lithiophilic and sulfiphilic dual linkages for cooperative affinity to polysulfides in lithium-sulfur batteries.* Energy Storage Materials, 2018. **12**: p. 252-259.
35. Wang, S., *Exfoliation of Covalent Organic Frameworks into Few-Layer Redox-Active Nanosheets as Cathode Materials for Lithium-Ion Batteries.* Journal of Americal Chemical Society, 2017. **139**: p. 4258−4261.
36. Karak, S., *Constructing Ultraporous Covalent Organic Frameworks in Seconds via an Organic Terracotta Process.* Journal of Americal Chemical Society, 2017. **139**: p. 1856−1862.
37. Maria S. Lohse, T.B., *Sequential Pore Wall Modification in a Covalent Organic Framework for Application in Lactic Acid Adsorption.* Chemistry of Materials, 2016. **28**: p. 626−631.
38. Ning Huang, R.K., and Donglin Jiang, *Tailor-Made Pore Surface Engineering in Covalent Organic Frameworks: Systematic Functionalization for Performance Screening.* Journal of American Chemical Society, 2015. **137**: p. 7079−7082.
39. Nagai, A., *Pore surface engineering in covalent organic frameworks*
Nature Communications, 2011. **2**(536): p. 1-8.
40. Sabrina Rager, T.B., *Pore wall fluorescence labeling of covalent organic frameworks*
Cryst.Eng.Comm, 2017. **19**: p. 4886–4891.
41. Xiao Feng, D.J., *High-Rate Charge-Carrier Transport in Porphyrin Covalent Organic Frameworks: Switching from Hole to Electron to Ambipolar Conduction*

Angewandte Communications, 2012. **51**: p. 2618-2622.

42. Talapaneni, S.N., et al., *Elemental-Sulfur-Mediated Facile Synthesis of a Covalent Triazine Framework for High-Performance Lithium-Sulfur Batteries.* Angew Chem Int Ed Engl, 2016. **55**(9): p. 3106-11.
43. Yang, X., *Sulfur impregnated in a mesoporous covalent organic framework for high performance lithium– sulfur batteries.* Royal Society of Chemistry, 2015. **5**: p. 86137-86143.
44. Xu, F., *Fluorinated,Sulfur Rich, Covalent Triazine Frameworks for Enhanced Confinement of Polysulfides in Lithium-Sulfur Batteries.* ACS Appl. Mater. Interfaces 2017. **9**: p. 37731-37738.
45. Liao, H., *Covalent-organic frameworks: potential host materials for sulfur impregnation in lithium–sulfur batteries.* Journal of Materials Chemistry A, 2014. **2**: p. 8854-8858.
46. Wang, J., *An imine-linked covalent organic framework as the host material for sulfur loading in lithium-sulfur batteries.* Journal of Energy Chemistry, 2017.
47. Zahid Ali Ghazi, Z.T., *Efficient Polysulfide Chemisorption in Covalent Organic Frameworks for High-Performance Lithium-Sulfur Batteries.* Advanced Energy Materials, 2016. **6**.
48. Haldar, S., *High and Reversible Lithium Ion Storage in Self- Exfoliated Triazole-Triformyl Phloroglucinol-Based Covalent Organic Nanosheets.* Advanced Energy Materials, 2018. **8**: p. 1702170- 1702181.
49. Yuan Yang, Y.C., *Improving the Performance of Lithium Sulfur Batteries by Conductive Polymer Coating.* ACS Nano, 2011. **5**(11): p. 9187-9193.
50. Z. Ullah, S.A., and S. Naseem, *Indexing the Diffraction Patterns and Investigating the Crystal Structure of Pb-doped Strontium Ferrites.* Journal of Scientific Research, 2013. **5**(2): p. 235-244.
51. Daimay, L.-V., *The Handbook of Infrared and Raman characteristic frequencies of organic molecules*. 1991, San Diego: ACADEMIC PRESS, INC.
52. Thommes, M., *Physisorption of gases, with special reference to the evaluation of surface area and pore size distribution (IUPAC Technical Report).* Pure Appl. Chem., 2015. **87**(9-10): p. 1051-1069.
53. Zhou, G., *Sulfiphilic Nickel Phosphosulfide Enabled Li2S Impregnation in 3D Graphene Cages for Li–S Batteries.* Advanced Materials, 2017: p. 1603366-1603376.
54. Pierre Kuhn, M.A., *From Microporous Regular Frameworks to Mesoporous Materials with Ultrahigh Surface Area: Dynamic Reorganization of Porous Polymer Networks* 2008. **Journal of American Chemical Society** (130): p. 13333-13337.
55. Landers, J., *Density functional theory methods for characterization of porous materials.* Colloids and Surfaces A: Physicochemical and Engineering Aspects, 2013. **437**: p. 3-32.
56. Seh, Z.W., *High-capacity Li2S–graphene oxide composite cathodes with stable cycling performance.* Chemical Science, 2014. **5**.
57. Kai Zhang, J.C., *Ultrasmall Li2S Nanoparticles Anchored in Graphene Nanosheets for High-Energy Lithium-Ion Batteries*
Scientific Reports, 2014. **4**(6467).
58. Chenji Hu, L.C., *In situ wrapping of the cathode material in lithium-sulfur batteries.* Nature Communications, 2017. **8**(479).
59. Patrick Bonnick, E.N., John Muldoon, *Lithium-Sulfur Batteries*
Journal of The Electrochemical Society, 2018 **165** (1): p. A6005-A6007.